The Dissertation Committee for Mychel Elizabeth Varner
certifies that this is the approved version of the following dissertation:

Theoretical Thermochemistry and Spectroscopy of Weakly Bound Molecules

Committee:

John F. Stanton, Supervisor

Peter J. Rossky

Graeme Henkelman

Eric V. Anslyn

G. Barney Ellison

Theoretical Thermochemistry and Spectroscopy of Weakly Bound Molecules

by

Mychel Elizabeth Varner, B.S.

DISSERTATION

Presented to the Faculty of the Graduate School of

The University of Texas at Austin

in Partial Fulfillment

of the Requirements

for the Degree of

DOCTOR OF PHILOSOPHY

THE UNIVERSITY OF TEXAS AT AUSTIN

December 2010

Dedicated to millie and emmalynne.

Acknowledgments

Thank you to Professor John F Stanton, Dr. Juana Vázquez, Professor G. Barney Ellison, Professor Marsha I. Lester, Dr. Michael E. Harding, Dr. Bradley A. Flowers, Dr. Yannick J. Bomble, Dr. Takatoshi Ichino and all those listed on page 122 and beyond.

Theoretical Thermochemistry and Spectroscopy of Weakly Bound Molecules

Publication No. _____

Mychel Elizabeth Varner, Ph.D.
The University of Texas at Austin, 2010

Supervisor: John F. Stanton

The weakly bound association products of atmospherically relevant radical species (O_2, OH, NO_2, HO_2 and NO) have been studied theoretically using quantum-chemical methods. The thermodynamic stabilities, which are crucial to determining the probability of formation in Earth's atmosphere, were calculated for the hydrotrioxy radical (HOOO) and peroxynitrous acid (HOONO, an isomer of nitric acid) relative to the radical dissociation products. In the case of HOONO, the experimentally determined values were confirmed. For HOOO, the predicted stability was significantly lower than the experimentally determined value; a conclusion that was supported by later experimental work and indicates that HOOO will not form in significant quantities in Earth's atmosphere. The fundamental and multi-quantum vibrational transitions were also predicted for both the HOONO and HOOO systems. The theoretical

work on the HOONO system aided the assignment of experimental spectra and was used to correct equilibrium rotational constants. The HOOO system presented a challenge for the methods used here and work to apply other approaches in describing the vibrational modes is ongoing. Second-order vibrational perturbation theory, combined with a correlated quantum-chemical method and a moderately sized basis set, provides a method for accurately predicting fundamental and low-order multi-quantum transition energies and intensities for many systems (HOOO being an exception). Here coupled cluster theory, at a level which treats one- and two-electron correlation with a correction for three-electron correlation, and atomic natural orbitals basis sets were used in the vibrational calculations. To predict the dissociation energies of weakly bound species with the precision required (due to the small energy differences involved), high-order correlation contributions (a full treatment of three-electron correlation and a correction for four-electron correlation) are included, as is extrapolation to the basis set limit. Other contributions, such as that for the zero-point energy, were also considered. For the HOOO system, one-dimensional potential curves along the dissociation and torsional coordinates were constructed with standard single-reference and equation-of-motion coupled-cluster methods. The latter is better able to describe the nature of a system in the bond-breaking region and the complex electronic structure of a species formed from two radical fragments, one doubly degenerate in the ground state: $\tilde{X}^2\Pi$ OH and $\tilde{X}^3\Sigma$ O_2. A possible barrier to dissociation and the torsional potential for HOOO were investigated.

Table of Contents

List of Figures

List of Tables

Chapter 1

Introduction

The molecules discussed in this work are the weakly bound products of association reactions involving species relevant in atmospheric chemistry. The importance of the fragments and previous studies of the association products will be introduced below, as will the contributions that theoretical chemistry can add to the understanding of these systems.

1.1 Atmospheric Chemistry

Peroxynitrous acid, HOONO, is formed in the three-body combination reaction of the hydroxyl radical, OH, and nitrogen dioxide, NO_2, or the reaction of the hydroperoxy radical, HO_2, and nitric oxide, NO. The hydrotrioxy radical, HOOO, forms from OH and molecular oxygen, O_2. The reactants are involved in many atmospheric processes making the study of the association products of interest. After beginning with a discussion of the interactions of the fragments with ozone,[a] the possible effects of the weakly bound association

[a]Ozone is a significant minor component in the Earth's atmosphere with a significance that varies with altitude. At mid altitudes, high concentrations of ozone absorb sunlight of wavelengths shorter than 290 nm filtering the radiation that reaches the Earth's surface and the life thereon. Near the Earth's surface, ozone is an oxidant and irritant to plants and people.[1]

products on ozone concentration will be mentioned along with possible effects on a few other atmospheric processes.

1.1.1 Ozone and the HO_x and NO_x Cycles

The production and destruction of ozone through reactions of only oxygen-containing species, termed the Chapman cycle presented in reactions 1.1-1.5, cannot account for the relatively steady-state concentrations observed.[2]

$$O_2 + h\nu \longrightarrow O + O \tag{1.1}$$

$$O + O_2 \xrightarrow{M} O_3 \tag{1.2}$$

$$O_3 + h\nu \longrightarrow O + O_2 \tag{1.3}$$

$$O + O_3 \longrightarrow O_2 + O_2 \tag{1.4}$$

$$O + O \xrightarrow{M} O_2 \tag{1.5}$$

Photodissociation of molecular oxygen produces atomic oxygen, creating odd-oxygen species (1.1). The combination reaction of atomic oxygen and molecular oxygen to produce ozone converts one odd-oxygen species to another (1.2). And photodissociation of ozone to produce atomic and molecular oxygen reverses the effect (1.3). Both conversion reactions (1.2 and 1.3) are fast and destruction or production of an odd-oxygen species is generally considered equivalent to destruction or production of ozone.[b] However, loss of odd-oxygen

[b] While production of ozone decreases with increasing altitude (and decreasing concentrations of molecular oxygen) and production of atomic oxygen increases with altitude (and increasing radiation) resulting in atomic oxygen being the dominate odd-oxygen species at high altitudes, ozone is the dominate species at altitudes relevant here.

species through either the combination reaction of atomic oxygen and ozone to produce two oxygen molecules (1.4), or two oxygen atoms to produce one (1.5), is insufficient to combat the production due to photolysis of O_2 (1.1). Catalytic cycles with a net result of either Eq. 1.4 or Eq. 1.5 make up for the deficit in loss (or excess production). For example

$$X + O_3 \longrightarrow XO + O_2 \tag{1.6}$$

$$XO + O \longrightarrow X + O_2 \tag{1.7}$$

Here X may be H, OH or NO (or Cl); with an OH, HO_2 or NO_2 (or ClO) intermediate. Processes involving these species make up the HO_x or NO_x (or ClO_x) catalytic cycles for ozone loss. In the stratosphere (altitudes of approximately 20 to 50 km), both processes are significant with the HO_x processes dominating in the upper portion of the region and NO_2 in the lower.[2]

Photodissociation of NO_2 to NO and atomic oxygen and conversion of atomic oxygen to ozone through Eq. 1.2 has no effect on the overall ozone concentration when followed by the reaction of NO with ozone to form NO_2 and molecular oxygen (1.6). But if NO is oxidized without converting ozone to molecular oxygen, the net result is ozone production. This scenario is responsible for photochemical smog.[1] The reaction of NO with the HO_2 (or an alkylperoxy radical, ROO) to form NO_2 and OH (or an alkoxy radical, RO)

$$HO_2 + NO \longrightarrow OH + NO_2 \tag{1.8}$$

$$ROO + NO \longrightarrow RO + NO_2 \tag{1.9}$$

oxidizes NO, produces hydroxyl radicals that can oxidize organic species leading to other NO oxidation processes and ties the fates of NO_x and HO_x species.

1.1.2 Peroxynitrous Acid - HOONO

The reaction of OH (or RO) with NO_2 forms nitric acid, $HONO_2$ (or an organic nitrate, $RONO_2$).[1]

$$OH + NO_2 \xrightarrow{M} HONO_2 \tag{1.10}$$

$$RO + NO_2 \xrightarrow{M} RONO_2 \tag{1.11}$$

This reaction removes NO_x and HO_x species from the atmosphere by forming a relatively stable molecule: nitric acid. At high pressure and given the formation of nitric acid as the only removal mechanism, the concentration of OH in the presence of NO_2 decays at rates greater than predicted based on low pressure observations. This led to the suggestion that a less stable isomer of nitric acid, HOONO, could be an alternate product in the association reaction of OH and NO_2 with the formation of the less stable isomer becoming significant at high pressure.[3] It was predicted that under certain conditions (high pressure or low temperature) the lifetime of HOONO would be long enough to affect the loss rate for OH observed experimentally, but that HOONO was not sufficiently stable to serve as a sink for NO_x and HO_x atmospherically. The rate constant for nitric acid formation determined from the rate of OH loss was adjusted to account for estimated HOONO formation.[4] The effect of this reduced rate constant on atmospheric models was examined. Among the

differences noted was a significant increase in NO_x at altitudes at which discrepancies between modeled and observed concentrations had previously been reported.[c]

Evidence for the formation of the HOONO isomer as an alternate product in the association reaction of OH and NO_2 was found through isotopic labeling[5] and a bi-exponential loss rate for OH in the presence of NO_2.[6] At high temperature the less stable product has a short lifetime and dissociates on the timescale of the experiment. Initially, the loss of OH indicates the formation of nitric acid and the less stable product, but as the less stable product begins to dissociate and OH is reformed, the concentration of OH decreases at a slower rate. The HOONO product was first observed spectroscopically in the gas phase in the infrared action experiments of Nizkorodov and Wennberg.[7] This technique, in which a weakly bound molecule is dissociated through vibrational excitation and one of the resulting fragments is detected through laser-induced fluorescence,[d] was subsequently used to determine the dissociation energy of HOONO.[8,9] In the time since the HOONO side product was first observed, work to clarify the outcome of the OH + NO_2 reaction under various conditions has continued through master-equation models,[10,11e] and experiment.[12–14]

[c]One-dimensional atmospheric models predict the distribution of atmospheric species as a function of altitude based on the rate of production and rate of loss. Two-dimensional models, such as that used in ref. 4, incorporate a latitudinal dependence.[2]

[d]A more detailed description of this experimental technique is included in section 2.4.3.

[e]Models to describe the overall reaction rate of the system as a function of temperature. Temperature dependent parameters for collisional energy transfer as well as reaction rates of possible side reactions contribute to the overall process.

Alkylperoxy radicals reacting with nitric oxide form alkoxy radicals and NO_2 (1.9). For large alkylperoxy radicals, alkyl nitrates are also formed (1.12), with a yield up to 30 to 40%.[1]

$$ROO + NO \xrightarrow{M} RONO_2 \tag{1.12}$$

With the formation of alkyl nitrates removing radical species, RO_x and NO_x, from the atmosphere (1.12) and the formation of RO accompanying the ozone-less oxidation of NO (1.9), ROO + NO is another reaction of atmospheric interest. The simpler HOO + NO reaction also oxidizes NO (1.8) and is attractive as a model system in the study of reactions 1.9 and 1.12. A HOONO or ROONO intermediate has been assumed in these processes. However, there is not an obvious low energy transition state between HOONO and nitric acid and it was thought that the nitrate product only becomes significant when large alkylperoxy radicals are involved — making HOONO seemingly irrelevant to the discussion of nitrate formation from peroxy radicals.

Recent studies indicate that nitric acid is formed (in small yield) from HOO + NO and that the presence of water increases the yield of this minor product,[15] with theoretical evidence supporting a HOONO intermediate.[16] Rate constants determined over a range of atmospheric temperatures and pressures[17] were incorporated into atmospheric models[18] to investigate the effect of this nitrate forming reaction

$$HOO + NO \xrightarrow{M} HONO_2 \tag{1.13}$$

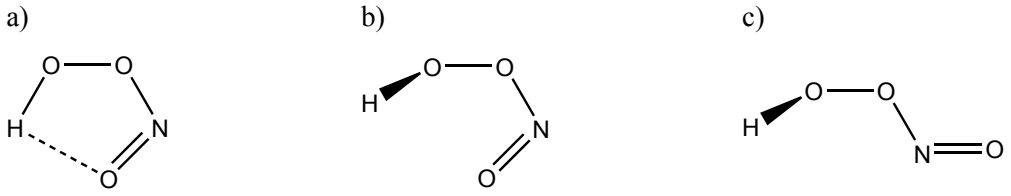

Figure 1.1: Three HOONO conformations: a) *cis,cis*, b) *cis,perp* and c) *trans,perp*.

on the concentrations of various atmospheric species. The inclusion of reaction 1.13 lead to lower predicted concentrations of NO_x and OH in the troposphere (from the Earth's surface to approximately 10 km), specifically the upper troposphere, and, under certain conditions, a slight increase the lifetime of methane and a decrease in ozone concentrations. The inclusion of reaction 1.13 also leads to larger differences between predicted and observed concentrations of various atmospheric species so this chemistry must be further investigated before the importance is known.

There are three main conformers of HOONO[19] (see figure 1.1), which are of varying importance. When both OONO and HOON torsional angles are zero (*cis,cis*-HOONO), an internal hydrogen bond forms stabilizing this isomer relative to the others (see figure 1.2[f]). A generalized valence bond analysis indicates that a HOON torsional angle of approximately 90 degrees

[f]The determination of the relative energies for the HNO_3 system presented in figure 1.2 is discussed in chapter 2 with the exceptions of the *cis,perp* conformer and the *perp,perp* transition state. The relative energies of the *cis,perp* and *perp,perp* conformers were calculated at the CCSD(T)/ANO1 (fc) level. See chapter 2 for a description of the computational methods.

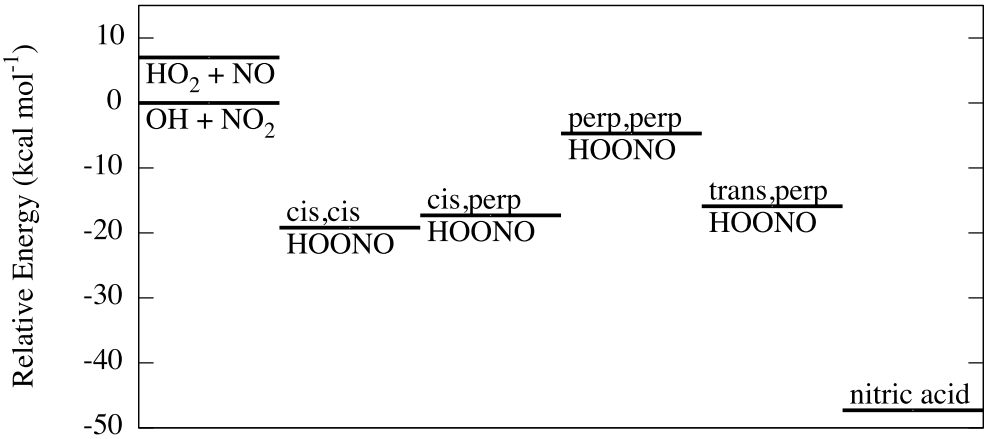

Figure 1.2: Potential energy diagram for the HNO_3 system.

(*perp*) is energetically most favorable, excepting the formation of an internal hydrogen bond as above, and that the heavy atoms will remain roughly in-plane resulting in *trans,perp* and *cis,perp* conformers.[20]

1.1.3 The Hydrotrioxy Radical - HOOO

The HO_3 species has been discussed as an intermediate in several atmospheric processes including the reaction of ozone with atomic hydrogen to produce vibrationally and rotationally excited OH (OH*) and O_2[21–26] and the reaction of the hydroperoxy radical with atomic oxygen.[22,27–29]

$$H + O_3 \longrightarrow O_2 + OH* \tag{1.14}$$

$$HOO + O \longrightarrow O_2 + OH \tag{1.15}$$

In a kinetic isotope study of reaction 1.15 carried out at room temperature, it was determined that OH is formed through an HO_3 intermediate rather

than through hydrogen abstraction by atomic oxygen.[27] In recent theoretical studies,[28,29] a planar structure for the HOOO intermediate was predicted and rate constants, which were roughly in agreement with experimental values, were calculated.[28] For reaction 1.14, two possible HOOO intermediates with planar and nonplanar structures described in an early theoretical study[21] were invoked to explain OH products that were either highly rotationally or vibrationally excited, respectively.[23,25] Following theoretical studies focused first on the nonplanar[22] then a planar HOOO intermediate similar to that of reaction 1.14.[26]

Vibrationally excited hydroxyl radicals (OH*) are produced in the upper atmosphere through reaction 1.14. Loss of this vibrational energy occurs through emission in the infrared and visible (i.e., the Meinel bands) and through collisions with N_2 and O_2.[2] The rate of vibrational energy loss is much greater for collisions with O_2, with the rate increasing with decreasing temperature.[30] A relatively large negative temperature dependence for collisional deactivation can indicate the formation of a complex. If the O_2-OH* complex forms, the rate of dissociation, which would regenerate O_2 and OH*, decreases with decreasing temperature. The decreased dissociation rate allows other processes to compete, such as redistribution of vibrational energy and the formation of O_2 and deactivated OH. This interaction is another indication that there is a bound HO_3 species.

Early theoretical studies on the thermodynamic stability of HO_3 yielded inconsistent results. At some levels of theory the structure of a stable radical

was determined[22,31–33] and at others HO_3 was found to be unstable[31,34–36] or possibly metastable[36] relative to OH + O_2. The first experimental estimate of the heat of formation of HO_3 ($\Delta H^\circ_{f,298K}$ = -1 ± 5 kcal mol^{-1}) was obtained by inferring an ionization energy of HO_3 (IE = 253 ± 4 kcal mol^{-1}) through examination of electron transfer efficiencies between a series of substrates and HO_3^+[37] and combining it with the heat of formation of HO_3^+ ($\Delta H^\circ_{f,298K}$ = 252 ± 3 kcal mol^{-1}).[38] This heat of formation for HO_3 indicates that the radical is stable relative to dissociation to OH + O_2 by 10 ± 5 kcal mol^{-1}. The HO_3 species was first detected through neutralization-reionization mass spectroscopy,[39] which confirmed that it is a relatively stable radical. The Fourier-transform microwave spectroscopy study that followed provided rotational constants and determined that the radical has a stable planar *trans*-HOOO geometry.[40] Infrared action exeriments provided an upper bound for the dissociation energy of HOOO to OH + O_2 ($D_0 \leq 6.12$ kcal mol^{-1}),[41] which was later revised based on the value determined for the deuterated species ($D_0 \leq 5.31$ kcal mol^{-1}).[42] This upper bound is consistent with the earlier experimental estimate, but significantly greater than recent theoretical predictions that cluster around 1 to 3 kcal mol^{-1} (see figure 1.3[g]).[26,28,43–45h]

The hydrotrioxy (HOOO) radical has been proposed as a sink for hydroxyl radicals in the Earth's atmosphere. Depending on the binding energy

[g]The determination of the stability of HOOO relative to OH and O_2 is presented in chapter 2. The experimental value for the HOOO stability is from ref. 42. The relative stabilities of H + O_3 and HOO + O were estimated from heats of formation.

[h]One exception being the work of ref. 44.

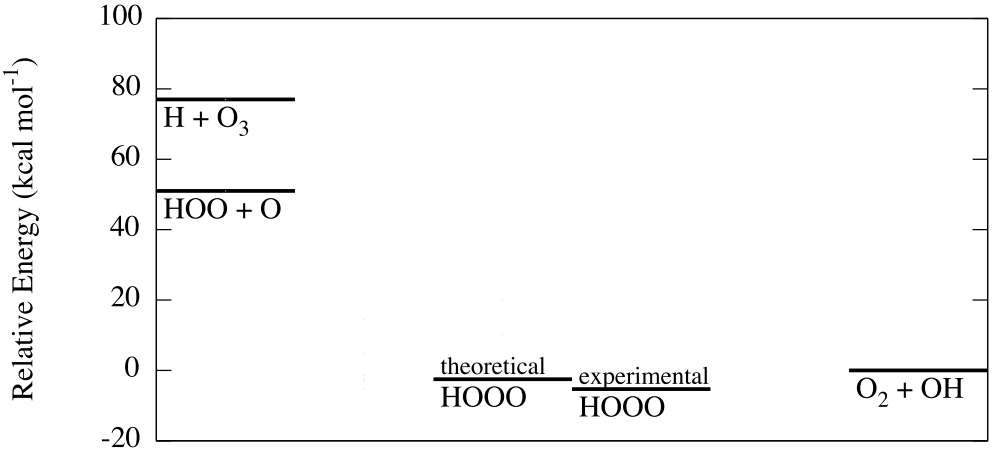

Figure 1.3: Potential energy diagram for the HO_3 system.

of HOOO, a significant portion of the hydroxyl radicals could be bound to O_2 at certain altitudes, up to 66%[41] for a D_0 of 6.12 kcal mol^{-1} (or 25%[46] for a D_0 of 5.31 kcal mol^{-1}). However, if the true dissociation energy is around 1 to 3 kcal mol^{-1} as predicted by theory, the formation of HOOO in the atmosphere will likely not be significant. A negative temperature dependence, similar to that noted above for deactivation of OH* through collisions with O_2, is expected for the formation of HOOO in the association reaction of OH and O_2. As a result, the highest predicted concentrations of HOOO would occur at approximately 10 km above the Earth's surface, at the boundary between the troposphere[i] and stratosphere[j] (the tropopause).

[i]From the Earth's surface to an altitude of approximately 10 km, temperature decreases with increasing altitude.

[j]Above approximately 10 km, temperature increases with altitude due to the absorption of solar radiation in the photolysis of O_2 and O_3 discussed above.

In addition to participation in the HO_x catalytic ozone destruction cycles of the stratosphere (see reactions 1.6 and 1.7), hydroxyl radicals are significant as a primary atmospheric oxidant and as a participant in the ozone formation and destruction cycles in the troposphere. By abstracting a hydrogen from alkanes, hydroxyl radicals initiate a chain of processes that result in ozone production through reaction 1.9.[k] The reaction of OH radicals with carbon monoxide to produce hydrogen atoms is another critical step in tropospheric ozone production in the presence of NO. Or, in remote regions where concentrations of NO are low, the reaction of OH with carbon monoxide results in loss of ozone. Thus reaction with hydroxyl radicals is a major sink for methane (and other hydrocarbons) and carbon monoxide in the troposphere. The behavior of hydroxyl radicals has been well-described in the stratosphere, however uncertainty remains concerning OH chemistry in the troposphere[47] (and the mesosphere[l 48]). Inclusion or dismissal of the HOOO radical as a sink for hydroxyl radicals in the atmosphere would be one step (of many) toward a clearer description of this important chemistry.

1.2 Applications of Computational Chemistry

Both HOONO[3] and HOOO[49] were proposed well before they were detected.[7,39,50] Weakly bound species can often only be studied under specific

[k] Alkyl radicals react with O_2 to form alkoxy radicals that can participate in reaction 1.9.

[l] From an altitude of approximately 50 to 90 km, temperature again decreases with increasing altitude.

conditions with interference by other more stable molecules. Identification through the observation of vibrational and rotational spectra is often critical to establish the existence of these species. The initial intent of this computational work was to aid the assignment of experimentally observed vibrational spectra. The calculation of vibrational energy levels beyond the harmonic approximation with high accuracy can provide a connection between one of the few experimentally observable properties, the vibrational frequencies, and the theoretical description. An accurate description of the molecular vibrations will also allow for comparison of the experimentally and theoretically determined structure. Work in these areas is described in chapter 3 and includes a comparison of predicted and observed vibrational frequencies and rotational constants for *trans,perp*-HOONO, *cis,cis*-HOONO and *trans*-HOOO.

An accurate determination of the thermodynamic stability for these weakly bound species is essential to the prediction of concentrations over a range of temperatures and pressures, i.e. at various altitudes in the Earth's atmosphere. The experimental technique, infrared action spectroscopy, used to determine bond energies of HOONO and HOOO, can only provide an upper bound to the dissociation energy. This approach can benefit from confirmation through accurate theoretical predictions. High-level quantum chemical methods are required to obtain a useful quantitative value. Special care is required with the fragments (NO_2, OH, NO, HO_2 and O_2) as all are species containing unpaired electrons. In the case of HOOO, the species of interest is itself a radical. The theoretical determination of dissociation energies for *cis,cis* and

trans,perp-HOONO and *trans* and *cis*-HOOO is discussed in chapter 2.

The ability to theoretically explore the potential energy surface of a species away from the local minima is also useful. For HOOO, where disagreement between theory and experiment has been commonly encountered, an examination of the *trans*-HOOO $\rightarrow$ OH + O_2 dissociation curve and the HOOO torsional potential is presented chapter 4.

Atmospheric models require rate constants for reactions of the relevant species. Often low-temperature rate constants can be extrapolated over the range of atmospheric conditions. However, complications can arise, as in the OH + NO_2 system as described above. Theory may not yet be capable of predicting quantitative rate constants *ab initio*,[51] but an accurate description of the potential energy surface and the prediction of molecular properties to support experimental observations may provide a better understanding of the system. The estimation of the concentration of species that form through weak interaction of common atmospheric molecules is dependent on the thermodynamic stability as well as spectroscopic constants such as vibrational frequencies and rotational constants — all of which can typically be accurately predicted with advanced electronic structure methods.[52] When discrepancies do arise between theoretical predictions and experimental determinations, theory may reveal abnormalities that could explain the differences.

Chapter 2

Dissociation Energies

High-level quantum-chemical methods were used to calculate the dissociation energies of several weakly bound molecules. The energy required to dissociate *trans,perp*-HOONO to OH and NO_2 is predicted to be 15.9 kcal mol^{-1}, for *cis,cis*-HOONO the value is 19.2 kcal mol^{-1}. These predictions agree with experimental determinations to within 1 kcal mol^{-1}. Theoretically, *trans*-HOOO is bound relative to OH and O_2 by 2.5 kcal mol^{-1}.

2.1 Introduction

2.1.1 Thermochemistry

In weakly bound systems, where dissociation energies are as small as a few kilocalories per mole, accurate heats of formation (or heats of reaction) are essential to the discussion of the stability of a species. Through the evaluation of experimental data, the heat of formation of a species can be determined from observations on many related species. A recent implementation of this concept, the Active Thermochemical Tables [ATcT] approach,[53,54] which utilizes selected experimental and theoretical data, has succeeded in substantially improving the quality of thermodynamic values for many species. Relation-

ships between available data are monitored while solving for values of interest and determining a reliable uncertainty. However, for short-lived, exotic species that have only been detected under certain conditions (or have not yet been observed) there is less (or no) data on which to base experimental values without theoretical predictions. Theoretical predictions also can provide consistency checks to experimental determinations in addition to estimates where no experimental data is available.[a] Thermochemical models have been developed to describe procedures by which heats of formation can be determined through the application of quantum-chemical methods.[58–63] These models vary in accuracy and reliance on empirical corrections.

2.1.2 Coupled Cluster Theory

Of the various thermochemical models developed, those that attempt to attain sub-kilojoule per mole (less than a quarter of a kcal mol^{-1}) accuracy use coupled-cluster methods for the calculation of electronic energies.[61–64] In this approach, an exponential operator is applied to a reference, usually single-determinate Hartree-Fock, wavefunction $[\Phi_0]$ to generate the coupled cluster wavefunction $[\Psi_{CC}]$.[65,66]

$$\begin{aligned}\Psi_{CC} &= e^{\hat{T}}\Phi_0 \\ &= (1 + \hat{T} + \tfrac{1}{2}\hat{T}^2 + \tfrac{1}{3!}\hat{T}^3 + \cdots)\Phi_0 \end{aligned} \tag{2.1}$$

[a]Theoretical thermochemistry has played a role in the examination of such species as OH,[55] HO_2,[54,56] and C[57] where experimental data is available but contradictory or error bars are larger than required. The work presented below focuses on weakly bound molecules where experimental observation has been limited.

where the cluster operator, $\hat{T}$, is defined as a series of terms

$$\hat{T} = \hat{T}_1 + \hat{T}_2 + \hat{T}_3 + \cdots \tag{2.2}$$

that promote one, two, three or more electrons from occupied orbitals [ϕ_i, ϕ_j, $\phi_k \ldots$] of the reference function [$\Phi_0 = \{\phi_i \phi_j \phi_k \ldots\}$] to unoccupied, or virtual, orbitals [ϕ_a, ϕ_b, $\phi_c \ldots$] as follows

$$\hat{T}_1 \Phi_0 = \sum_{\substack{i \\ a}} t_i^a \Phi_i^a \tag{2.3a}$$

$$\hat{T}_2 \Phi_0 = \sum_{\substack{i>j \\ a>b}} t_{ij}^{ab} \Phi_{ij}^{ab} \tag{2.3b}$$

$$\hat{T}_3 \Phi_0 = \sum_{\substack{i>j>k \\ a>b>c}} t_{ijk}^{abc} \Phi_{ijk}^{abc} \tag{2.3c}$$

These single (equation 2.3a), double (equation 2.3b), triple (equation 2.3c), etc. excitations make possible the calculation of corrections, due to electron correlation, to the electronic energy obtained through the self-consistent field [SCF] approach in which an electron interacts with the average field generated by its peers.[66] The magnitude of the coupled cluster amplitudes [t_i^a, t_{ij}^{ab}, $t_{ijk}^{abc} \ldots$] associated with the $\hat{T}_1$, $\hat{T}_2$, $\hat{T}_3 \ldots$ operators indicates the importance of the associated excitation to the wavefunction of the system.

To obtain information from the coupled cluster wavefunction, $\Psi_{CC} = e^{\hat{T}} \Phi_0$ is inserted into the Schrödinger equation, which is then multiplied on the

left by the reference function to obtain and expression for the energy.[67]

$$\hat{H}|\Psi\rangle = E|\Psi\rangle \tag{2.4a}$$

$$\hat{H}e^{\hat{T}}|\Phi_0\rangle = Ee^{\hat{T}}|\Phi_0\rangle \tag{2.4b}$$

$$\langle\Phi_0|\hat{H}e^{\hat{T}}|\Phi_0\rangle = E\langle\Phi_0|e^{\hat{T}}|\Phi_0\rangle \tag{2.4c}$$

If the Schrödinger equation is instead projected onto an excited wavefunction, such as those of equations 2.3a-2.3c, an equation for the corresponding coupled cluster amplitude is obtained.

$$\langle\Phi_{ij\ldots}^{ab\ldots}|\hat{H}e^{\hat{T}}|\Phi_{ij\ldots}^{ab\ldots}\rangle = E\langle\Phi_{ij\ldots}^{ab\ldots}|e^{\hat{T}}|\Phi_{ij\ldots}^{ab\ldots}\rangle \tag{2.5}$$

Multiplying by $e^{-\hat{T}}$ prior to multiplication by the reference or excited wavefunction yields equations which can separately be solved for the energy and amplitudes (rather than dealing with the energy dependence of equation 2.5).

$$\langle\Phi_0|e^{-\hat{T}}\hat{H}e^{\hat{T}}|\Phi_0\rangle = E\langle\Phi_0|e^{-\hat{T}}e^{\hat{T}}|\Phi_0\rangle = E \tag{2.6a}$$

$$\langle\Phi_{ij\ldots}^{ab\ldots}|e^{-\hat{T}}\hat{H}e^{\hat{T}}|\Phi_0\rangle = E\langle\Phi_{ij\ldots}^{ab\ldots}|e^{-\hat{T}}e^{\hat{T}}|\Phi_0\rangle = 0 \tag{2.6b}$$

The coupled cluster energy as given by equation 2.6a is not variational, but equations 2.6a and 2.6b can more readily be solved for E and all possible t_i^a, t_{ij}^{ab}, etc.

The exponential form of the operator,[b] and the expansion demonstrated in equation 2.1, ensures that higher order excitations are included when the

[b]Here $e^{\hat{T}}$ also ensures size-consistency, i.e. that calculated properties are "additive for noninteracting systems."[68]

cluster operator of equation 2.2 is truncated.[69] Use of the first two terms from equation 2.2, which generate single and double excitations from the reference wavefunction, leads to the coupled cluster singles and doubles method [CCSD].[70] When the $\hat{T}_1 + \hat{T}_2$ operator is applied to the reference function and expanded as shown in equation 2.7, higher excitations are generated as well.

$$\begin{aligned}\Psi_{CCSD} &= (1 + (\hat{T}_1 + \hat{T}_2) + \tfrac{1}{2}(\hat{T}_1 + \hat{T}_2)^2 + \cdots)\Phi_0 \\ &= \Phi_0 + \sum_{\substack{i \\ a}} t_i^a \Phi_i^a + \sum_{\substack{i>j \\ a>b}} t_{ij}^{ab} \Phi_{ij}^{ab} \\ &\quad + \tfrac{1}{2}\sum_{\substack{i>j \\ a>b}} t_i^a t_j^b \Phi_{ij}^{ab} + \sum_{\substack{i>j>k \\ a>b>c}} t_i^a t_{jk}^{bc} \Phi_{ijk}^{abc} + \tfrac{1}{2} \sum_{\substack{i>j>k>l \\ a>b>c>d}} t_{ij}^{ab} t_{kl}^{cd} \Phi_{ijkl}^{abcd} + \cdots \end{aligned} \tag{2.7}$$

Here the higher excitations are the triple and quadruple excitations for the final two terms shown.[c]

A correction that estimates the effect of the $\hat{T}_3$ term can be made by approximating the triples contributions according to perturbation theory and determining the relevant t_{ijk}^{abc} coefficients from the converged t_{ij}^{ab} and t_i^a coefficients.[66] Use of this correction following application of the CCSD method yields the standard CCSD(T) method.[71] Calculations to account for additional correlation may be carried out, but contributions beyond those of the $\hat{T}_4$ term are typically small[d] when the goal is accuracy of 1 kJ mol^{-1}.[72,73]

[c]These are considered disconnected triples and quadruples. Connected triples are those of equation 2.3c.

[d]Among the exceptions are cases where nondynamical correlation is large. HOOO may be such a case and this topic will be discussed further in Section 2.4.2.

2.1.3 Basis Sets

Along with a series of increasingly accurate, and increasingly demanding, coupled-cluster methods, a series of basis sets are employed by high-level thermochemical models. Using a large number of basis functions to describe the reference wavefunction allows for increased flexibility, but also complexity, in the calculation of the energy. Since the use of an infinite basis set is impossible, energies calculated with a series of basis sets are extrapolated to approximate the infinite basis set limit.[69]

Prior to the basis set extrapolation described below, Almlöf and Taylor used atomic natural orbitals [ANO][74] to select basis functions that contributed significantly to the description of the wavefunction to minimize the effect of basis truncation. Basis sets may be constructed from contracted functions which are linear combinations of Gaussian functions, or primitives. These primitives are defined by the exponent of the Gaussian and multiplied by an expansion coefficient.[75] Using a large number of primitives and the configuration interaction method for atomic wavefunctions, Almlöf and Taylor determined the expansion coefficients for the natural orbitals.[76] These coefficients were used as in constructing the contracted functions. Orbital occupation numbers determined which functions would be excluded to obtain a basis set of reasonable size. This resulted in basis sets for which calculated atomic correlation energies did not differ significantly from those obtained with large uncontracted sets of Gaussians. As only the valence electrons were correlated in the optimization of the coefficients, these basis sets were not designed for core correlation.[74] The

$[4s3p2d1f/4s2p1d]$ contraction of the ANO basis set has been labelled ANO1.[77]

Building on the work of Almlöf and Taylor and others in designing basis sets for correlated wavefunctions, Dunning and co-workers constructed a series of correlation-consistent basis sets.[78] Each basis set in the series has additional functions chosen so that the correlation energy computed with each set increases systematically. This allows for the fitting of a model to the calculated energies for extrapolation to the basis set limit. The Hartree-Fock self-consistent field [HF-SCF] energies calculated with the correlation-consistent polarized valence sets [cc-pVXZ, X = D,T,Q,5...][78,79] can be fit to the following three-parameter exponential model[80,81]

$$E_{\mathrm{HF}}^{X} = E_{\mathrm{HF}}^{\infty} + ae^{-bX} \tag{2.8}$$

where E_{HF}^{∞} is the (estimated) HF-SCF energy at the basis set limit, E_{HF}^{X} is the HF-SCF energy calculated with the cc-pCVXZ basis set, X is 2, 3, 4... for X = D, T, Q... while a and b are additional parameters to be fit. Using this model, the HF-SCF energy at the basis set limit can be predicted from energies calculated with three basis sets from the series of correlation-consistent basis sets.

The correlation energy is not well described by an exponential model. Instead a two-parameter inverse power equation is used[81]

$$\Delta E_{\mathrm{corr}}^{X} = \Delta E_{\mathrm{corr}}^{\infty} + \frac{a}{X^3} \tag{2.9}$$

here $E_{\mathrm{corr}}^{\infty}$ is the (estimated) value determined for the correlation energy at the basis set limit, E_{corr}^{X} is the correlation energy calculated with the cc-pCVXZ

basis set and a is a parameter to be fit. While the requirements for the validity of this extrapolation are often not fullfilled,[e] the results obtained are typically good[64] though some refinement is possible[73]. Diffuse functions or functions for the proper treatment of core electron correlation may be added to the cc-pVXZ series to obtain the aug-cc-pVXZ series[82] and the cc-pCVXZ series,[78] respectively, or when both are included the aug-cc-pCVXZ series.

2.1.4 Other Factors

Accurate treatment of the electron correlation and the completeness of the basis set are not the only factors that must be considered when calculating atomic or molecular energies for comparison to experimental observables. The zero-point vibrational energy of molecules can have a considerable effect on relative energies of the species. Other, more minor factors that are relevant at the kJ mol^{-1} level are: spin-orbit interaction, other relativistic effects and failings of Born-Oppenheimer approximation.[64,72] The nonrelativistic Hamiltonian does not account for the splitting of states due to coupling of spin and orbital angular momentum. By calculating the energy of a molecule with a Hamiltonian that includes this coupling and comparing to a state-averaged nonrelativistic value, the lowering of the ground state energy of a molecule due to spin-orbit coupling can be obtained.[64] The effect of the relativistic electron mass on the electronic kinetic energy and on nuclear attraction, through the

[e] As noted in ref. 64, these systems are not spherically symmetric, nor, for example, is the aug-cc-pCVTZ basis set saturated with f functions.

effect on the effective radius,[83] can (for first- and second-row elements) largely be accounted for by the mass-velocity and one-electron Darwin terms, respectively.[84]

Within the Born-Oppenheimer, approximation we fix the nuclei of a molecule and determine the electronic energy. By examining how the electronic energy changes with varying internuclear distances, we may construct potential energy surfaces (see chapter 3). From these surfaces the energy of the zero-point vibrational motion of a molecule can be determined. This potential energy surface description can break down when nuclear and electronic motion cannot be separated. This failing of the Born-Oppenheimer approximation will not be considered here. However, the finite nuclear mass (rather than an infinite nuclear mass associated with the fixed-nuclei, Born-Oppenheimer approach) can have an effect on the nuclear kinetic energy even for systems with electronic states that are well-described by separable potential energy surfaces. The diagonal Born-Oppenheimer correction [DBOC] takes this effect into account without disrupting the potential energy surface description. Use of a correlated electronic wavefunction in the calculation of the correction is possible, but not generally necessary.[68,85f] The specific treatment of each of the components to the total molecular energy discussed in this section as applied to the systems of interest, HOONO and HOOO, will be described in sections 2.2.1 and 2.2.2.

[f]The effect on the calculated DBOC correction due to use of correlated wavefunctions, was investigate for one of the systems here but was not found to be significant.

2.2 Methods

The goal of this work was the prediction of the thermodynamic stability of several molecules relative to fragmentation. The dissociation energy, D_0, of each species was computed directly from the molecular energies of the species of interest and its fragments according to the following equations. Each contribution in (2.10) is calculated from the energies of fragments A and B and the bound product AB according to (2.11)

$$D_0 = E_{\mathrm{a}} + E_{\mathrm{b}} + E_{\mathrm{c}} + \cdots \tag{2.10}$$

$$E_x = E_x(\mathrm{A}) + E_x(\mathrm{B}) - E_x(\mathrm{AB}) \tag{2.11}$$

The contributions in equation 2.10, which are summed to determine D_0, are described below.

2.2.1 HOONO

A procedure similar to the HEAT (high accuracy *ab initio* thermochemistry) protocol[64] was used to calculate dissociation energies for two isomers of the HOONO molecule (see table 2.1[g] for a summary of the HEAT protocol and the differences in the approach as applied to the HNO_3 system). Geometries[h] were optimized at the CCSD(T) level employing a restricted Hartree-Fock [RHF] reference wavefunction. For the open-shell dissociation fragments an

[g] Tables are collected at the end of the chapter.
[h] Molecular geometries are compiled in appendix A.

unrestricted Hartree-Fock [UHF] reference wavefunction was employed. The cc-pVQZ basis set was used and all electrons were correlated. The largest contributions to the electronic energy are the (restricted or unrestricted) HF-SCF energy and the CCSD(T) correlation energy. The HF-SCF energy at the basis set limit [E^{∞}_{HF}] was determined according to equation 2.8 from energies calculated with the aug-cc-pCVXZ [X = T,Q,5] basis sets. Using the CCSD(T) correlation energy calculated with the aug-cc-pCVXZ [X = Q,5] basis sets and equation 2.9, the extrapolated CCSD(T) correlation energy [$\Delta E^{\infty}_{\mathrm{CCSD(T)}}$] was determined. To correct for deficiencies in the perturbative treatment of triple excitations, the difference in the extrapolated correlation energy at the coupled cluster singles, doubles and triples level [CCSDT],[86–88] and the extrapolated CCSD(T) correlation energy was included, $\Delta E_{\mathrm{CCSDT}}$. The two-parameter model of equation 2.9 was used in the extrapolations required for the CCSDT correction, but due to the computational demand of the full triples calculations, the smaller cc-pVXZ [X = D,T] basis sets were used. The final correlation contribution included here was the difference in the coupled cluster singles, doubles and triples energy with a perturbative treatment of quadruple excitations [CCSDT(Q)][89,90] and the CCSDT energy, both calculated with the cc-pVDZ basis set, $\Delta E_{\mathrm{CCSDT(Q)}}$. Core correlation effects were not included in the CCSDT or CCSDT(Q) corrections.

The first-order correction due to spin-orbit interaction [ΔE_{SO}] considered here will only be nonzero for species with with singly-occupied degenerate orbitals, i.e. the fragments excluding NO_2 and HO_2. These values were taken

from the HEAT data set[64] where a spin-orbit configuration interaction [CI] procedure was used in conjuction with a cc-pVDZ basis set and relativistic effective core potentials [RECP].[91] The scalar relativistic correction [ΔE_{rel}] was calculated at the CCSD(T)/aug-cc-pCVTZ level from the one-particle density matrix and the mass-velocity and one-electron Darwin terms. A RHF electronic wavefunction calculated with the aug-cc-pVTZ[82] basis set was used to determine the DBOC correction [ΔE_{DBOC}]. For the open-shell systems, the restricted open-shell Hartree-Fock [ROHF] wavefunction was used.[64]

To calculate the zero-point energy correction [ΔE_{ZPE}], geometry optimizations and second-order vibrational perturbation theory [VPT2] calculations (see chapter 3) were carried out at the CCSD(T) level with the ANO1 basis set and the frozen core approximation [(fc)], which excludes core electrons from the correlation treatment. The constant G_0 term from the expression for the vibrational energy levels was included in the calculation of the zero-point energy.[64]

With the above descriptions of the included contributions, the equation for D_0 (2.10) becomes

$$\begin{aligned} D_0 = {} & E_{\mathrm{HF}}^{\infty} + \Delta E_{\mathrm{CCSD(T)}}^{\infty} + \Delta E_{\mathrm{CCSDT}} + \Delta E_{\mathrm{CCSDT(Q)}} \\ & + \Delta E_{\mathrm{SO}} + \Delta E_{\mathrm{rel}} + \Delta E_{\mathrm{DBOC}} + \Delta E_{\mathrm{ZPE}} \end{aligned} \tag{2.12}$$

2.2.2 HOOO

Geometry optimizations,[i] anharmonic force field calculations and the remaining calculations for the determination of the HOOO dissociation energy were carried out as described in section 2.2.1 with the exceptions of the $\Delta E_{\mathrm{CCSDT}}$ and $\Delta E_{\mathrm{CCSDT(Q)}}$ contributions and the type reference wavefunction used (see table 2.1 for a summary of the HEAT protocol and the differences in the approach as applied to the HO_3 and HNO_3 systems). For all but the force field calculations, a UHF reference function was employed for the open-shell HOOO species and dissociation fragments. An ROHF reference wavefunction was used to avoid issues of spin-contamination[92] in calculating the anharmonic frequencies[j] required to determine the zero-point correction. In determining $\Delta E_{\mathrm{CCSDT}}$, the larger pVXZ [X = T,Q] basis sets were used. For $\Delta E_{\mathrm{CCSDT(Q)}}$, the pVTZ basis set was used.[k]

The CFOUR[95] program package was used in all calculations except those to determine ΔE_{SO}; for those at the CCSDT(Q) level the MRCC[96] package was also used.

[i] Molecular geometries are compiled in chapter 4.

[j] Anharmonic force fields were determined for *trans* and *cis*-HOOO with both UHF and ROHF wavefunctions. For *trans* the results were nearly indistinguishable. For *cis*, spin-contamination had a large effect on the resulting frequencies of some modes.

[k] Double zeta basis sets seem to be insufficient for this system (see refs. 93, 94 and chapter 4).

2.3 Results

2.3.1 HOONO

The contributions to dissociation energies calculated for *trans,perp* and *cis,cis*-HOONO are compiled in Tables 2.2 and 2.3.[1] Energies of dissociation to OH and NO_2 are compared to experimentally determined values in Table 2.2; nitric acid is included for comparison. The predicted binding energies of the HOONO isomers; 15.9 kcal mol^{-1} for *trans,perp* and 19.2 kcal mol^{-1} for *cis,cis*; are less than half that of nitric acid, 47.7 kcal mol^{-1}. The internal hydrogen bond of the *cis,cis* isomer of HOONO stabilizes it by 3.3 kcal mol^{-1} relative to the *trans,perp* isomer. All predicted values for dissociation of HNO_3 to OH and NO_2 are within 1 kcal $mol^{-1}$of the experimental values.

Results for dissociation of HOONO to HO_2 and NO are presented in Table 2.3. The central NO bond is approximately 7 kcal mol^{-1} stronger than the OO bond, the weakest bond in the HOONO molecule. D_0 for the central NO bond has not been measured directly, but the experimental stabilities of HOONO relative to OH and NO_2 presented in Table 2.2 can be combined with the experimental heats of formation of NO, HO_2, OH and NO_2 to determine the experimental stabilities HOONO relative to HO_2 and NO as follows

$$\begin{aligned} D_0^{\mathrm{HO_2+NO}}(\mathrm{HOONO}) = {} & \Delta H^\circ_{\mathrm{f,0K}}(\mathrm{HO_2}) + \Delta H^\circ_{\mathrm{f,0K}}(\mathrm{NO}) \\ & - \Delta H^\circ_{\mathrm{f,0K}}(\mathrm{OH}) - \Delta H^\circ_{\mathrm{f,0K}}(\mathrm{NO_2}) \\ & + D_0^{\mathrm{OH+NO_2}}(\mathrm{HOONO}) \end{aligned} \tag{2.13}$$

[1]Tables are collected at the end of the chapter.

These experimental predictions are presented in Table 2.3 with the calculated results.

2.3.2 HOOO

The calculated dissociation energy of the *trans*-HOOO radical is presented in Table 2.4, along with the corresponding values for *cis*-HOOO and the FOO radical for comparison. This theoretical value of 2.5 kcal mol^{-1} for the central OO bond energy of *trans*-HOOO is approximately 3 kcal mol^{-1} below the upper bound to the dissociation energy determined in the infrared action experiment, 5.31 kcal mol^{-1}.[42] However, the predicted value is in good agreement with the value for D_0 derived from a very recent kinetics experiment: 2.96 kcal mol^{-1}.[97]

2.4 Discussion

2.4.1 HOONO

HOONO is larger than the typical system studied at the sub-kilojoule per mole ($\approx$ 0.24 kcal mol^{-1}) level. The largest species in the original HEAT test set had three heavy atoms (and one less hydrogen atom than HOONO). Due to the computational cost of certain methods in the HEAT protocol, some adjustments were necessitated when the model was applied to a system with four heavy atoms such as HOONO. The first deviation was in the size of the basis sets used to calculate the first correction to account for high-level correlation: the $\Delta E_{\mathrm{CCSDT}}$ contribution. The double and triple zeta basis sets were

used to extrapolate the CCSDT, and the required associated CCSD(T), correlation energy rather than the larger prescribed triple and quadruple zeta basis sets. This change is solely due to the computational cost of the CCSDT/cc-pVQZ calculation for the *trans,perp* isomer of HOONO. The use of the smaller basis sets is not expected to have a large effect on the dissociation energies for this system. The $\Delta E_{\mathrm{CCSDT}}$ contribution was calculated with the HEAT mandated triple and quadruple zeta basis sets for *cis,cis*-HOONO, which has a plane of symmetry that reduces the cost of the CCSDT/cc-pVQZ calculation. The effect on the final D_0 was negligible, 0.03 kcal mol^{-1} for dissociation to OH and NO_2, -0.04 kcal mol^{-1} for dissociation to HO_2 and NO. Therefore, the use of the cheaper $\Delta E_{\mathrm{CCSDT}}$ correction is justified and without significant loss of accuracy.

The other deviation from the HEAT protocol was in the basis set used to calculate the anharmonic force field for the determination of the ΔE_{ZPE} contribution. Computational cost was a factor, but use of the called-for cc-pVQZ basis set would have been feasible had it been necessary. However, our previous work on the prediction of the vibrational energies of the HOONO isomers and nitric acid has shown that the smaller triple zeta atomic natural orbital basis set of Almlöf and Taylor (ANO1)[74] generally yields very good results for the vibrational energies of this system,[20,98–100] and therefore should also reproduce the zero-point energy accurately.

If the intended (and demonstrated for the chosen test set, see ref. 64) accuracy of the HEAT model ($\pm$ 0.24 kcal mol^{-1}) is assumed when applied

to HOONO, then the experimental and theoretical uncertainties overlap for the oxygen-oxygen bond energies (in dissociation to OH and NO_2). The error relative to experimental values for the theoretical nitrogen-oxygen HOONO bond energies (in dissociation to HO_2 + NO) is 0.1 kcal mol^{-1} greater than the error in the oxygen-oxygen HOONO bond energies. An examination of the $\Delta E_{\mathrm{CCSDT}}$ and $\Delta E_{\mathrm{CCSDT(Q)}}$ contributions to the HOONO dissociation energies in Tables 2.2 and 2.3 suggests that inadequate treatment of high-level correlation may be the cause of the increased error in the HOONO nitrogen-oxygen bond energies. In Table 2.2, the $\Delta E_{\mathrm{CCSDT}}$ and $\Delta E_{\mathrm{CCSDT(Q)}}$ contributions to the oxygen-oxygen bond energies are of similar magnitude and opposite sign, with the magnitude of the quadruples correction slightly smaller than the magnitude of the triples correction. In Table 2.3, the $\Delta E_{\mathrm{CCSDT}}$ and $\Delta E_{\mathrm{CCSDT(Q)}}$ corrections to the nitrogen-oxygen bond energies are also of similar magnitude and opposite sign, however the magnitude of the quadruples correction is slightly larger than that of the triples correction. The similar magnitudes of the triples and quadruples corrections indicate that a pentuples correction may be significant. The increased contribution from the high-level correction, $\Delta E_{\mathrm{CCSDT(Q)}}$, relative to the $\Delta E_{\mathrm{CCSDT}}$ correction suggests that this possible effect may be greater for the nitrogen-oxygen bond energies.

The agreement between the experimental and theoretical dissociation energies for nitric acid is similar to the HOONO results. When studying an exotic species such as HOONO, a very throughly studied isomer such as nitric

acid[m] provides a tempting molecule for calibration of the theoretical methods. However, it is difficult to make a strict comparison of D_0 for $HONO_2 \rightarrow OH + NO_2$ to either D_0 for $HOONO \rightarrow OH + NO_2$ or D_0 for $HOONO \rightarrow HO_2 + NO$. In the former case, the discrepancy is in the nature of the bond that is broken, an oxygen-nitrogen bond vs. an oxygen-oxygen bond. And in the latter the dissociation products differ, $OH + NO_2$ vs. $HO_2 + NO$. The much smaller magnitude of the $\Delta E_{\mathrm{CCSDT(Q)}}$ contribution to the nitric acid dissociation energy relative to the $\Delta E_{\mathrm{CCSDT}}$ contribution does indicate that the theoretical value is essentially converged in terms of high-level correlation. In this respect the nitric acid dissociation energy may not be strictly comparable to either the nitrogen-oxygen or oxygen-oxygen bond energies of HOONO.

One might wonder why the additional corrections are necessary when, in the case of HOONO, the E^{∞}_{HF}, $\Delta E^{\infty}_{\mathrm{CCSD(T)}}$ and ΔE_{ZPE} contributions alone produce a D_0 which agrees with the experimental value.[104n] It was shown above that the additional corrections can indicate when the theoretical methods have likely converged, as in the case of the $HONO_2$ dissociation energy, and when the

[m]Many studies have examined various aspects of the photodissociation of nitric acid to OH and NO_2, but the often cited dissociation energy[101] is dependent on the heat of formation of nitric acid[102] and the heats of formation of the fragments.[102,103] Revised heats of formation are available for OH and NO_2.[54] In the calculation of relative energies, it can be risky to replace the heats of formation for some, but not all, interrelated species.[102] However, as the heat of formation for OH used in ref. 101 was from a different data set[103] than that used for the nitrogen-containing species,[102] it may be safe to use the revised value for $\Delta H^{\circ}_{\mathrm{f,0K}}(\mathrm{OH})$ in calculating $D_0^{exp}(\mathrm{HONO_2})$. It is interesting to note that this calculation of $D_0^{exp}(\mathrm{HONO_2})$ best agrees with the theoretical prediction, see the final entry for $HONO_2$ in Table 2.2.

[n]Ref. 104 also included a correction for the scalar relativistic effects.

results might be improved through the application of higher levels of theory, as in the case of the HOONO dissociation energy. And, in the following section, it will be shown that these contributions can become important. It is necessary to demonstrate the unimportance of further corrections lest the agreement with experiment be coincidental.

2.4.2 HOOO

The loss of electrons with the loss of a nitrogen atom in moving from the HOONO system to the HOOO system, as well as the plane of symmetry present in both *trans* and *cis* isomers, allows for the use of larger basis sets in the calculation of the high-level correlation contributions: $\Delta E_{\mathrm{CCSDT}}$ and $\Delta E_{\mathrm{CCSDT(Q)}}$. The long, very weak central oxygen-oxygen bond of HOOO requires a more thorough description of the electron correlation than the HOONO system. The use of a basis set beyond the smaller cc-pVDZ basis set allows for more flexibility in that description.[94] The calculation of the HOOO energy only differed from the HEAT model in the use of the larger cc-pVTZ basis set in the determination the $\Delta E_{\mathrm{CCSDT(Q)}}$ contribution and in the use of an ANO basis set for the zero-point correction. Comparison of experimental vibrational energies and those calculated at the CCSD(T)/ANO1 level of theory are not as encouraging as the HOONO results, but the fault does not seem to lie in the choice of basis set (see chapter 3). The effects of the vibrational problem on the theoretical dissociation energy of HOOO will be discussed near the end of this section.

Previous theoretical studies of the HOOO system have occasionally found the *cis* conformation to be the most stable species rather than the *trans*.[33,105,106] However, *cis*-HOOO has not yet been observed[o] while *trans*-HOOO has been detected under jet-cooled conditions in infrared action[41,107,108] and Fourier-transform microwave[40] spectroscopy experiments. In this work, it is the inclusion of the correction to account for quadruple excitations that reverses the relatives stabilities of the conformers, with the equilibrium geometry of *trans*-HOOO becoming the global minimum on the HO_3 potential energy surface. In other recent theoretical studies that have found the *trans* isomer to be the minimum energy structure, multi-reference methods were used.[28,40,p] The multi-reference methods better accounted for nondynamical electron correlation. The single-reference methods used in refs. 33,105,106 were insufficient as these methods did not account for high-level correlation beyond a perturbative treatment of triple excitations. The following discussion of HOOO dissociation will focus on the *trans* isomer as it is the most stable conformer and the only observed species.

The theoretical dissociation energy of the *trans*-HOOO radical presented in Table 2.4, $D_0 = 2.5$ kcal mol^{-1}, is approximately 3 kcal mol^{-1} below the value inferred from the infrared action experiment, $D_0^{exp} = 5.31$ kcal mol^{-1}.[42] Such disagreement is unexpected as the experimental approach and

[o]Broad features in the infrared action spectra of HOOO have been assigned to *cis*-HOOO,[41] but due to the lack of rotational structure this assignment cannot be confirmed.

[p]Another recent study finding *trans*-HOOO to be the global minimum fit an analytic potential surface to energies determined using a hybrid density functional.[44]

the theoretical methods are very similar to those applied to the dissociation of HOONO and the agreement of the two determinations was demonstrated in the previous section. However, there are a few challenging aspects associated the HOOO system which should be addressed.

The first issue is the presumed multi-reference character and the proposed inability of single-reference methods to properly treat the HOOO radical. The second, related issue is the rather large contribution of the quadruple excitations to the calculated bond energy of *trans*-HOOO, $\Delta E_{\mathrm{CCSDT(Q)}} = 1.39$ kcal mol^{-1}.[q] To address these potential problems, our thermochemical model was also applied to the isoelectronic radical FOO, which would presumably present similar difficulties concerning the electronic structure. The contribution of perturbative triples to the total atomization energy, %TAE[(T)], and the largest T_2 amplitude have proven useful as diagnostics of the multi-reference character of, or the effect of nondynamical correlation on, a species.[109] The high %TAE[(T)] values for *trans*-HOOO and FOO, 8% and 16% respectively, as well as the largest T_2 amplitudes, 0.06 and 0.16, suggest that these systems must be treated with care and highly correlated methods. While FOO appears to be the more troublesome of the two radicals with a %TAE[(T)] twice that of *trans*-HOOO, as well as the larger T_2 amplitude, the calculated energy for

[q]The perturbative treatment of quadruple excitations tends to overestimate the quadruples contribution to calculated energies. To estimate the effect of a full treatment of quadruple excitations, the difference the in the CCSDTQ and CCSDT(Q) frozen core energies calculated with the cc-pVDZ basis set was added to the quadruples correction calculated with CCSDT(Q) and the cc-pVTZ basis set. The resulting bond energies are D_0(*trans*-HOOO) = 2.13 kcal mol^{-1} and D_0(FOO) = 12.0 kcal mol^{-1}.

dissociation to F + O_2 is in quite good agreement with the experimental value (see Table 2.4 and ref. 110). This would seem to indicate that our treatment of correlation is sufficient for these systems. In a study of hydrogen polyoxides, Denis and Ornellas[45] dealt with the issue of higher-order correlation in *trans*-HOOO through the use of an isodesmic reaction,[r] which tends to cancel such effects[56]. Based on their calculated heat of formation for *trans*-HOOO, $\Delta H^{\circ}_{\mathrm{f,298K}} = 5.46$ kcal mol^{-1},[s] the radical is approximately 3 kcal mol^{-1} less stable than indicated by the value derived from experimental data, $\Delta H^{\circ}_{\mathrm{f,298K}} \geq 2.51$ kcal mol^{-1}, a disagreement between theory and experiment which is comparable to that seen here.

Another issue encountered in the HOOO system (alluded to above) is one not seen in the triatomic FOO system. It has been noted in chapter 3 and ref. 94 that, due to a very low frequency torsional mode, second-order vibrational perturbation theory, VPT2,[111] may not be appropriate for the prediction of fundamental vibrational modes for the HOOO radical. As VPT2 was used in the current calculation of zero-point energies, the ΔE_{ZPE} contribution is a possible source of error in the determination of the dissociation energy, but it is not expected to be large enough to explain the difference between theory and experiment. Fundamental vibrational frequencies for *trans*-HOOO have been inferred from observed combination bands.[108] These vibrational energies,[t] ν_i,

[r] A reaction in which bond types are preserved, e.g. HOO + FOO → HOOO + FO.

[s] Combined with $\Delta H^{\circ}_{\mathrm{f,298K}}(\mathrm{OH}) = 8.93$ kcal mol^{-1}of ref. 54, this corresponds to a bond energy of of 3.47 kcal mol^{-1}at 298 K compared to an estimated experimental bond energy of 6.42 kcal mol^{-1}at 298 K.

[t] A combination band involving the terminal OO stretch, ν_2, was not observed so the

and those of the OH and O_2 fragments[u] were used with the harmonic formula, $E_{\mathrm{ZPE}} = \frac{1}{2}\sum \nu_i$, to estimate the zero-point correction to the dissociation energy yielding $\Delta E_{\mathrm{ZPE}} = -2.33$ kcal mol^{-1}. The difference between this and our VPT2 determination of the same correction, $\Delta E_{\mathrm{ZPE}} = -2.74$ kcal mol^{-1}, allows us to predict the error in our calculated D_0 introduced by the use of VPT2 zero-point energies — the result is less than 0.5 kcal mol^{-1}. The effects due to this error in the zero-point vibrational energy as well as residual correlation (discussed above) may not be negligible, but they cannot account for the nearly 3 kcal mol^{-1} discrepancy currently seen when comparing the theoretical determination of the bond energy for *trans*-HOOO and the value inferred from the infrared action experiment. The experimental determinations of the binding energies of HOOO, as well as HOONO, will be discussed below.

2.4.3 Experimental Determinations

There are two experimentally determined values for the dissociation energy of *trans,perp*-HOONO presented in Table 2.2. Both values are derived from the same experiment through two different methods of analysis. In the infrared action spectroscopy experiments, an OH fundamental or overtone stretch is excited. The energy of the vibrational excitation is sufficient to break the weak oxygen-oxygen bond in HOONO or HOOO. Following dissociation,

theoretical value of 1331 cm^{-1} was used for ν_2.

[u]Values of 3568 cm^{-1} and 1556 cm^{-1} were used for the vibrational energies of the OH and O_2 fragments respectively.

the populations of the rotational energy levels of the OH fragment are determined through laser-induced fluorescence. With knowledge of the the initial excitation energy and the maximum rotational energy of the OH fragment, an upper bound to the oxygen-oxygen bond energy can be determined through a straightforward consideration of energy conservation.[v] Or, the populations of the OH rotational levels may be used in conjuction with a statistical model to estimate the bond energy.[98,107] In the case of *trans,perp*-HOONO, these two analyses agree very well. The statistical model yielded D_0^{exp}(*tp*-HOONO) = 16.2 ± 0.1 kcal mol^{-1}. The upper bound from the energy balance equation and the maximum OH rotational energy is 16.1 kcal mol^{-1}.[98] These values also agreed well with our theoretical determination.

Statistical analysis of the populated OH rotational levels following dissociation of *trans*-HOOO due to excitation of the OH fundamental stretch indicated that the bond energy is 7.20 ± 0.11 kcal mol^{-1}.[107] A value of 6.76 ± 0.16 kcal mol^{-1} was obtained for dissociation due to excitation of the OH overtone. These contradictory values also are inconsistent with the upper bound, D_0^{exp}(*tr*-HOOO) ≤ 6.12 kcal mol^{-1}, determined from the energy balance equation and the maximum observed rotational energy of the OH fragment following dissociation due to excitation of the OH overtone. The experiment was repeated with the deuterated species yielding D_0^{exp}(*tr*-DOOO) ≤ 5.31 kcal mol^{-1}.[42] The dissociation energies of *trans*-HOOO and DOOO differ only in the effect of the zero-point energies, with the dissociation energy of DOOO likely being the

[v]See refs. 98,107 for the full energy balance equation.

larger to the two values. The smaller rotational energies of the OD fragment provide a more precise measurement of the excess energy following dissociation. Based on the *trans*-DOOO dissociation energy, the *trans*-HOOO value was revised: D_0^{exp}(*tr*-HOOO) $\leq$ 5.3 kcal mol^{-1}.[46] In a recent study of the OH + O_2 reaction at low temperatures, equilibrium constants for the process were determined and D_0^{exp} was extracted. The new value is $D_0^{exp} = 2.96 \pm 0.07$ kcal mol^{-1}.[97] Discussion of the dissociation energy of *trans*-HOOO will continue in chapter 4, but first, chapter 3 contains an examination of the anharmonic force fields of HOOO and HOONO.

Table 2.1: The HEAT thermochemical model and the differences in the approaches used for the HNO_3 and HO_3 systems.

	HEAT[a]	HNO_3	HO_3
geometry	CCSD(T)[b]	✓	✓
	cc-pVQZ	✓	✓
E^{∞}_{HF}	HF-SCF	✓	✓
	aug-cc-pCVXZ [X = T,Q,5]	✓	✓
$\Delta E^{\infty}_{\mathrm{CCSD(T)}}$	CCSD(T) - HF-SCF	✓	✓
	aug-cc-pCVXZ [X = Q,5]	✓	✓
$\Delta E_{\mathrm{CCSDT}}$	CCSDT (fc) - CCSD(T) (fc)[c]	✓	✓
	cc-pVXZ [X = T,Q]	❖	✓
$\Delta E_{\mathrm{CCSDT(Q)}}$	CCSDTQ (fc) - CCSDT (fc)	★	★
	cc-pVDZ	✓	✶
ΔE_{SO}	CI	✓	✓
	cc-pVDZ with RECP	✓	✓
ΔE_{rel}	CCSD(T)	✓	✓
	aug-cc-pCVTZ	✓	✓
ΔE_{DBOC}	HF-SCF	✓	✓
	aug-cc-pVTZ	✓	✓
ΔE_{SO}	CI	✓	✓
	cc-pVDZ	✓	✓
ΔE_{ZPE}	CCSD(T)	❇	❇
	cc-pVQZ	✣	✣

[a] A more complete description of the methods and basis sets can be found section 2.2.1. [b] All electrons correlated. [c] Core electrons excluded from correlation treatment. ✓ Same as HEAT.

❖ cc-pVXZ [X = D,T] ★ CCSDT(Q) (fc) - CCSDT (fc) ✶ cc-pVTZ ❇ CCSD(T) (fc) ✣ ANO1

Table 2.2: Contributions to D_0 for dissociation of HOONO (both *trans,perp* and *cis,cis* isomers) and $HONO_2$ to OH + NO_2.

	tp-HOONO[a]	*cc*-HOONO[a]	$HONO_2$[a]
E_{HF}^{∞}	-17.09	-17.02	18.23
$\Delta E_{CCSD(T)}^{\infty}$	36.70	40.20	35.84
ΔE_{CCSDT}	-0.36	-0.47	-0.68
$\Delta E_{CCSDT(Q)}$	0.22	0.43	0.01
ΔE_{rel}	0.06	0.06	-0.20
ΔE_{DBOC}	0.07	0.08	0.10
ΔE_{SO}[b]	-0.19	-0.19	-0.19
ΔE_{ZPE}	-3.55	-3.92	-5.77
D_0	15.9	19.2	47.3
D_0^{exp}	16.2[c]	19.9[d]	47.8[e]
D_0^{exp}	$\leq$16.1[f]		47.6[g]
D_0^{exp}			47.4[h]

[a] All energies are in kcal mol^{-1}. [b] Value for OH from Ref. 64. [c] Ref. 98: error bar $\pm$ 0.1 kcal mol^{-1}. [d] Ref. 112: error bar $\pm$ 0.5 kcal mol^{-1}. [e] Ref. 101. [f] Ref. 98. [g] Ref. 102: $\Delta H_{f,0K}^{\circ}(HONO_2)$; Ref. 54: $\Delta H_{f,0K}^{\circ}$(OH) and $\Delta H_{f,0K}^{\circ}(NO_2)$. [h] Ref. 102: $\Delta H_{f,0K}^{\circ}(HONO_2)$ and $\Delta H_{f,0K}^{\circ}(NO_2)$; Ref. 54: $\Delta H_{f,0K}^{\circ}$(OH).

Table 2.3: Contributions to D_0 for dissociation of HOONO (both *trans,perp* and *cis,cis* isomers) to HO_2 + NO.

	tp-HOONO[a]	*cc*-HOONO[a]
E_{HF}^{∞}	-19.25	-19.18
$\Delta E_{CCSD(T)}^{\infty}$	45.42	48.92
ΔE_{CCSDT}	-0.71	-0.82
$\Delta E_{CCSDT(Q)}$	0.79	1.00
ΔE_{rel}	-0.03	-0.04
ΔE_{DBOC}	0.06	0.08
ΔE_{SO}[b]	-0.17	-0.17
ΔE_{ZPE}	-2.75	-3.12
D_0	23.4	26.7
D_0^{exp}	23.8[c,d]	27.5[c,e]

[a] All energies are in kcal mol^{-1}. [b] Value for NO from ref. 64. [c] Ref. 54: $\Delta H_{f,0K}^{\circ}$ for HO_2, NO, OH and NO_2. [d] Ref. 98: D_0^{exp}(*tp*-HOONO); [e] Ref. 112: D_0^{exp}(*cc*-HOONO).

Table 2.4: Contributions to D_0 for dissociation of HOOO (both *trans* and *cis* isomers) to OH + O_2, as well as dissociation of FOO to F + O_2.

	trans-HOOO[a]	*cis*-HOOO[a,b]	FOO[a]
E_{HF}^{∞}	-50.75	-48.13	-62.05
$\Delta E_{\mathrm{CCSD(T)}}^{\infty}$	54.39	51.94	73.54
$\Delta E_{\mathrm{CCSDT}}$	0.34	0.27	0.37
$\Delta E_{\mathrm{CCSDT(Q)}}$	1.39	1.14	2.13
ΔE_{rel}	-0.01	-0.01	0.00
ΔE_{DBOC}[c]	0.03	0.04	-0.03
ΔE_{SO}[d]	-0.19	-0.19	-0.37
ΔE_{ZPE}	-2.74	-3.00	-1.30
D_0	2.47	2.06	12.3
D_0^{exp}	$\leq$5.31[e]		11.9[f]
D_0^{exp}	2.96[g]		

[a] All energies are in kcal mol^{-1}. [b] No D_0^{exp} available. [c] Values for O_2, OH and F from ref. 64. [d] DBOC corrections were calculated at the CCSD/aug-cc-pVTZ level but did not have a significant effect for these systems. [e] Ref. 42. [f] Ref. 110: error bar ± 0.24 kcal mol^{-1}. [g] Ref. 97: error bar ± 0.07 kcal mol^{-1}.

Chapter 3

Spectroscopic Features and Constants

The vibrational energy levels of HOONO and HOOO were calculated to aid the identification of the species. Vibrational corrections to the rotational constants were calculated to aid the determination of the molecular structure.

3.1 Introduction

3.1.1 Spectroscopy of HOONO and HOOO

The vibrational spectroscopy techniques of matrix-isolation and infrared action[a] have played a critical role in establishing the existence and expanding the knowledge of the weakly bound HOONO and HOOO species. While studies of nitric acid formation in the reaction of OH with NO_2 suggested an alternate HOONO product,[3,113] some time passed before the species was observed, first in solid argon[50] and nearly a decade later in the gas phase.[7] For HOOO, the first vibrational spectrum was recorded in an argon matrix as well,[114] long after it was first proposed as a stable species.[49] Through deposition in solid argon these elusive species can be isolated, but band positions can be perturbed by the surroundings causing matrix shifts and interfering

[a]Discussion of this experimental technique is included in sections 2.4.3 and 4.4.2.

bands can appear due to other species deposited in addition to the species of interest.[115]

Both the HOONO[7–9,116] and HOOO[41,42,107,108] systems have been studied through infrared action spectroscopy. This IR pump-UV probe technique allows for the detection of species that, due to low yields or the intrusion of more strongly absorbing species, may be otherwise unobservable.[8] With vibrational excitation, a molecule may absorb sufficient energy for cleavage of a weak bond. By monitoring production of fragments through laser-induced fluorescence as a function of infrared excitation energy, the vibrational bands can be identified. Since only transitions to vibrational levels above the dissociation threshold can be detected with this approach, the infrared action experiments commonly examine the region of the overtone (multiple quanta of excitation in one vibrational mode) and combination band (multiple quanta of excitation in multiple vibrational modes), rather than the fundamental (one quanta of excitation) modes. By selectively detecting only weakly bound species, with the limitation that only vibrational bands above the dissociation limit can be observed, the infrared action approach is complementary to the matrix-isolation technique. Confining the weakly bound species in a solid matrix prevents dissociation and the infrared absorption spectrum can be probed directly. With this technique, the observable vibrational modes are not limited to those above the dissociation threshold. However, as stated above, interfering species and matrix shifts may complicate the spectra obtained through matrix-isolation.

Experimental structural parameters, obtained for *trans*-HOOO[40] and

cis,cis-HOONO[117] from rotational spectroscopy and for *trans,perp*-HOONO[98] from rotationally resolved vibrational spectroscopy, may be compared to equilibrium structures provided the appropriate vibrational corrections can be calculated. Isotopic substitution is necessary for the determination of experimental structures for molecules with more than two independent structural parameters. In addition, isotopic substitution shifts vibrational frequencies in a calculable manner providing a means of confirming the assignments of experimental spectra. The *cis,cis* conformer of deuterated peroxynitrous acid, DOONO, has been studied with rotational[117] and vibrational[20,100] spectroscopy. Rotational[40] and vibrational spectroscopy[114] have been used to study the deuterated trioxy species, DOOO.

3.1.2 Second-Order Vibrational Perturbation Theory - VPT2

For the accuracy required to aid assignment of spectra obtained through matrix-isolation, for the prediction of overtone and combination bands commonly observed through infrared action spectroscopy and for the comparison of theoretical equilibrium structures to experimentally-determined, vibrationally-averaged structures, the typical harmonic oscillator description of the molecular vibrational modes is insufficient. To explain the shortcomings of this approach and introduce the subject of this section's heading, the initial model must first be described.

Beginning with expressions for the kinetic $[T]$ and potential $[V]$ energy

as a function of displacement, T is given by[118]

$$T = \tfrac{1}{2}\sum_{i=1}^{3n} m_i \dot{x}_i^2 \tag{3.1}$$

Here half the product of the mass $[m_i]$ of one of n atoms and the square of the derivative of its displacement $[x_i]$ from equilibrium (given by the minimum of $V(x_i)$) along one of the three Cartesian coordinates gives one component of the kinetic energy of the atom. The sum of the products over the three Cartesian coordinates and n atoms, $3n$, gives twice the total kinetic energy. Or, after defining a new mass weighted coordinate $X_i = m_i^{1/2} x_i$

$$T = \tfrac{1}{2}\sum_{i=1}^{3n} \dot{X}_i^2 \tag{3.2}$$

The analytic functional form of V is not known, but by assuming the deviations from equilibrium are small, the function can conveniently be written as a Taylor series in the above displacement coordinates.

$$V = (V)_0 + \sum_i \left(\frac{\partial V}{\partial X_i}\right)_0 X_i + \tfrac{1}{2}\sum_{i,j}\left(\frac{\partial^2 V}{\partial X_i \partial X_j}\right)_0 X_i X_j + \cdots \tag{3.3}$$

As the partial derivative of the potential energy with respect to displacement will be zero at equilibrium and the constant term is uninteresting (or set to zero), and assuming that the higher terms are unimportant (an assumption that will be addressed below), the above function is approximated by

$$V^{(0)} = \tfrac{1}{2}\sum_{i,j}^{3n} f_{ij} X_i X_j \tag{3.4}$$

where f_{ij} is the partial derivative of V with respect to coordinates X_i and X_j. Choosing a set of coordinates $[Q_i]$, termed normal coordinates, for which

$\partial^2 V/\partial Q_i \partial Q_j$ is zero when $i \neq j$ the problem is reduced to a set of $3n-6$[b] independent harmonic oscillators.

$$V^{(0)} = \tfrac{1}{2} \sum_{i}^{3n-6} \lambda_i Q_i^2 \tag{3.5}$$

where λ_k is the second derivative of V with respect to the mass weighted normal coordinate Q_i. If the momentum associated with the mass weighted normal coordinate is given by the time derivative of the coordinate, $P_i = \dot{Q}_i$, T becomes

$$T = \tfrac{1}{2} \sum_{i=1}^{3n-6} P_i^2 \tag{3.6}$$

With classical expressions for T and V of equations 3.5 and 3.6, the quantum mechanical operator for the harmonic oscillator $[\hat{H}^{(0)}]$, is written as[118]

$$\hat{H}^{(0)} = \hat{T} + \hat{V}^{(0)} \tag{3.7a}$$

$$= \tfrac{1}{2} \sum_{i=1}^{3n-6} \left(\hat{P}^2 + \lambda_i \hat{Q}_i^2 \right) \tag{3.7b}$$

$$= \tfrac{1}{2} \sum_{i=1}^{3n-6} \left(\frac{-\hbar^2 \partial^2}{\partial Q_i^2} + \lambda_i Q_i^2 \right) \tag{3.7c}$$

The above Hamiltonian can be rewritten in yet another set of coordinates, this time *dimensionless* normal coordinates, given by $q_i = \gamma_i^{1/2} Q_i$ and $p_i = P_i/\gamma_i^{1/2}\hbar$

[b]The force constants associated with translation or rotation of the molecule along each of the three axes will be zero. For linear molecules, the number of independent coordinates, or vibrational degrees of freedom, is $3n-5$. Below it will be assumed that the system is nonlinear.

where $\gamma_i = \lambda_i^{1/2}/\hbar = 2\pi c\omega_i/\hbar$ and ω_i is the harmonic frequency (in wavenumbers [cm^{-1}]) of the ith normal mode, *i.e.* along the normal coordinate q_i. Divided by hc to produce energies that are in wavenumbers and written in terms of dimensionless normal coordinates, the harmonic oscillator Hamiltonian is[111]

$$\hat{H}^{(0)} = \tfrac{1}{2}\sum_{i=1}^{3n-6} \omega_i(\hat{p}_i^2 + \hat{q}_i^2) \tag{3.8a}$$

$$= \tfrac{1}{2}\sum_{i=1}^{3n-6} \omega_i \left(\frac{-\partial^2}{\partial q_i^2} + q_i^2\right) \tag{3.8b}$$

Because our Hamiltonian can be written as the sum of $3n-6$ separable operators, the vibrational eigenfunctions [Ψ] may be written as the product of $3n-6$ independent functions of q_i [$\psi_{\upsilon_i}(q_i)$].[118]

$$\begin{aligned}\Psi(q_1, q_2 \ldots q_{3n-6}) &= \prod_i^{3n-6} \psi_{\upsilon_i}(q_i) \\ &= \psi_{\upsilon_1}(q_1)\psi_{\upsilon_2}(q_2)\ldots\psi_{\upsilon_{3n-6}}(q_{3n-6})\end{aligned} \tag{3.9}$$

where υ_i is the principle quantum number of mode i. The set of $3n-6$ eigenvalue equations

$$-\frac{d^2\psi_{\upsilon_i}}{dq_i^2} + q_i^2\psi_{\upsilon_i} = \frac{2E_{\upsilon_i}^{(0)}}{\omega_i}\psi_{\upsilon_i} \tag{3.10}$$

yield energies of the form

$$E_{\upsilon_i}^{(0)} = \omega_i(\upsilon_i + \tfrac{1}{2}) \tag{3.11}$$

where both ω_i and $E_{\upsilon_i}^{(0)}$ are in units of wavenumbers.

The energy of a transition from one harmonic vibrational state (given by equation 3.11) to another can be predicted, using equation 3.12.

$$\Delta E^{(0)}_{\upsilon_i'' \rightarrow \upsilon_i'} = \omega_i(\Delta \upsilon_i) \tag{3.12}$$

where υ_i'' is the quantum number of mode i in the initial vibrational state and υ_i' is the quantum number of mode i in the final vibrational state. Within this model, the vibrational levels are evenly spaced and the energy of a multi-quantum transition, such as the first overtone of mode i, is the product of the change in quantum number, $\Delta\upsilon_i = 2$, and the harmonic frequency of the ith normal mode, $\Delta E^{(0)}_{0\rightarrow 2} = 2\omega_i$. Combination bands, multi-quantum transitions with excitation in more than one mode, are simply the sum of the contributions from each mode. This results from the separable Hamiltonian of equation 3.8b.

In reality, the potential energy does not approach infinity as a bond is stretched as the quadratic potential assumed in equation 3.4 would indicate and the observed transition energies deviate significantly from the harmonic predictions. For example, the harmonic frequency of the OH stretching mode [ω_1] in nitric acid is 3746[c] cm^{-1}, which would result in a predicted transition energy for the first overtone of 7492 cm^{-1} — the true transition energies for $\Delta\upsilon_1 = 1$ and $\Delta\upsilon_1 = 2$ are 3551 cm^{-1} and approximately 6940 cm^{-1}.[119] The fundamental transition energy, $\Delta E_{0\rightarrow 1}$ or ν_1, is lower than predicted due to deviation of the true potential from the harmonic model, *i.e.* anharmonicity, and the frequency of the first overtone is not twice the harmonic frequency. The

[c]Calculated at the CCSD(T)/ANO2 (fc) level, see appendix B.

combination band of the OH and the asymmetric NO_2 stretching frequencies, $\omega_2 = 1763^{c}$ cm^{-1} compared to $\nu_2 = 1710$ cm^{-1},[120] has a theoretical value of 5509 cm^{-1} — the experimentally observed band is at 5254 cm^{-1}.[99]

The energies of multi-quantum transitions can be predicted (though not accurately) using the harmonic approximation, but these transitions are not theoretically allowed within the model. This can be demonstrated by calculating the absorption intensity for single-quantum and multi-quantum transitions. The absorption intensity is proportional to the square of the vibrational transition dipole moment [$\mathbf{P}$], which is given by[118]

$$\boldsymbol{P}_{m0} = \langle \Psi_m | \boldsymbol{\mu} | \Psi_0 \rangle \tag{3.13}$$

where Ψ_0 is the reference and Ψ_m is the excited vibrational wavefunction as defined in equation 3.9. The dipole moment [$\boldsymbol{\mu}$] can be expanded about the equilibrium as was the potential energy function in equation 3.3.

$$\begin{aligned} \boldsymbol{\mu} &= (\boldsymbol{\mu})_0 + \sum_i \left(\frac{\partial \boldsymbol{\mu}}{\partial q_i} \right)_0 q_i + \tfrac{1}{2} \sum_{ij} \left(\frac{\partial^2 \boldsymbol{\mu}}{\partial q_i \partial q_j} \right)_0 q_i q_j + \cdots \\ &= \boldsymbol{\mu}^{(0)} + \sum_i \boldsymbol{\mu}_i^{(1)} q_i + \tfrac{1}{2} \sum_{ij} \boldsymbol{\mu}_{ij}^{(2)} q_i q_j + \cdots \end{aligned} \tag{3.14}$$

Truncation of $\boldsymbol{\mu}$ after the second term yields

$$\boldsymbol{P}_{m0}^{(0)} = \boldsymbol{\mu}^{(0)} \langle \Psi_m | \Psi_0 \rangle + \sum_i \boldsymbol{\mu}_i^{(1)} \langle \Psi_m | q_i | \Psi_0 \rangle \tag{3.15}$$

where due to the orthogonal functions of $\Psi = \psi_{\upsilon_1} \psi_{\upsilon_2} \psi_{\upsilon_3} \ldots \psi_{\upsilon_{3n-6}}$, the first term of equation 3.15, dependent on the static dipole at equilibrium [$(\boldsymbol{\mu})_0$ or $\boldsymbol{\mu}^{(0)}$] does not contribute to the transition dipole as $\langle \Psi_m | \Psi_0 \rangle$ yields zero unless

$m = 0$ (meaning no transition occurs) and all matrix elements of $\langle \Psi_m | q_i | \Psi_0 \rangle$ are zero except $\langle \psi_{\upsilon'_k} | q_i | \psi_{\upsilon''_k} \rangle$ where $\upsilon'_k = \upsilon''_k \pm 1$. As a result, only single-quantum transitions result in a nonzero absorbance within the harmonic approximation and the linear dipole approximation.

One way to acknowledge the interaction of the molecular vibrations is to move beyond the harmonic approximation by retaining additional terms in the Taylor series expansion of the potential energy (and the dipole moment) function(s). The Taylor expansion of V from equation 3.3 rewritten in dimensionless normal coordinates is given in wavenumbers by[111]

$$\begin{aligned} V &= \tfrac{1}{2} \sum_i \frac{\partial^2 V}{\partial q_i^2} q_i^2 + \tfrac{1}{6} \sum_{ijk} \frac{\partial^3 V}{\partial q_i \partial q_j \partial q_k} q_i q_j q_k + \tfrac{1}{24} \sum_{ijkl} \frac{\partial^4 V}{\partial q_i \partial q_j \partial q_k \partial q_l} q_i q_j q_k q_l + \cdots \\ &= \tfrac{1}{2} \sum_i \omega_i q_i^2 + \tfrac{1}{6} \sum_{ijk} \phi_{ijk} q_i q_j q_k + \tfrac{1}{24} \sum_{ijkl} \phi_{ijkl} q_i q_j q_k q_l + \cdots \end{aligned} \tag{3.16}$$

The first, second and third terms are dependent on the quadratic, cubic and quartic force constants [ω_i, ϕ_{ijk} and $\phi_{ijkl} \ldots$] (the second, third and fourth partial derivatives with respect to the dimensionless normal coordinates), respectively.

Perturbation theory[121] provides a method for sorting and calculating corrections to a zeroth order model. The potential energy function V is written as[118]

$$V = V^{(0)} + \lambda V^{(1)} + \lambda^2 V^{(2)} + \cdots \tag{3.17}$$

where the zeroth order model [$V^{(0)}$] and corrections are taken from equation

3.16 as follows[d]

$$V^{(0)} = \tfrac{1}{2}\sum_i \omega_i q_i^2 \tag{3.18a}$$

$$V^{(1)} = \tfrac{1}{6}\sum_{ijk} \phi_{ijk} q_i q_j q_k \tag{3.18b}$$

$$V^{(2)} = \tfrac{1}{24}\sum_{ijkl} \phi_{ijkl} q_i q_j q_k q_l \tag{3.18c}$$

When the parameter λ is equal to zero, the potential as described in equation 3.17 becomes the zeroth order model of equation 3.18a, the harmonic oscillator. When the corrections to the zeroth order model are small the expansion of equation 3.17 converges rapidly.[121] The vibrational energy may be similarly expanded.

$$E = E^{(0)} + \lambda E^{(1)} + \lambda^2 E^{(2)} + \cdots \tag{3.19}$$

As the zeroth order model is the harmonic oscillator, $E^{(0)}$ is known.

$$E^{(0)} = \omega_i(\upsilon_i + \tfrac{1}{2}) \tag{3.20a}$$

The first order correction to the energy is the expectation value of the first order operator acting on the zeroth order wavefunction.[121]

$$E^{(1)} = \langle \Psi | V^{(1)} | \Psi \rangle \tag{3.20b}$$

Here the average effect of the first order operator $V^{(1)}$ (the cubic potential term from equation 3.18b) on the zeroth order wavefunction Ψ (which is the

[d]The sums of equations 3.18b and 3.18c are restricted as above, here and in the following discussion.

product of $3n-6$ orthogonal harmonic oscillator functions) is given by[118]

$$E^{(1)} = \tfrac{1}{6}\sum_{ijk}\phi_{ijk}\langle\psi_{v_1}\psi_{v_2}\psi_{v_3}\ldots\psi_{v_{3n-6}}|q_iq_jq_k|\psi_{v_1}\psi_{v_2}\psi_{v_3}\ldots\psi_{v_{3n-6}}\rangle$$

For $i \neq j \neq k$, equation 3.20b becomes[e]

$$E^{(1)} = \tfrac{1}{6}\sum_{ijk}\phi_{ijk}\langle\psi_{v_i}|q_i|\psi_{v_i}\rangle\langle\psi_{v_j}|q_j|\psi_{v_j}\rangle\langle\psi_{v_k}|q_k|\psi_{v_k}\rangle$$

where the odd functions of each matrix element integrate to zero.

For $i \neq j = k$

$$E^{(1)} = \tfrac{1}{6}\sum_{ij}\phi_{ijj}\langle\psi_{v_i}|q_i|\psi_{v_i}\rangle\langle\psi_{v_j}|q_j^2|\psi_{v_j}\rangle$$

where again, $\langle\psi_{v_i}|q_i|\psi_{v_i}\rangle$ integrates to zero, so the whole term will be zero.

And finally, $i = j = k$

$$E^{(1)} = \tfrac{1}{6}\sum_{i}\phi_{iii}\langle\psi_{v_i}|q_i^3|\psi_{v_i}\rangle$$

is an odd function which will integrate to zero. The first order correction to the vibrational energy therefore vanishes.

The second order correction to the energy $E^{(2)}$ includes contributions from the second order operator $V^{(2)}$ acting on the zeroth order wavefunction Ψ_m and the interaction of the first order operator $V^{(1)}$ with the zeroth order and an excited vibrational wavefunction Ψ_n. Here Ψ_m and Ψ_n are the wavefunctions that correspond to the zeroth order energies $E_m^{(0)}$ and $E_n^{(0)}$.[118]

$$E^{(2)} = \langle\Psi_m|V^{(2)}|\Psi_m\rangle + \sum_{m\neq n}\frac{\langle\Psi_m|V^{(1)}|\Psi_n\rangle\langle\Psi_n|V^{(1)}|\Psi_m\rangle}{E_m^{(0)} - E_n^{(0)}} \qquad (3.20c)$$

[e]The remaining $3n-9$ basis functions will have no effect on the integral and are neglected.

Elements of the $V^{(2)}$ term from above that are of the form

$$\phi_{iiii}\langle\psi_i|q_i^4|\psi_i\rangle \quad \text{and} \quad \phi_{\mathrm{iijj}}\langle\psi_\mathrm{i}|\mathrm{q_i^2}|\psi_\mathrm{i}\rangle\langle\psi_\mathrm{j}|\mathrm{q_j^2}|\psi_\mathrm{j}\rangle$$

contribute to the second order correction to the energy as

$$\tfrac{3}{2}\sum_i \phi_{iiii}((\upsilon_i+\tfrac{1}{2})^2+\tfrac{1}{4})+\sum_{ij}\phi_{iijj}(\upsilon_i+\tfrac{1}{2})(\upsilon_j+\tfrac{1}{2})$$

Elements of the second term in equation 3.20c containing the force constants ϕ_{ijk}^2, ϕ_{iij}^2, ϕ_{iii}^2, $\phi_{iii}\phi_{ijj}$ and $\phi_{iik}\phi_{jjk}$ contribute to the contribute to the second order correction as well.

In the above discussion, molecular rotation and its interaction with vibrational motion have been ignored. The second order correction to the vibrational energy is of the $\kappa^2\nu$ order of magnitude, where κ is the fourth root of the ratio of the electron mass to a typical nuclear mass, approximately 1/10, and ν is a typical frequency of molecular vibration.[111] At the $\kappa^2\nu$ order of magnitude the coupling of vibrational modes through rotation becomes significant. This coupling is described for normal modes i and j and rotation about axis α by the Coriolis zeta constant $[\zeta_{ij}^{(\alpha)}]$.[122] The expressions for the effective vibrational angular momenta about each of the three principal axes (π_A, π_B and π_C correspond to A, B and C) are given in terms of the $\zeta_{ij}^{(\alpha)}$ constants.

$$\pi_{(\alpha)}=\sum_{ij}\zeta_{ij}^{(\alpha)}q_ip_j\left(\frac{\omega_j}{\omega_i}\right)^{1/2} \tag{3.21}$$

The equilibrium rotational constants [A_e, B_e and C_e, or the "B_e's"] are inversely proportional to the moments of inertia and so may easily be determined

for the equilibrium molecular configuration.

$$B_e^{(\alpha)} = \frac{\hbar^2}{2hcI_e^{(\alpha)}} \tag{3.22}$$

Here the rotational constant about the α axis is $\hbar$ squared divided by twice the moment of inertia about the α axis $[I_{(\alpha)}]$. Dividing by hc yields the value in wavenumbers. The sum over the three principal axes of the product of equilibrium rotational constant and the square of the vibrational angular momentum, *i.e.* $\sum_\alpha B_e^{(\alpha)}\pi_{(\alpha)}^2$, contributes to the vibrational energy at the second order.

Combining the zeroth, first and second order operators discussed above, the second order vibrational perturbation theory [VPT2] operator becomes[111]

$$\begin{aligned}\hat{H}^{\mathrm{VPT2}} = {} & \tfrac{1}{2}\sum_i \omega_i(\hat{p}_i^2 + \hat{q}_i^2) + \tfrac{1}{6}\sum_{ijk}\phi_{ijk}\hat{q}_i\hat{q}_j\hat{q}_k \\ & + \tfrac{1}{24}\sum_{ijkl}\phi_{ijkl}\hat{q}_i\hat{q}_j\hat{q}_k\hat{q}_l + \sum_\alpha B_e^{(\alpha)}\left[\sum_{ij}\zeta_{ij}^{(\alpha)}q_ip_j\left(\frac{\omega_j}{\omega_i}\right)^{1/2}\right]\end{aligned} \tag{3.23}$$

where the summation of the fourth term is over the three principal axes. The resulting energies for a vibrational state υ_i hasthe form[f]

$$E^{\mathrm{VPT2}}(\upsilon_i) = G_0 + \sum_i \omega_i(\upsilon_i + \tfrac{1}{2}) + \sum_{i\geq j} x_{ij}(\upsilon_i + \tfrac{1}{2})(\upsilon_j + \tfrac{1}{2}) + \ldots \tag{3.24}$$

The G_0 term is a constant term that can be neglected in spectroscopic analysis.[64] The largest contribution to the energy of the vibrational state specified

[f]For diatomics, the VPT2 energy, $E^{\mathrm{VPT2}}(\upsilon_i) = G_0 + \omega_i(\upsilon_i + \frac{1}{2}) + x_{ii}(\upsilon_i + \frac{1}{2})^2$, is exact for the Morse oscillator and so provides a very good description of typical stretching potentials.

by the set vibrational quantum numbers υ_i is the sum of the harmonic vibrational energy levels of the second term. The third term, which accounts for the coupling of modes through the anharmonicity constants $[x_{ij}]$ comes from the second order correction to the vibrational energy of equation 3.20c and the angular momentum operator of equation 3.21.[g] The anharmonicity constant x_{ij} for vibrational modes i and j is determined by the harmonic frequencies of all $3n-6$ modes, the cubic force constants for modes i and j and those coupled to mode k, the quartic force constants along one (ϕ_{iiii}) or both normal modes (ϕ_{iijj}) and the Coriolis zeta constants coupling modes i and j. When i is equal to j:

$$x_{ii} = \tfrac{1}{16}\phi_{iiii} - \tfrac{1}{16}\sum_k \phi_{iik}^2 \frac{8\omega_i^2 - 3\omega_k^2}{\omega_j(4\omega_i^2 - \omega_k^2)} \tag{3.25a}$$

When i is not equal to j:

$$\begin{aligned} x_{ij} = \frac{1}{4}\phi_{iijj} - \frac{1}{4}\sum_k \frac{\phi_{iik}\phi_{kjj}}{\omega_k} - \tfrac{1}{2}\sum_k \phi_{ijk}^2 \omega_k \frac{\omega_k^2 - \omega_i^2 - \omega_j^2}{\Delta_{ijk}} \\ + [A_e(\zeta_{i,j}^A)^2 + B_e(\zeta_{i,j}^B)^2 + C_e(\zeta_{i,j}^C)^2]\left(\frac{\omega_i}{\omega_j} + \frac{\omega_j}{\omega_i}\right) \end{aligned} \tag{3.25b}$$

where:

$$\Delta_{ijk} = (\omega_i + \omega_j + \omega_k)(\omega_i - \omega_j - \omega_k)(-\omega_i + \omega_j - \omega_k)(-\omega_i - \omega_j + \omega_k)$$

By calculating second (ω_i), third (*e.g.* ϕ_{ijk}) and select fourth (ϕ_{iiii} and ϕ_{iijj}) derivatives[h] of the molecular energy with respect to displacement along the

[g] As discussed above, the first order correction to the vibrational energy is zero.

[h] The method by which these derivatives are calculated will be discussed in section 3.2.

vibrational modes, the anharmonic vibrational energy levels can be determined and vibrational excitation energies can be predicted for comparison to spectra.

When the vibrational energy is described as independent of rotational excitation (as above), an "effective" rotational Hamiltonian can be defined that is associated with a specific vibrational state (υ).[111]

$$\hat{H}_{\upsilon}^{rot} = A_{\upsilon}\hat{J}_A^2 + B_{\upsilon}\hat{J}_B^2 + C_{\upsilon}\hat{J}_C^2 + \frac{1}{4}\sum_{\alpha,\beta}(\tau'_{\alpha\alpha\beta\beta})_{\upsilon}\hat{J}_{\alpha}^2\hat{J}_{\beta}^2 + \ldots \tag{3.26}$$

The resulting rotational energies are dependent on the effective rotational constants [A_{υ}, B_{υ} and C_{υ}, or the "B_{υ}'s"], which are the rotational constants associated with a specific vibrational state (υ), the components the total rotational angular momentum along the three principal axes [J_A, J_B and J_C] and the certain centrifugal distortion constants. Only those centrifugal distortion constants related to rotation about two principal axes (α and β), through dependence on the moments of inertia ($I^{(\alpha)_e}$ and $I_e^{(\beta)}$) and the $a_i^{(\alpha\beta)}$ constants, are significant at the level considered here. These constants [$(\tau'_{\alpha\alpha\beta\beta})_{\upsilon}$] vary with υ as well. The vibrationally dependent rotational constants, B_{υ}'s, can be related to the rotational constants of the equilibrium structure, B_e's, through

$$B_{\upsilon} = B_e - \sum_i \alpha_i^B(\upsilon_i + \tfrac{1}{2}) + \ldots \tag{3.27}$$

where the α_i^B constant is the first vibration-rotation interaction constant coupling vibrational mode i and the principal axis of rotation B. The α constants [α_i^A, α_i^B and α_i^C] of normal mode i for each of the three principal axes of

rotation are given by[i]

$$-\alpha_i^B = \frac{2B_e^2}{\omega_i}\left[\sum_\xi \frac{3(a_i^{(B\xi)})^2}{4I_\xi} + \sum_j (\zeta_{i,j}^B)^2\left(\frac{3\omega_i^2+\omega_j^2}{\omega_i^2+\omega_j^2}\right)\right.$$
$$\left. + \pi\left(\frac{c}{h}\right)^{1/2}\sum_j \phi_{iij} a_j^{(BB)}\left(\frac{\omega_i}{\omega_j^{3/2}}\right)\right] \qquad (3.28)$$

where the first term (dependent on the moments of inertia and the $a_i^{(\alpha\beta)}$ constants, which are given by the partial derivatives of the inertia tensor elements with respect to the normal coordinates at equilibrium $[a_i^{(\alpha\beta)} = (\partial I^{(\alpha\beta)}/\partial Q_i)_e]$) is summed over the three principal axes of rotation. And the second (dependent on the harmonic frequencies and the Coriolis zeta constants) and third (dependent on the harmonic frequencies, cubic force constants and $a_i^{(B\xi)}$ constants) are summed over the remaining $3n-7$ ($3n-6$ for linear systems). The equilibrium rotational constants, B_e's, are inversely proportional to the moments of inertia and so may easily be determined for the equilibrium molecular geometry.

Rotational spectroscopy determines the differences between rotational energy levels distorted by the molecular vibrations. The rotational constants determined by fitting the spectra to the Hamiltonian in equation 3.26 are the B_v's rather than the theoretical B_e's. In equation 3.28, the VPT2 description of the α constants requires the harmonic energy levels, as well as cubic force constants. The α_i constant is usually on the order of B_e^2/ω_i.[111] In wavenumbers, B_e values are typically on the order of 10^{-1} to 10^0 and the

[i]Here π is 3.14159... not the vibrational angular momentum.

order of magnitude of harmonic frequencies typically ranges from 10^2 to 10^3. At most each α correction should shift the equilibrium rotational constant on the order of 1%, with the effect being greater for low frequency vibrational modes. It is possible to determine effective structural parameters for the vibrational ground state [r_0's] by fitting to experimentally determined ground state rotational constants [B_0's, B_v's where $v = 0$].

$$B_0 = B_e - \tfrac{1}{2}\sum_i \alpha_i^B \tag{3.29}$$

However, comparison of the effective structure to the molecular parameters of a theoretical equilibrium structure [r_e's] cannot be made without some knowledge of the effect of vibrations on the rotational constants.[j]

Shifts in vibrational bands upon isotopic substitution and relative relative absorption intensities are both useful in the assigning of observed spectral features to vibrational modes. The calculation of isotopic shifts is straightforward; the calculation of transition moments beyond the harmonic approximation expressed in equation 3.15 is less so. While the Coulombic forces between the atoms are independent of the nuclear masses, the vibrational frequencies do depend on mass and the potential surface is expressed in mass weighted coordinates. The force constants must be converted or recalculated for the new set of mass weighted coordinates and the vibrational energy levels must be determined for the isotopic masses. Due to the density of vibrational

[j]The equilibrium structure of HOOO and the effective structure fit to experimental rotational constants will be discussed — but not strictly compared — in chapter 4.

states beyond the fundamental modes, predicted intensities can be crucial to the assignment of combination bands and overtones. Calculation of transition moments at the VPT2 level has not previously been common, but recent work on this subject[77] made possible the assignment of certain combination bands.

3.2 Methods

The second derivatives of the molecular energy with respect to position that are needed for the calculation of the harmonic frequencies may be calculated analytically for most quantum-chemical methods provided a high-quality program package is used.[95] However, the third and fourth analytic derivatives needed for the calculation of the cubic and quartic force constants are currently nonexistent. The higher-order derivatives may be calculated through numerical differentiation of analytic second derivatives.[123]

$$\phi_{ijk} = \frac{\partial^3 V}{\partial Q_i \partial Q_j \partial Q_k} = \frac{(\phi_{ij})_{Q_{k^+}} - (\phi_{ij})_{Q_{k^-}}}{2\Delta} \tag{3.30a}$$

$$\phi_{ijkk} = \frac{\partial^4 V}{\partial Q_i \partial Q_j \partial Q_k \partial Q_k} = \frac{(\phi_{ij})_{Q_{k^+}} + (\phi_{ij})_{Q_{k^-}} - 2\phi_{ij}}{\Delta^2} \tag{3.30b}$$

The cubic force constants ϕ_{ijk} (third derivatives of the potential with respect to normal coordinates Q_i, Q_j and Q_k) are determined by calculating the quadratic force constants ϕ_{ij} (the second derivatives with respect to coordinates Q_i and Q_j) at displaced points Q_{k^+} and Q_{k^-} (positive and negative displacements of magnitude Δ along normal coordinate k).[k] The quartic force constants

[k] At the displace points, the second derivatives of the potential are no longer equivalent to the harmonic frequencies ω_i.

are calculated in a similar manner.[1] When analytic second derivatives are unavailable, the quadratic force constants may be calculated numerically from analytic gradients.

$$\phi_{ij} = \frac{\partial^2 V}{\partial Q_i \partial Q_j} = \frac{\left(\frac{\partial V}{\partial Q_i}\right)_{Q_{j+}} - \left(\frac{\partial V}{\partial Q_i}\right)_{Q_{j-}}}{2\Delta} \tag{3.30c}$$

The electronic energy, energy gradients and in some cases analytic second derivatives were calculated with the CCSD(T) method.[71] As demonstrated in appendix B, the use of the ANO1 basis sets[74] yields vibrational energies which are more accurate than does use of the similarly sized, but more widely used cc-pVTZ basis sets.[78] Consequently, the ANO1 basis set was used in the calculations of the anharmonic force fields. As the ANO basis sets were not designed with correlation of the core molecular orbitals in mind, these orbitals were excluded from the correlation treatment (the frozen core [(fc)] approximation was made). In calculations on the singlet HOONO species, a restricted Hartree-Fock, RHF, reference wavefunction was used. The *trans* conformer of the doublet HOOO species required an unrestricted Hartree-Fock, UHF, reference function. For historical reasons, the HOONO force constants were calculated through numerical differentiation of analytic gradients. The *trans*-HOOO force constants were calculated from analytic second derivatives. In both cases, the molecular geometries were optimized such that the root mean square deviation of the molecular energy gradient with respect to displacement along

[1]As only the ϕ_{iiii} and ϕ_{iijj} are needed, calculating quartic constants of the form ϕ_{ijkk} exceeds what is required.

the internal coordinates was less than 10^{-10} hartree bohr^{-1}. For numerical differentiation of analytic gradients, the Hartree-Fock density was converged to 10^{-11} and the parameters of the CCSD wavefunction and lambda equations were converged to 10^{-13}. For analytic second derviatives, the Hartree-Fock density, CCSD wavefunction and lambda equation parameters were converged to 10^{-10}. In the calculations presented here, resonances were not present. For the calculation of the vibrationally corrected rotational constants, the equilibrium rotational constants were determined with the ANO1 and the larger cc-pVQZ basis set[78] and the corrections calculated from the ANO1 anharmonic force field were applied to both.

The CFOUR[95] program package was used in all calculations.

3.3 Results

3.3.1 HOONO

The fundamental vibrational modes of *trans,perp*-HOONO are listed in Table 3.1.[m] The first and second overtones of the OH stretching mode (ν_1) are also included, as is the combination band involving two quanta of excitation in the OH stretching mode and one in the HOON torsional mode (ν_8). For these overtone and combination bands gas phase experimental values[98,124] are available for comparison to the calculated values; the differences are all less than 25 cm^{-1}. For the fundamental vibrations agreement between calculated

[m]Tables are collected at the end of the chapter.

values and the matrix-isolation data[125] is quite good for all the observed modes with the exception of ν_1. Due to the effect of the argon matrix, two peaks were observed for each of the five fundamental modes detected. The theoretical predictions were within 10 cm^{-1} of at least one, and often both, of the peaks for ν_2 through ν_5. The observed absorbance of the OH stretching mode is split by nearly 20 $cm^{-1}$and differs from the prediction by at least 20 cm^{-1}. This mode appears to be most affected by the surrounding matrix in *trans,perp*-HOONO.

In addition to the fundamental modes of *cis,cis*-HOONO listed in Table 3.2, overtones of the OH stretching mode (ν_1) and the two lowest frequency modes, a combination of the NOO and ONO bending modes (ν_7) and the OONO torsional mode (ν_9) are included. Agreement with experiment[20,100,126,127] is relatively good for these transitions with the exception of the central ON stretching mode (ν_6) and perhaps the ν_7 and ν_9 overtones. Comparison of predicted and observed[20,100] transition energies for the deuterated species (Table 3.3) show similar agreement.

The equilibrium rotational constants for *trans,perp cis,cis*-HOONO and *cis,cis*-DOONO at two levels of theory are presented in tables 3.4, 3.5 and 3.6 along with vibrationally corrected values. The vibrational corrections from the anharmonic force field calculated with the ANO1 basis set were applied to both equilibrium constants determined with the ANO1 basis set and those determined with the cc-pVQZ basis set. For the *trans,perp* conformer, rotational constants of the vibrational state in which the OH stretching mode

is doubly excited are presented in addition to those of the ground vibrational state. Experimentally determined rotational constants are included for comparison.[98,117] The largest difference in the predicted and observed rotational constants for *trans,perp*-HOONO occurs for the A constant when both the equilibrium constants and the vibrational corrections are calculated at the CCSD(T)/ANO1 (fc) level. The percent difference is less than 1.5% for both the ground and excited state constants. The error in the A constant is reduced to approximately 0.5% when the cc-pVQZ equilibrium constants are used, however the relative error in the B constant increases slightly to approximately 1 and 2% for the ground and excited states. For both *cis,cis*-HOONO and DOONO the largest difference occurs for the A constant as well when both components are calculated with the ANO1 basis set. The percent differences are approximately 1% initially and reduced to approximately 0.1 % when cc-pVQZ equilibrium constants are used. But here the relative error in both the B and C constants increases to approximately 1% when the alternate equilibrium constants are used in the calculation of the vibrationally corrected rotational constants.

3.3.2 HOOO

Vibrational transition energies for *trans*-HOOO are listed in Table 3.8 along with available experimental values. For the OH stretching mode (ν_1) and the overtone ($2\nu_1$), the agreement with respect to gas-phase experimental values[107] is as expected based on the above results. For gas-phase observa-

tions of the combination bands involving one quantum of excitation in the OH stretching mode and one in another mode ($\nu_1 + \nu_x$)[108] substantial differences of approximately 60 to 100 cm^{-1} are seen. Similar disagreement is seen for the *trans*-DOOO vibrational bands. These inconsistencies will be discussed, but not resolved, in section 3.4, as will the more minor issues noted above concerning the HOONO vibrational energies.

The equilibrium and vibrationally-corrected rotational constants for *trans*-HOOO are presented in table 3.9. As large discrepancies between theory and experiment have already been observed for the vibrational energies calling into question the anharmonic force field, agreement between observed[40] and predicted rotational constants, with corrections that are determined from the anharmonic force field, might not be expected — and is not found. The difference between the experimentally determined constants and those based on the ANO1 equilibrium constants are between 300 and 500 MHz, the percent difference being about 4 to 5% for the B and C constants compared to approximately 1% for HOONO. The situation does not improve, and indeed worsens, when the cc-pVQZ equilibrium constants are used.

3.4 Discussion

3.4.1 HOONO

The rather remarkable agreement between theory and experiment for vibrational energies in the region of the first and second overtone of the OH stretching mode for *trans,perp*-HOONO demonstrates the accuracy that is

achievable for anharmonic force fields using the methods described above. Similar, and indeed greater, accuracy has been seen for the HOONO isomer nitric acid (see appendix B for fundamental frequencies and ref. 99 for overtone and combination bands.) Matrix effects that slightly perturb the isolated *trans,perp*-HOONO and produce multiple absorption peaks make evaluation of the predicted vibrational energies in the fundamental region more difficult. For the transitions observed, the agreement seems to be quite good, though perhaps not as good as seen previously[115] with the deviation likely due to matrix effects on the OH stretching mode.

The three quantum transition $2\nu_1 + \nu_8$ was assigned based on the calculated position and absorption intensity.[98] The difference between the predicted and observed values appears to be largely due to the error in $2\nu_1$ indicating that for *trans,perp*-HOONO, VPT2 properly describes the HOON torsional motion, at least to the first excited state.

The predicted transition energies were used to aid the assignment of the *cis,cis*-HOONO and DOONO matrix-isolation vibrational spectra in the fundamental and overtone regions.[20,100] The latter predictions extended the understanding of the *cis,cis*-HOONO force field by refining the previous matrix-isolation data in the fundamental region[50,125] and adding to the infrared action data in the overtone region,[7,112,127] Large disagreements between theory and experiment appear for two transitions, which begin to demonstrate the limitations of the theoretical methods used here or possibly those of the experimental techniques (the matrix-induced shift of vibrational levels).

If the band at 601 cm^{-1} in the *cis,cis*-HOONO spectrum is indeed the first overtone of ν_9, then the agreement with the VPT2 prediction is astonishing. However, recent calculations[128] indicate that it is most likely the second overtone of ν_9. The ν_9 mode is the HOON torsional motion that connects the *cis,cis* and *cis,perp* structures. The *cis,perp* region of the potential energy surface creates a "shelf" in the HOON torsional potential at approximately 600 to 700 cm^{-1} (see figure 3.1).[n] With this significant deviation from harmonic behavior, VPT2 is expected to fail.[o] The $\nu_7 + \nu_9$ band in the experimental *cis,cis*-DOONO spectrum agrees fairly well the the predicted value. Below the *cis,perp* energy the HOON torsional potential is well-behaved, and the fundamental of ν_9 is properly predicted with VPT2.

The second discrepancy between theoretical prediction and experimental observation of vibrations in the *cis,cis* conformer involves the central ON stretching mode, ν_6. In both the HOONO and DOONO spectra, the observed frequency is about 50 cm^{-1} lower than predicted. The dipole moment is particularly sensitive to this mode, which may cause an unusual matrix effect.[20] A potential gas-phase study could resolve this issue.[130]

[n]Stationary points along the torsional potential were optimized and confirmed at the CCSD(T)/ANO1 (fc) level of theory. The curve was generated using the energies of the optimzed structures and cubic splines.

[o]A torsional barrier of approximately 750 cm^{-1} for isomerization, or approximately 1000 cm^{-1} for free rotation,[129] may have a similar effect for the overtone of ν_9 in *trans,perp*-HOONO.

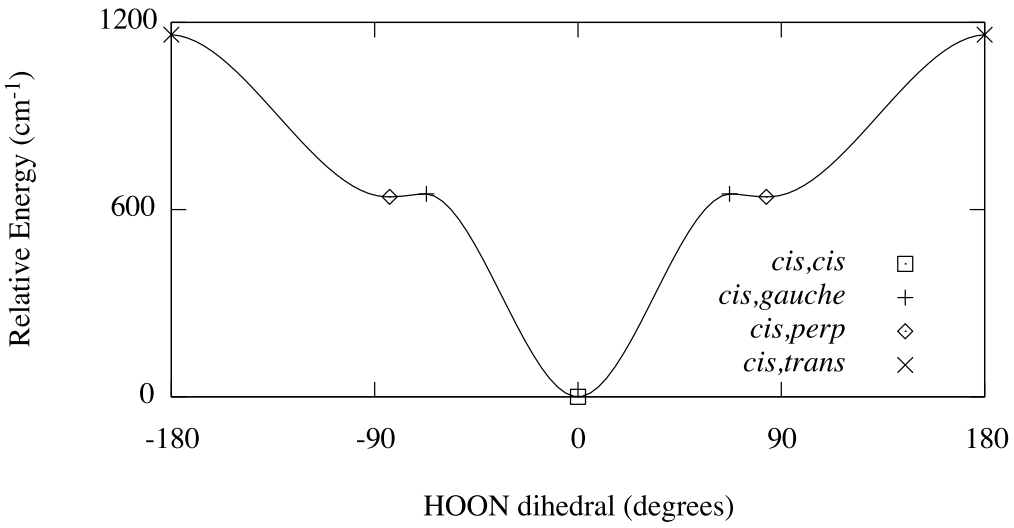

Figure 3.1: HOON torsional potential for the *cis*-HOONO system. The OONO dihedral is zero, or approximately zero, degrees for each of the four stationary points: *cis,cis*; *cis,perp*; *cis,gauche* and *cis,trans*.

3.4.2 HOOO

Comparison of the predicted vibrational energies to those of the infrared action spectrum for *trans*-HOOO presents a very different picture from that of HOONO. For the OH stretching mode and its overtone the results are very good, however almost no agreement can be claimed when comparing the energies of the combination bands. The predicted combination band for excitation of the OH stretching and HOOO torsional modes is approximately 60 cm^{-1} lower than the observed band, while the combination bands involving the coupling of the OH stretching motion with the central OO stretching motion (ν_5) and the OOO (ν_4) and HOO (ν_3) bending frequencies are predicted to be approximately 70 to 110 cm^{-1} higher than observed. It has been

noted that, due to significant deviation from harmonic behavior, VPT2 will most likely not be able to properly treat the very low-frequency torsional mode (ν_6). Coupling of modes may allow the improperly treated ν_6 to cause this drastic deviation from the VPT2 approximation for the bending and central OO stretching modes, while leaving the OH stretching mode relatively unaffected. However, of the in-plane modes for which conbination bands have been observed, only the cross anharmonicity term with ν_3 is large ($x_{36} = -17$ cm^{-1}). The cross anharmonicity term for the terminal OO stretching mode (ν_2) and the torsional mode is significant ($x_{26} = -14$ cm^{-1}). Observation of a band involving the terminal OO stretching mode ν_2 could perhaps provide some insight.[p] The cross anharmonicity terms between ν_3, ν_4 and ν_5 are relatively large, from 15 to 20 cm^{-1}, and negative. If VPT2 is not adequately describing the mixing of these in-plane relative motions of the OH and O_2 moieties (the bending motions and the central stretching mode), the modes may be sufficiently anharmonic to cause the descrepancies seen between theory and experiment independent of the torsional motion. While it has been shown to be reliable in the past, the level of theory used to describe the potential surface may also contribute to disagreement. This will be explored to some extent in chapter 4.

[p]The terminal OO stretching frequency (ν_2) may theoretically be observable depending on the dissociation energy of HOOO, but for technical reasons this region ($\sim$1300 cm^{-1}) and that of the $\nu_1 + \nu_2$ combination band ($\sim$4900 cm^{-1}) cannot be probed using the experimental setup of ref. 108. A search for the overtone of ν_2 was carried out, but was unsuccessful. The overtone is predicted to lie at 2630 cm^{-1} with a absorption intensity of 6.3 km mol^{-1} — roughly equivalent to that of the overtone of the OH stretching mode.

An alternate approach for describing anharmonic vibrations to that discussed in section 3.1.2 is direct calculation of the vibrational levels from an analytic potential surface fit to energies determined for a large set of molecular configurations, which avoids the harmonic approximation altogether.[44] A potential surface for HOOO was produced[44] by calculating energies with a density functional choosen to reproduce the experimentally determined dissociation energy.[41] A variational procedure[131] was used to calculate the rovibrational energy levels of the analytic surface. The resulting vibrational energies were also not in agreement with the fundamental frequencies inferred from the observed combination bands. The description of the torsional mode was in better agreement with experiment than that of VPT2 with the predicted frequency only 48 cm^{-1} higher than the experimentally inferred value compared to the VPT2 value which was 67 cm^{-1} low. However, the variationally predicted values for modes ν_5, ν_4 and ν_3 are between 125 and 170 cm^{-1} higher than the experimentally inferred values.[q] There is no experimental estimate for ν_2 and vibrational levels were not calculated beyond approximately 1450 cm^{-1}. While this variational approach is better able to describe low-frequency modes, the nature of the HOOO system requires high-level quantum chemical

[q]Coupling between ν_1 and ν_x would lead to combination bands that are not simply the sum of the fundamental vibrations. The cross anharmonicity terms from VPT2 indicate that only ν_3 is strongly coupled to ν_1 ($x_{13} = -21$ cm^{-1}). Thus, the value for ν_3 inferred from the combination band would be lower than the true fundamental by 21 cm^{-1} — not 140 cm^{-1} as predicted by the variational calculations. This VPT2 estimate of coupling may not be reliable, but a true comparison of the experimentally observed bands and the variational calculations cannot be made as no bands below the ν_1 (3569 cm^{-1}) fundamental have been observed for *trans*-HOOO and no levels above the ν_2 (1352 cm^{-1}) fundamental were predicted variationally.

methods for a proper description of the potential surface, which makes the calculation of energies for the large number of molecular configurations required for potential fitting a challenging endevor. An investigation of the torsional potential and the resulting torsional levels will be presented in chapter 4, but a full six-dimensional potential surface at the level of theory required for this molecule, and the prediction of the resulting vibrational energies has not yet been attempted.

Table 3.1: Fundamental vibrational frequencies of *trans,perp*-HOONO, as well as the first and second overtone of the OH stretching mode and a combination band, compared to available experimental values.

mode	theoretical[a,b]	experimental[a,c]
$3\nu_1$	10219	10195.3[d]
$2\nu_1 + \nu_8$	7254	7237[e]
$2\nu_1$	6989	6971.351[e]
ν_1	3583	3563.4, 3545.7[f]
ν_2	1701	1708.0, 1703.5[f]
ν_3	1367	1372.6, 1364.1[f]
ν_4	953	957.3, 952.1[f]
ν_5	792	782.1, 772.9[f]
ν_6	483	
ν_7	352	
ν_8	270	
ν_9	206	

[a] All frequencies are in cm^{-1}. [b] From the RHF CCSD(T)/ANO1 (fc) VPT2 force field. [c] No experimental values available for fundamentals ν_6 through ν_9. [d] Ref. 124 (gas phase). [e] Ref. 98 (gas phase): $2\nu_1 \pm 0.004$ cm^{-1}. [f] Ref. 125 (Ar matrix): due to the effect of the Ar matrix, two peaks were observed for each of the ν_1 through ν_5 fundamentals.

Table 3.2: Fundamental vibrational frequencies of *cis,cis*-HOONO, as well as selected overtones, compared to experimental values.

mode	theoretical[a,b]	experimental[a,c]
$2\nu_1$	6378	6370[d], 6350[e]
ν_1	3320	3306[f], 3303[g]
ν_2	1593	1600.6[g]
ν_3	1411	1392[g]
ν_4	935	922.8[g]
$3\nu_9$	832	601[d]
ν_5	792	789.7[g]
$2\nu_7$	744	716, 721[e]
ν_6	668	617[g]
$2\nu_9$	598	601[e]
ν_8	474	462[g]
ν_7	376	
ν_9	321	

[a] All frequencies are in cm^{-1}. [b] From the RHF CCSD(T)/ANO1 (fc) VPT2 force field. [c] No experimental values available for ν_7 or ν_9. [d] Ref. 127 (gas phase). [e] Ref. 100 (Ar matrix): The original assignment of the band at 601 cm^{-1} to $2\nu_9$ was "tentative" and recently reassignment to $3\nu_9$ has been supported.[128] Due to the effect of the Ar matrix, two peaks were observed for $2\nu_7$. [f] Ref. 126 (gas phase). [g] Ref. 20 (Ar matrix): $\nu_1 \pm 1$ cm^{-1}, $\nu_2 \pm 0.6$ cm^{-1}, $\nu_3 \pm 1$ cm^{-1}, $\nu_4 \pm 0.5$ cm^{-1}, $\nu_5 \pm 0.4$ cm^{-1}, $\nu_6 \pm 1$ cm^{-1}, $\nu_8 \pm 1$ cm^{-1}.

Table 3.3: Fundamental vibrational frequencies of *cis,cis*-DOONO, and an overtone and a combination band, compared to experimental values.

mode	theoretical[a,b]	experimental[a,c]
$2\nu_1$	4775	4767[d]
ν_1	2458	2447.2[e]
ν_2	1585	1595.7[e]
ν_3	1098	1089.1[e]
ν_4	900	888.1[e]
ν_5	793	786.6[e]
ν_6	672	613.9[e]
$\nu_7 + \nu_9$	603	588[d]
ν_8	460	456.5[e]
ν_7	361	
ν_9	255	

[a]All frequencies are in cm^{-1}. [b]From the RHF CCSD(T)/ANO1 (fc) VPT2 force field. [c]No experimental values available for ν_7 or ν_9. [d]Ref. 100. [e]Ref. 20: $\nu_1 \pm 0.6$ cm^{-1}, $\nu_2 \pm 0.7$ cm^{-1}, $\nu_3 \pm 0.4$ cm^{-1}, $\nu_4 \pm 0.4$ cm^{-1}, $\nu_5 \pm 0.5$ cm^{-1}, $\nu_6 \pm 0.9$ cm^{-1}, $\nu_8 \pm 0.5$ cm^{-1}.

Table 3.4: Equilibrium and vibrationally corrected rotational constants for *trans,perp*-HOONO compared to available experimental values.

	theoretical[a,b,d]	theoretical[a,b,d]	experimental[a,e]
A_e	54203	55112	
B_e	4972	5022	
C_e	4623	4672	
A_0	53732	54642	54391
B_0	4928	4978	4909
C_0	4577	4626	4602
$A(v_1 = 2)$	53424	54333	54116
$B(v_1 = 2)$	4925	4975	4864
$C(v_1 = 2)$	4577	4626	4625

[a]All rotational constants are in MHz. [b]From the RHF CCSD(T)/ANO1 (fc) VPT2 force field. [c]Equilibrium constants from the RHF CCSD(T)/ANO1 (fc) structure. [d]Equilibrium constants from the RHF CCSD(T)/cc-pVQZ structure. [e]Ref. 98.

Table 3.5: Equilibrium and vibrationally corrected rotational constants for *cis,cis*-HOONO compared to available experimental values.

	theoretical[a,b,c]	theoretical[a,b,d]	experimental[a,e]
A_e	21267	21544	
B_e	8078	8155	
C_e	5855	5916	
A_0	21148	21426	21406
B_0	7945	8022	7948
C_0	5769	5831	5791

[a]All rotational constants are in MHz. [b]From the RHF CCSD(T)/ANO1 (fc) VPT2 force field. [c]Equilibrium constants from the RHF CCSD(T)/ANO1 (fc) structure. [d]Equilibrium constants from the RHF CCSD(T)/cc-pVQZ structure. [e]Ref. 117.

Table 3.6: Equilibrium and vibrationally corrected rotational constants for *cis,cis*-DOONO compared to available experimental values.

	theoretical[a,b,c]	theoretical[a,b,d]	experimental[a,e]
A_e	20147	20398	
B_e	8041	8117	
C_e	5747	5806	
A_0	20023	20274	20245
B_0	7912	7988	7913
C_0	5666	5725	5685

[a]All rotational constants are in MHz. [b]From the RHF CCSD(T)/ANO1 (fc) VPT2 force field. [c]Equilibrium constants from the RHF CCSD(T)/ANO1 (fc) structure. [d]Equilibrium constants from the RHF CCSD(T)/cc-pVQZ structure. [e]Ref. 117.

Table 3.7: Fundamental vibrational frequencies of *trans*-HOOO, as well as the overtone of the OH stretching mode and selected combination bands, compared to available experimental values.

mode	theoretical[a,b]	experimental[a,c]
$2\nu_1$	6990	6974.18[d]
$\nu_1 + \nu_2$	4912	
$\nu_1 + \nu_3$	4674	4567.20[e]
$\nu_1 + \nu_4$	4120	4051.18[e]
$\nu_1 + \nu_5$	3885	3812.96[e]
$\nu_1 + 2\nu_6$	3651	3798.00[e]
$\nu_1 + \nu_6$	3642	3698.02[e]
ν_1	3578	3569.30[d]
ν_2	1336	
ν_3	1117	997.9[f]
ν_4	544	481.9[f]
ν_5	307	228.7[f]
ν_6	62	128.7[f]

[a] All frequencies are in cm^{-1}. [b] From the UHF CCSD(T)/ANO1 (fc) VPT2 force field. [c] No experimental values available for ν_2 or the $\nu_1 + \nu_2$ combination band. [d] Ref. 107: $2\nu_1 \pm 0.05$ cm^{-1} and $\nu_1 \pm 0.05$ cm^{-1}. [e] Ref. 108: all combination bands ± 0.05 cm^{-1}. [f] Inferred from combination bands of ref. 108.

Table 3.8: Fundamental vibrational frequencies of *trans*-DOOO, as well as the overtone of the OH stretching mode and selected combination bands, compared to available experimental values.

mode	theoretical[a,b]	experimental[a,c]
$2\nu_1$	5196	5182.42[d]
$\nu_1 + \nu_2$	3986	
$\nu_1 + \nu_3$	3493	3419.1[e]
$\nu_1 + \nu_4$	3162	3098.0[e]
$\nu_1 + \nu_5$	2954	2880.4[e]
$\nu_1 + \nu_6$	2709	2737.3[e]
ν_1	2642	2635.06[d]
ν_2	1343	
ν_3	861	783.9[f]
ν_4	522	463.0[f]
ν_5	312	245.3[f]
ν_6	66	102.2[f]

[a]All frequencies are in cm^{-1}. [b]From the UHF CCSD(T)/ANO1 (fc) VPT2 force field. [c]No experimental values available for ν_2 or the $\nu_1 + \nu_2$ combination band. [d]Ref. 108: $2\nu_1 \pm 0.05$ cm^{-1} and $\nu_1 \pm 0.05$ cm^{-1}. [e]Ref. 108: all combination bands ± 0.05 cm^{-1}. [f]Inferred from combination bands of Ref. 108.

Table 3.9: Equilibrium and vibrationally corrected rotational constants for *trans*-HOOO compared to available experimental values.

	theoretical[a,b,c]	theoretical[a,b,d]	experimental[a,e]
A_e	71839	73141	
B_e	10698	10904	
C_e	9311	9489	
A_0	71117	72419	70778
B_0	10437	10643	9987
C_0	9107	9285	8750

[a]All rotational constants are in MHz. [b]From the UHF CCSD(T)/ANO1 (fc) VPT2 force field. [c]Equilibrium constants from the UHF CCSD(T)/ANO1 (fc) structure. [c]Equilibrium constants from the UHF CCSD(T)/cc-pVQZ structure. [d]Ref. 40.

Chapter 4

HOOO Potential Curves and Structures

Equation-of-motion coupled-cluster methods were used to calculate the minimum energy path for dissociation of *trans*-HOOO to OH + O_2. The HOOO torsional potential was examined as well. Molecular structures and harmonic frequencies at stationary points along the torsional potential will be compared to results obtained with standard single-reference coupled-cluster methods.

4.1 Introduction

Due to the curious discrepancies between theory and experiment for nearly all aspects of the HOOO system studied to date, a closer examination of the potential surface is warranted. This chapter will focus on the calculation of the potential energy as a function of the dissociation coordinate (the central OO bond) and the HOOO torsional motion (which converts between the *trans* and *cis* conformers). The dissociation curve could reveal a potential cause for the large difference between the predicted dissociation energy and the experimental upper bound, which is thought to be close to the actual value. Through study of the torsional potential, it may be possible to begin

to reconcile the observed and predicted vibrational frequencies as it is the torsional vibration that severely challenges the theoretical approach by deviating significantly from harmonic behavior. As the full anharmonic force field is not yet well-described and the vibrational effects on the molecular structure are not well-understood (see section 3.3.2), a comparison of the experimentally determined structure to the equilibrium structures presented here cannot yet be made. However, discussion of the theoretical equilibrium structures is possible — and worthwhile — and therefore included.

4.1.1 Dissociation Curve

To extend our understanding of the central OO bond, equation-of-motion coupled-cluster methods (discussed further in section 4.1.4) have been used to investigate the minimum energy path for the dissociation of HOOO to OH + O_2. Standard single-reference coupled-cluster methods are not well-suited for the study of bond-breaking processes,[132] but the nature of equation-of-motion methods[133] is such that they can be applied with confidence to certain bond-breaking situations[a] for example, the one discussed in this work.

4.1.2 Torsional Potential

Single-reference methods may be used to map the molecular energy as a function of the HOOO dihedral angle as no bonds are broken in this process.

[a] In the present context, the "certain bond-breaking situations" referred to are those in which one of the fragments of the reference state is a closed-shell species.

However, as seen table 2.4, it is only with the inclusion of high-level correlation corrections that the *trans* conformer is predicted to be more stable than the *cis* conformer. High-level correlation applied to a single-reference wavefunction may be able to properly describe a system with some degree of multi-reference character, but the equation-of-motion methods can be used, in most cases, to treat non-dynamical correlation, or the multi-reference character, directly. As high-level correlation need not be included, less computational effort is required. Both standard single-reference and equation-of-motion approaches will be applied to the torsional potential for comparison, but one should not expect the single-reference methods to yield results that are qualitatively correct for the *cis*-*trans* energy difference unless high-level correlation corrections are applied.

Large amplitude motions, with a frequency of oscillation much lower than that of typical molecular vibrations, may be separable from the other vibrational modes.[134] This separability is desirable as these vibrational modes are not amenable to the standard harmonic approximation followed by a perturbation theory treatment. The low-frequency torsional mode in HOOO may be separable from the remaining vibrational modes simplifying the calculation of the torsional energy levels to a one-dimensional problem. For *trans*-HOOO at the CCSD(T)/ANO1 (fc) level of theory, the VPT2 cross anharmonicity terms,[b] a measure of the coupling of the torsional mode ($\nu_6 = 62$ cm^{-1}) to the in-plane modes, are low for the second ($\nu_5 = 307$ cm^{-1}, $x_{56} = -6$ cm^{-1}) and

[b]See section 3.4.2.

third ($\nu_4 = 544$ cm^{-1}, $x_{46} = 6$ cm^{-1}) lowest frequency motions. Those modes with significant cross anharmonicity terms ($x_{36} = -17$ cm^{-1}and $x_{26} = -14$ cm^{-1}) are higher frequency modes ($\nu_3 = 1117$ cm^{-1}and $\nu_2 = 1336$ cm^{-1}). By calculating the zero-point energy of the five higher-frequency modes along the torsional potential, the vibrational effects of these other modes on the HOOO torsional motion may be taken into account.[134c] The resulting (one-dimensional) potential is known as a "vibrationally adiabatic" potential.

4.1.3 The Structural Issue

Rotational constants for HOOO and the deuterated species, DOOO, were determined by Endo and co-workers through Fourier-transform microwave spectroscopy.[40] An effective molecular structure was fit to the experimentally determined rotational constants. A very long central OO bond distance ($r_0 = 1.688$ Å) seemed to challenge the ability of single-reference coupled-cluster methods to properly treat the HOOO species as only with multi-reference methods had equilibrium structures been obtained which had a central OO bond distance of a similar length.[28,40,43,44] The central OO bond length at the minimum of the dissociation curve will be discussed and compared to central OO bond lengths determined at other levels of theory.

[c]The choice of a coordinate for the large amplitude motion and the projection of the frequencies calculated along the potential can be a very complicated problem, however we have taken a very simple approach below.

4.1.4 Equation-of-Motion Coupled Cluster Theory

If an operator $[\hat{R}_k]$, which when acting on a reference wavefunction $[\Psi_0]$ with n electrons generates the wavefunction of an ionized state with $n-1$ electrons[135]

$$\hat{R}_k \Phi_0(n) = \Phi(n-1) \tag{4.1}$$

and the coupled cluster [CC] Hamiltonian of 2.6a

$$\bar{H} = e^{-\hat{T}} \hat{H} e^{\hat{T}} \tag{4.2}$$

are combined

$$\bar{H} \hat{R}^k |\Phi_0\rangle = E_k \hat{R}_k |\Phi_0\rangle \tag{4.3}$$

the ionization energy $[E_k]$ for the kth target state can be determined relative to the CC energy of the reference state. By determining the energy of the target statethrough diagonalizing the transformed Hamiltonian $[\bar{H}]$ in a basis of $n-1$ wavefunctions,[136] which are obviously orthogonal to the n electron reference function,[133] a multi-reference target state can be described without a reference state bias.[d] This equation-of-motion coupled-cluster [EOM-CC] method is better suited for the multi-reference bond-breaking region along the dissociation curve than standard coupled-cluster methods. And, as stated above, the EOM approach directly treats the nondynamic correlation of the

[d] Provided the n electron reference state is well-described by a single determinate.

trans and *cis* conformers of HOOO and may yield a qualitatively correct description of the *cis*-*trans* energy difference without the high-level correlation used in chapter 2.

4.2 Methods

4.2.1 Dissociation Curve

The dissociation curve of *trans*-HOOO was determined by calculating the minimum energy for fixed values of the central OO bond. The remaining internal coordinates were optimized utilizing gradients determined through finite difference of energies. To calculate the energies a method originally presented by Stanton and Gauss[137,138], with some adjustments later made by Saeh and Stanton[136] was used. In this approach, termed EOMIP-CCSD*, a noniteritive correction allows for the inclusion of some terms neglected in the traditional EOMIP-CCSD method.[139] For the HOOO radical, the reference wavefunction used was that of the triplet HOOO anion, as it will properly dissociate to O_2 and the closed-shell species OH^-. By ejecting the appropriate electron a balanced treatment of the HOOO radical dissociating to the OH radical and O_2 may be obtained. Equation-of-motion methods for open-shell reference states are limited. The underutilized EOMIP-CCSD* approach was taken as it includes more dynamical correlation than the standard EOMIP-CCSD method.

In addition to the EOMIP-CCSD* constrained optimizations carried out to produce the dissociation curve, *trans*-HOOO and the dissociation prod-

ucts OH and O_2 were fully optimized at the same level of theory.[e] To estimate the effect of zero-point energy, ZPE, on the dissociation curve, the harmonic frequencies were calculated at the *trans* minimum, near the transition state to dissociation and for the fragments. Prior to the frequency calculations[f] the molecular geometries were optimized such that the root mean square deviation of the molecular energy gradient with respect to displacement along the internal coordinates was less than 10^{-8} hartree bohr^{-1} — the exception being the central OO distance near the transition state which was converged to on the order of 10^{-5} hartree bohr^{-1}.[g] As analytic gradients are not available for the EOMIP-CCSD* level of theory, the quadratic force constants were calculated through finite difference of energies at displaced points. For numerical differentiation to produce the quadratic force constants, the Hartree-Fock density was converged to 10^{-11} and the CCSD wavefunction parameters and EOMIP eigenvectors were converged to 10^{-13} Hartree.[h] Frequency calculations were carried out for the deuterated species DOOO to estimate the change in zero-point energy upon substitution. The cc-pVQZ basis set[78] was used in both the constrained optimizations to produce the curve as well as the full optimiza-

[e]The OH fragment was treated with the EOMIP approach from the closed-shell OH^- reference species, but for O_2 the single-reference CCSD method was used.

[f]The default convergence of 10^{-5} hartree bohr^{-1} was used for all other constrained optimizations.

[g]The transition state was found through constrained optimizations at increments of 0.0005 Å (approximately 0.001 Bohr) for the central OO distance near the maximum along the minimum energy dissociation curve. In this region the energy varies on the order of 10^{-8} with a change in the central OO bond length on the order of 10^{-3} Bohr.

[h]The default convergence of 10^{-7} was used for each of the three components for all but the frequency calculations.

tions and frequency calculations. At the global minimum, near the transition state and for the fragments, the energy was calculated with the larger cc-pV5Z basis set as well.[78] And for the same three points along the dissociation curve, the energy was calculated with the EOMIP coupled-cluster singles, doubles and triples method [EOMIP-CCSDT][140] and the cc-pVTZ basis set.[78] In all EOMIP calculations reported here, the frozen core [(fc)] approximation was made, meaning the core electrons were not correlated.

4.2.2 Torsional Potential

The torsional potential of HOOO was constructed in a manner similar to the dissociation curve of *trans*-HOOO. Constrained optimizations were carried out for fixed values of the HOOO dihedral angle between 0°, the *cis* minimum, and 180°, the *trans* minimum. With the plane of symmetry broken as the HOOO dihedral angle is varied, the computational cost increases. The ANO1[74] basis set was used in the constrained optimizations along the potential curve rather than the cc-pVQZ basis set used for the dissociation curve. Use of the triple-ζ ANO1 basis set, rather than a quadruple-ζ basis set such as cc-pVQZ (or ANO2), reduces the computational cost but the differences in results obtained with the triple- and quadruple-ζ contractions of the Almlöf and Taylor basis sets tend to be smaller than the differences in results obtained with the cc-pVTZ and cc-pVQZ. Optimizations at the *cis* and *trans* minima and near the torsional transition state (HOOO dihedral angel equal to 80°) were carried out with the cc-pVQZ basis set as well to demonstrate

the similarity in results obtained with the ANO1 and cc-pVQZ basis sets for this system.

For calculations at the EOMIP-CCSD*/ANO1 level of theory, parameters were converged such that the root mean square deviation of the molecular energy gradient was less than 10^{-8} hartree bohr^{-1}. The harmonic frequencies were then calculated through numerical differentiation of EOMIP-CCSD* energies converged as described above in section 4.2.1. The vibrationally adiabatic torsional potential was calculated by including the harmonic zero-point energy neglecting the contribution from the torsion. At the *cis* and *trans* minima and near the torsional transition state (HOOO dihedral angel equal to 80°) geometry optimizations and harmonic frequency calculations were carried out at the CCSD(T)/ANO1 level in addition to the EOMIP calculations.

4.2.3 Additional Equilibrium Structures

At the *trans*-HOOO minimum, the molecular parameters were optimized at the EOMIP-CCSD* and CCSD(T) levels of theory with a series of correlation consistent basis sets with and without additional diffuse functions. At the CCSD(T) level the cc-pVXZ [X = T,Q,5] and aug-cc-pVXZ [X = T,Q] basis sets introduced in section 2.1.3 and d-aug-cc-pVTZ basis set, which is a triple-ζ basis set that includes an additional set of diffuse functions.[141] At the EOMIP-CCSD* level of theory, the cc-pVXZ [X = T,Q] and aug-cc-pVXZ [X = T,Q] basis sets were employed.

The CFOUR[95] program package was used in all calculations; for those

at the EOMIP-CCSDT level the MRCC[96] package was also used.

4.3 Results

4.3.1 Dissociation Curve

The dissociation curve for *trans*-HOOO $\rightarrow$ OH + O_2 is presented in figure 4.1.[i] A barrier to dissociation is revealed with a maximum at a central OO distance of approximately 2.072 Å. The inclusion of the zero-point energy increases the entrance barrier, the difference in energy between the transition state and the fragments, and reduces the exit barrier, the energy difference between the transition state and the *trans*-HOOO minimum. The exit barrier is slightly decreased for the deuterated species. Based on the EOMIP-CCSD*/cc-pV5Z and EOMIP-CCSDT/cc-pVTZ energies calculated at the *trans* minimum and the transition state relative to dissociation, we can estimate the effect of increased basis size and high-level dynamic correlation. Both stabilize *trans*-HOOO relative to dissociation and reduce the barrier.

[i] All points are plotted relative to the dissociated fragments. Near an O_2-OH distance of 3 Å, there is a slight van der Waals interaction, but by approximately 5 Å the energy converges to the dissociation limit.

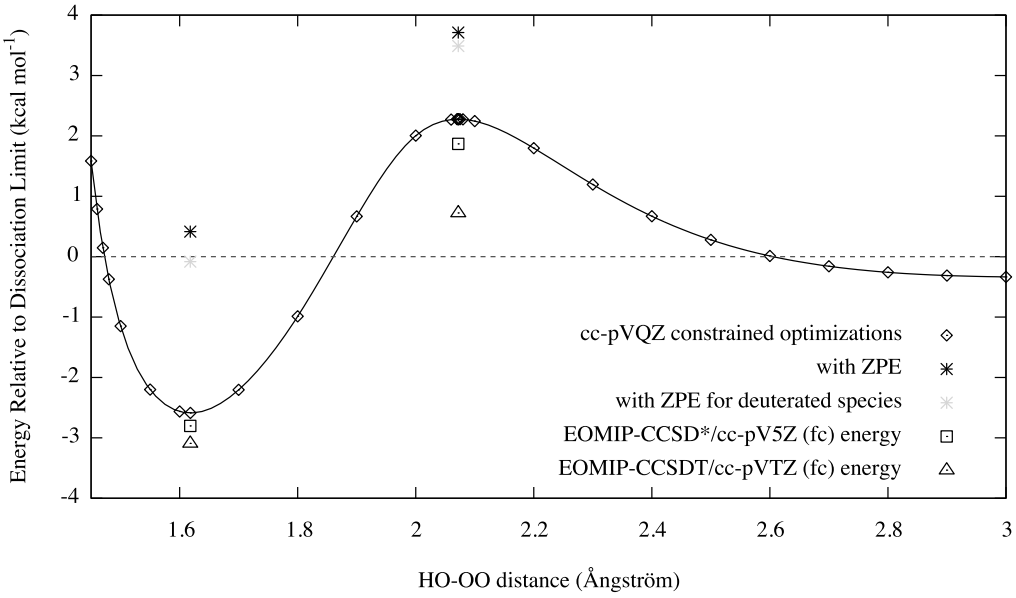

Figure 4.1: The EOMIP-CCSD*/cc-pVQZ (fc) minimum energy path for dissociation of *trans*-HOOO to OH + O_2.

4.3.2 Torsional Potential

The torsional potential from *cis* to *trans*-HOOO is presented in figure 4.2. The relative energies of the *cis* and *trans* conformers calculated with the cc-pVQZ and ANO1 basis sets are very similar, and indeed indistinguishable on the plot. The energy of the torsional transition state is slightly greater with the larger cc-pVQZ basis set, but qualitatively there appear to be no significant changes in the nature of the torsional potential when calculated with the more efficient ANO1 basis set. The inclusion of the ZPE does have a greater effect on the torsional potential. The frequency of the HOO bending mode is significantly greater at the *cis* minimum compared to the *trans*. This increases the ZPE at the *cis* minimum destabilizing it relative to *trans*. The frequency of the OOO bend increases as well while the frequency of the OH stretch decreases. These effects are possibly due to a slight hydrogen bond between the terminal oxygen atom and the hydrogen atom, which is made possible in the *cis* conformation. Near the torsional transition state the stretching frequency of the terminal OO bond is less than that of the *trans* structure. Therefore the ZPE is less and the barrier is reduced slightly.

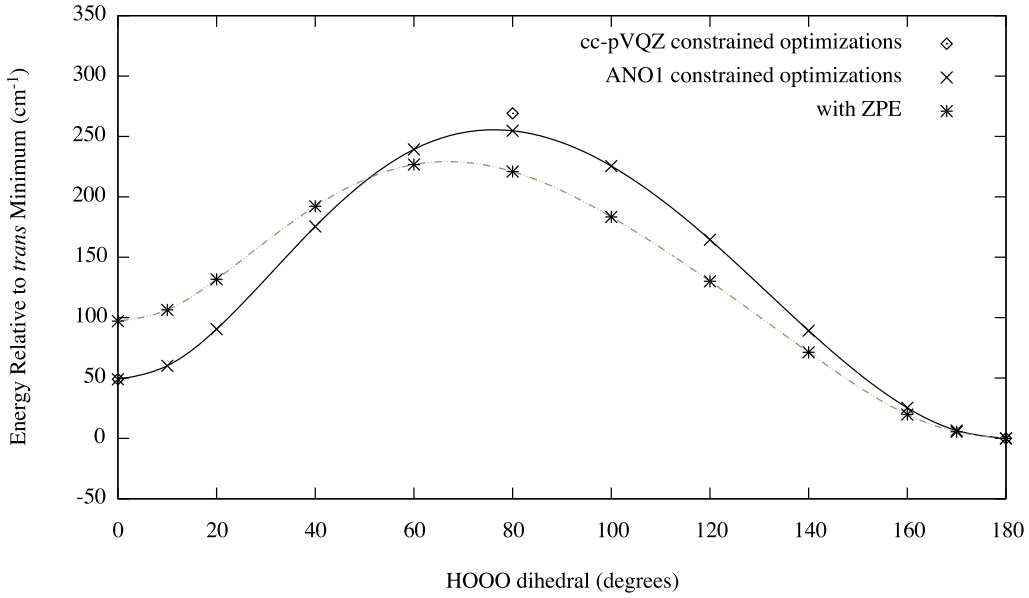

Figure 4.2: The EOMIP-CCSD* (fc) torsional potential from *cis* to *trans*-HOOO.

4.3.3 Equilibrium Structures

The structural parameters optimized at the EOMIP-CCSD*/cc-pVQZ (fc) level of theory for the *cis* and *trans*-HOOO conformers, the torsional transition [TS], the *trans* dissociation transition state, the dissociation fragments OH and O_2, as well as FOO for comparison, are included in table 4.2.[j] For all the previous species, with the exception of the dissociation transition state, structural parameters optimized at the CCSD(T)/cc-pVQZ level of theory are presented in table 4.1. The optimized parameters of *cis* and *trans*-HOOO, the torsional transition state and FOO determined with the ANO1 basis set at the CCSD(T) (fc) and EOMIP-CCSD* (fc) levels of theory are contained in tables 4.3 and 4.4 with the associated harmonic frequencies in tables 4.5 and 4.6. Additional sets of structural parameters for *trans*-HOOO determined at the two levels of theory, CCSD(T) (fc) and EOMIP-CCSD* (fc), with a series of correlation consistent basis sets with and without diffuse functions are gathered in table 4.7. The largest differences in the HOOO parameters calculated with the standard coupled-cluster method and the equation-of-motion method occur for the terminal and central OO bond lengths, approximately 0.01 and 0.02-0.03 Å respectively. The differences in the optimized parameters using the standard verses equation-of-motion approach for the isoelectronic FOO are significantly smaller, $\leq$ 0.005 and 0.01 Å for the OO distance and the FO distance respectively. In going from *trans* to *cis*-HOOO, the terminal OO distances increases, the central OO distance decreases and the OH distance

[j] Tables are collected at the end of the chapter.

increases in all the calculations presented here. The predicted harmonic frequency of the OH stretching mode (ω_1) decreases by approximately 40 to 50 cm^{-1} for both standard and equation-of-motion coupled-cluster approaches. For the harmonic frequency of the terminal OO stretch (ω_2) there is a significant *cis-trans* shift only for the equation-of-motion approach. However, the harmonic frequency near the torsional transition state is much lower at both levels of theory. At both levels of theory both the HOO and OOO bending frequencies increase in going from *trans* to *cis*, as does the central OO stretching frequency.

4.4 Discussion

4.4.1 Dissociation Curve

The barrier along the path to dissociation has been discussed as a possible source of the discrepancy between the experimental upper bound to the dissociation energy and the theoretical prediction.[142] As described in section 2.4.3, the upper bound to the dissociation energy of a weakly bound molecule can be determined through infrared action spectroscopy. For HOOO, the fundamental or overtone of the OH stretch is excited. The vibrational energy is sufficient to break the weak central OO bond following intramolecular vibrational redistribution. Following dissociation, the populations of the rotational levels of the OH fragment are determined through laser-induced fluorescence. If the energy available to the products [E_{avail}], the difference between the known vibrational energy [$E_{h\nu}$] and the energy required for dissociation [D_0],

is partitioned statistically among the available degrees of freedom, the total excess energy can be determined from the highest rotational level populated for OH [E_{rot}^{max}(OH)].[k]

$$E_{h\nu} = D_0 + E_{avail} \tag{4.4a}$$

$$E_{h\nu} \geq D_0 + E_{rot}^{max}(\mathrm{OH}) \tag{4.4b}$$

$$D_0 \leq E_{h\nu} - E_{rot}^{max}(\mathrm{OH}) \tag{4.4c}$$

The difference of $E_{h\nu}$ and E_{rot}^{max}(OH) is generally taken to be the upper limit to the dissociation energy, rather than the actual bond energy. There may be a portion of E_{avail} that is unaccounted for as the spacing between rotational energy levels limits the precision of the measurement and the energy distribution amongst the product states may not be statistical. In the case of *trans,perp*-HOONO, the upper bound is very close to the true bond energy (see table 2.4).

When there is a barrier to dissociation, E_{avail} may be described as the sum of the impulsive energy [E_{imp}], equal to the difference in the energy of the transition state and the energy of the dissociation fragments, and the statistical energy [E_{stat}], equal to the difference in $E_{h\nu}$ and the energy of the transition state (see figure 4.3).[143]

$$E_{h\nu} = D_0 + E_{stat} + E_{imp} \tag{4.5}$$

[k]See ref. 41 for the full energy balance equation.

It is assumed that at the transition state the excess energy, or E_{stat}, is partitioned statistically among the available degrees of freedom. However, as the rupturing bond continues to lengthen to dissociation the additional energy, or E_{imp}, may be preferentially directed into relative translational or rotational energy of one of the fragments. If the energy of the apparent entrance barrier in figure 4.1 is preferentially directed into relative translational energy of the fragments or rotation of the O_2 fragment, this portion of E_{avail} would be undetermined in the infrared action experiments and could explain the unexpected difference in the experimental upper bound to the dissociation energy and the theoretically predicted value.

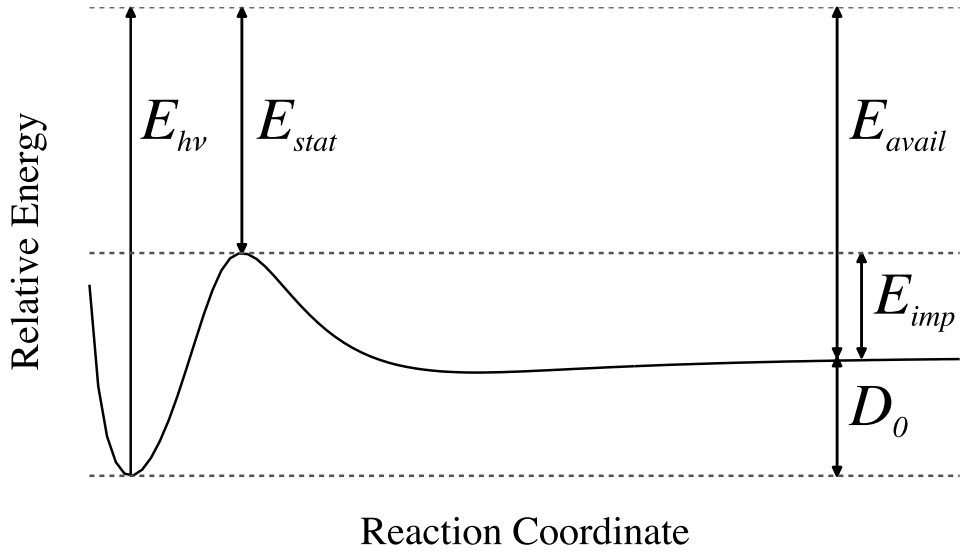

Figure 4.3: The partitioning of available energy in the presence of a barrier to dissociation.

The height of the apparent dissociation barrier is much more challenging to predict than is the dissociation energy. Single-reference methods with high-level correlation corrections can be applied at the *trans*-HOOO minimum and to the fragments that cannot be reliably applied to the transition state in the bond breaking region due to the multi-reference character of the species. The equation-of-motion methods used in the examination of the dissociation curve treat the non-dynamical correlation, but the degree of dynamical correlation treated with in the EOMIP-CCSD* method is much less than in the methods used to calculate the dissociation energy in chapter 2. The basis sets used here are less complete as well. The dissociation energy neglecting zero-point effects at the EOMIP-CCSD*/cc-pVQZ level is approximately 2.5 kcal mol^{-1} compared to 5.21 kcal mol^{-1} using the HEAT approach described in chapter 2. With harmonic ZPE corrections, *trans*-HOOO is not stable relative to dissociation on the EOMIP-CCSD*/cc-pVQZ curve. The dissociation curve presented in figure 4.1 should be taken as qualitative, rather than a quantitative, description. By calculating the relative energy at the EOMIP-CCSD*/cc-pV5Z and EOMIP-CCSDT/cc-pVTZ levels of theory at the EOMIP-CCSD*/cc-pVQZ optimized geometries, the effect of increased basis size and increased dynamic correlation on the barrier height can be estimated. Both effects decrease the height of the barrier; the increased correlation significantly decreases the barrier. At higher levels of theory the barrier may be negligible or disappear entirely. There is experimental evidence that there is no barrier in the association reaction of OH + O_2. Smith and coworkers

monitored the concentration of OH in the presence of O_2 at temperatures between 55.7 and 110.8 K and found no evidence for a barrier in the formation of HO_3.[97] If there is no barrier to dissociation for *trans*-HOOO, the reason for the discrepancy between theoretical and experimental bond energies is still in question.

The HF dimer is also a weakly bound system with a dissociation energy similar to that of HOOO. Dissociation of the HF dimer following vibrational excitation results in one fragment that is highly rotationally excited and one that is not.[144] The determination of the dissociation energy required monitoring of the rotational and kinetic energy of both fragments. The preferential rotational excitation of one fragment was attributed to the impulsive dissociation[144] in the absence of a barrier to dissociation.[145] A similar implusive dissociation of HOOO could explain the discrepancy between theoretical and experimental bond energies without invoking a barrier to dissociation.

4.4.2 Torsional Potential

The *cis*-*trans* energy difference on the EOMIP-CCSD*/ANO1 torsional potential is in qualitative agreement with results from the high-level calculations presented in table 2.4. The *trans* conformer is slightly (approximately 50 cm^{-1}) more stable than the *cis* with the inclusion of zero-point effects widening the gap significantly. The torsional barrier is sufficiently low that above 300 to 400 K, HOOO would convert freely between conformers. At 200 to 300 K, kT is sufficient for conversion of *cis* to *trans*.

Preliminary calculations carried out by Beames and coworkers[146] of the vibrational levels for a torsional potential obtained by scaling the data of figure 4.2 reproduce the inferred torsional band positions of *trans* and *cis* conformers of HOOO, *trans* conformer of DOOO and the torsional overtone of *trans*-HOOO quite well. The torsional barrier height relative to the *trans* minimum for the scaled potential is approximately 50 cm^{-1} higher than the barrier height obtained at the EOMIP-CCSD*/ANO1 (fc) level. Calculations of the EOMIP-CCSD* energy with larger basis sets (including cc-pVQZ, cc-pV5Z and aug-cc-pVQZ) indicate that the barrier height relative to the *trans* minimum does increase slightly with a more complete basis — converging toward the scaled potential which reproduces the experimentally determined torsional frequencies. However, due to the reduced terminal OO frequency near the torsional transition state, the zero-point energy effects reduce the barrier height for the vibrationally adiabatic curve — deviating from the potential prescribed by the scaled curve. The reduction in the terminal OO frequency may be an artifact of the calculations, but the effect is more difficult to dismiss as it occurs when both standard and equation-of-motion coupled-cluster methods are applied.

The *cis* well of the scaled potential is more difficult to correlate with the theoretical description. The increase in the HOO and OOO bending frequencies at the *cis* minimum increases zero-point energy relative to that of the other conformers. This, combined with the decrease in the barrier height with the inclusion of zero-point corrections, results in a very shallow *cis* well on the

vibrationally adiabatic curve. The barrier height relative to the *cis* minimum is approximately 125 cm^{-1} and unable to support a torsionally excited state 150 cm^{-1} above the ground vibrational state. Again, the zero-point corrections are taken from a force field that is not consistent with experiment, but as the trend is seen for both standard and equation-of-motion approaches (and with other basis sets), it is difficult to dismiss entirely. The effect of larger basis sets on the depth of the *cis* is not significant at the cc-pVQZ level (the cc-pVQZ and ANO1 energies are indistinguishable in figure 4.2), but when diffuse functions are included, the *cis* well again becomes extremely shallow (approximately 100 cm^{-1} before zero-point corrections). These effects which would appear to decrease the *cis* well depth may be counteracted at higher levels of theory by increased correlation shaping the theoretical torsional potential into a curve that reproduces the semi-empirical scaled potential. However, only the experimentally inferred *cis*-HOOO, not the *cis*-DOOO, band is reproduced well by the scaled potential. Also, a band originally assigned to the combination of the doubly excited torsional mode and the OH stretching frequency is now in question as the scaled potential will not support a second excited torsional state. This suggests that perhaps the alignment of the experimentally inferred torsional frequency and the predicted transition was coincidental and that the band from which the *cis* torsional frequency was inferred is attributable to another transition. The lack of rotational structure in the bands assigned to the *cis* conformer and the lack of a large shift in the OH stretching frequency[1]

[1]The predicted OH stretching frequency of the *cis* conformer is red-shifted relative to

relative to that of the *trans* conformer support this possibility.

4.4.3 The Equilibrium Structure

It has been noted that proper treatment of the *trans*-HOOO radical requires a basis set of at least triple-ζ quality and correlation beyond the singles and doubles approximation of CCSD.[94] Similar requirements have been noted for difluorodioxirane — which at the time had the distinction of having the longest OO bond ever measured or calculated.[93] The three-electron correlation effects treated by the perturbative triples correction of CCSD(T) are understandably important in a species formed from doublet OH and triplet O_2. In a study of the HOOO anion, Cremer and coworkers stated that in addition to a basis set of at least triple-ζ quality, diffuse functions and *f*-type polarization functions should be included. The cc-pVQZ and ANO1 basis sets used to determine the HOOO geometries for the calculation of the dissociation energy (see chapter 2), the anharmonic frequencies (chapter 3) and the potential curves (above) include *f* functions and in the calculation of the dissociation energy diffuse functions were included. A brief examination of the effect of diffuse functions on the equilibrium structure of *trans*-HOOO will follow below.

The use of a basis set that includes diffuse functions does allow for the description of a central OO bond length which is slightly longer, leaving the

that of the *trans* conformer by approximately 50 cm^{-1}. The experimentally observed band assigned to the OH stretching mode in the *cis* conformer lacks rotational structure which could confirm the assignment and is within 10 cm^{-1} of the *trans* band.

other parameters relatively unaffected at the CCSD(T) level of theory. The significant extension of the central OO bond seen when diffuse functions are added to a basis set of triple-ζ quality, approximately 0.02 Å is not increased, and in fact slightly decreases, with the additional diffuse functions of the d-aug-cc-pVTZ basis set. With a basis set of quadruple-ζ quality the effect of the addition of diffuse functions on the central OO bond length is not as great, the difference being less than 0.005 Å, at the CCSD(T) level of theory. However, at the EOMIP-CCSD* level of theory, the effect is greater.

Use of the equation-of-motion method extends the central OO bond significantly with an accompanying decrease in the terminal OO bond length. In calculations at the CCSDT level with the cc-pVTZ basis set a slightly longer central OO bond is obtained than at the CCSD(T) level[94] due to increased correlation. In the weakly bound *trans*-HONO molecule electron correlation at the CCSDTQ level was required to obtain a proper treatment of the central NO bond.[147] It was previously stated that as CCSD(T)/cc-pVQZ equilibrium structure for the isoelectronic FOO is consistent with the experimentally derived structure when vibrational effects are accounted for, it would be difficult to justify the need for additional correlation or multi-reference treatment for HOOO.[94] The similarity of the FOO structures determined with the standard and equation-of-motion coupled-cluster methods suggests that a multi-reference approach is not necessary for a proper description of the FOO system. The relatively large differences in the central OO distance of HOOO contradicts the statement that standard coupled cluster theory at the CCSD(T) level

properly describes HOOO as well.

The results here do not provide a definitive equilibrium structure for *trans*-HOOO, and any potential equilibrium structure cannot be directly compared to the structural parameters obtained experimentally[40] without vibrational corrections from a quality anharmonic force field,but some possibly important factors in the calculation of an equilibrium structure for *trans*-HOOO may be noted. Treatment of high-level dynamic correlation at the CCSDTQ level or nondynamic correlation through equation-of-motion methods should be considered. Diffuse functions may be required to obtain an accurate central OO bond.

Table 4.1: Equilibrium structural parameters for XOO (X = OH and F) and dissociation fragments calculated at the CCSD(T)/cc-pVQZ level of theory. For HOOO, the *cis* and *trans* conformers and an approximate torsional transition state are included.

molecular parameter	*cis*[a,b]	tor. TS[a,c]	*trans*[a,b]	$OH + O_2$[a,b]	FOO[a,b]
OO distance	1.244	1.237	1.226	1.206	1.190
XO distance	1.538	1.568	1.584		1.630
XOO angle	111.7	111.4	109.8		110.9
OH distance	0.970	0.966	0.966	0.968	
OOH angle	97.1	97.6	97.2		

[a]Distances in Ångströms and angles in degrees. [b]Root mean square deviation of the molecular energy gradient less than 10^{-5} hartree $bohr^{-1}$. [c]Root mean square deviation of the molecular energy gradient less than 10^{-5} Hartree $Bohr^{-1}$, except along the torsion, which was not optimized but fixed at 80°.

Table 4.2: Equilibrium structural parameters for XOO (X = OH and F) and dissociation fragments calculated at the EOMIP-CCSD*/cc-pVQZ (fc) level of theory. For HOOO, the *cis* and *trans* conformers, an approximate torsional transition state and the dissociation transition state of the *trans* conformer are included.

molecular parameter	*cis*[a,b]	tor. TS[a,c]	*trans*[a,b]	dis. TS[a,b]	$OH + O_2$[a,b]	FOO[a,b]
OO distance	1.231	1.222	1.215	1.187	1.197[d]	1.187
XO distance	1.562	1.613	1.618	2.072		1.625
XOO angle	112.3	111.7	110.0	112.1		110.8
OH distance	0.968	0.965	0.966	0.968	0.969	
OOH angle	97.0	96.7	96.8	91.8		

[a]Distances in Ångströms and angles in degrees. [b]Root mean square deviation of the molecular energy gradient less than 10^{-8} Hartree $Bohr^{-1}$. [c]Root mean square deviation of the molecular energy gradient less than 10^{-5} Hartree $Bohr^{-1}$, except along the torsion, which was not optimized but fixed at 80°. [d]Optimized at the CCSD/cc-pVQZ level of theory.

Table 4.3: Equilibrium structural parameters for XOO (X = OH and F) and calculated at the CCSD(T)/ANO1 level of theory. For HOOO, the *cis* and *trans* conformers and an approximate torsional transition state are included.

molecular parameter	*cis*[a,b]	tor. TS[a,b]	*trans*[a,b]	FOO[a,b]
OO distance	1.253	1.243	1.231	1.198
XO distance	1.536	1.585	1.605	1.641
XOO angle	111.6	111.4	109.7	110.9
OH distance	0.974	0.970	0.971	
OOH angle	97.2	97.2	96.9	

[a]Distances in Ångströms and angles in degrees. [b]Root mean square deviation of the molecular energy gradient less than 10^{-10} Hartree Bohr^{-1}. [c]Root mean square deviation of the molecular energy gradient less than 10^{-10} Hartree Bohr^{-1}, except along the torsion, which was not optimized but fixed at 80°.

Table 4.4: Equilibrium structural parameters for XOO (X = OH and F) and calculated at the EOMIP-CCSD*/ANO1 level of theory. For HOOO, the *cis* and *trans* conformers and an approximate torsional transition state are included.

molecular parameter	*cis*[a,b]	tor. TS[a,b]	*trans*[a,b]	FOO[a,b]
OO distance	1.236	1.228	1.220	1.193
XO distance	1.568	1.615	1.624	1.632
XOO angle	112.2	111.6	109.9	110.8
OH distance	0.971	0.968	0.969	
OOH angle	97.0	96.7	96.7	

[a]Distances in Ångströms and angles in degrees. [b]Root mean square deviation of the molecular energy gradient less than 10^{-9} Hartree Bohr^{-1}. [c]Root mean square deviation of the molecular energy gradient less than 10^{-8} Hartree Bohr^{-1}, except along the torsion, which was not optimized but fixed at 80°.

Table 4.5: Harmonic frequencies of *cis* and *trans*-HOOO, as well as an approximate torsional transition state, at the CCSD(T)/ANO1 level of theory.

mode[a]	*cis*[b]	TS[b,c]	*trans*[b]
ω_1	3707	3757	3758
ω_2	1374	1284	1370
ω_3	1220	1194	1184
ω_4	642	603	573
ω_5	380	319	328
ZPE	3662	3578	3606

[a]The torsional mode [ω_6] was not used in the calculation of the zero-point energy for the construction of the vibrationally adiabatic torsional potential. [b]In units of cm^{-1}. [c]The HOOO dihedral was fixed at 80°.

Table 4.6: Harmonic frequencies of *cis* and *trans*-HOOO, as well as an approximate torsional transition state, at the EOMIP-CCSD*/ANO1 (fc) level of theory.

mode[a]	*cis*[b]	TS[b,c]	*trans*[b]
ω_1	3743	3785	3785
ω_2	1421	1375	1438
ω_3	1271	1174	1188
ω_4	629	597	572
ω_5	370	338	355
ZPE	3717	3635	3669

[a]The torsional mode [ω_6] was not used in the calculation of the zero-point energy for the construction of the vibrationally adiabatic torsional potential. [b]In units of cm^{-1}. [c]The HOOO dihedral was fixed at 80°.

Table 4.7: Equilibrium structural parameters for *trans*-HOOO calculated at the CCSD(T) level with the cc-pVXZ [X = T,Q,5], aug-cc-pVXZ [X = T,Q] and d-aug-cc-pVTZ basis sets.

molecular parameter[a]	cc-pVTZ	cc-pVQZ	cc-pV5Z
terminal OO distance	1.233	1.227	1.226
central OO distance	1.590	1.589	1.586
OOO angle	109.8	109.8	109.7
OH distance	0.969	0.968	0.968
OOH angle	96.8	97.1	97.3
	aug-cc-pVTZ	aug-cc-pVQZ	
terminal OO distance	1.230[b]	1.226	
central OO distance	1.607[c]	1.594	
OOO angle	109.7[d]	109.8	
OH distance	0.972[d]	0.969	
OOH angle	97.1[d]	97.3	

[a]Distances in Ångströms and angles in degrees. [b]With d-aug-cc-pVTZ: 1.231 Å. [c]With d-aug-cc-pVTZ: 1.603 Å. [d]With d-aug-cc-pVTZ: unchanged.

Table 4.8: Equilibrium structural parameters for *trans*-HOOO calculated at the EOMIP-CCSD* level with the cc-pVXZ [X = T,Q] and aug-cc-pVXZ [X = T,Q] basis sets.

molecular parameter[a]	cc-pVTZ	cc-pVQZ
terminal OO distance	1.221	1.215
central OO distance	1.614	1.618
OOO angle	110.0	110.0
OH distance	0.967	0.966
OOH angle	96.5	96.8
	aug-cc-pVTZ	aug-cc-pVQZ
terminal OO distance	1.218	1.213
central OO distance	1.656	1.649
OOO angle	109.9	110.0
OH distance	0.969	0.966
OOH angle	96.5	96.6

[a]Distances in Ångströms and angles in degrees.

Chapter 5

Summary

This work provided predictions for the vibrational transitions of two HOONO isomers that aided the assignment of experimental spectra. Calculations also confirmed the experimentally determined dissociation energies for these species. Agreement between theory and experiment for *trans*-HOOO is more difficult to obtain. The theoretical prediction provided here, that *trans*-HOOO is only bound by approximately 2.5 kcal mol^{-1} relative to dissociation to OH and O_2, has very recently been supported experimentally. This work indicates that significant concentrations of *trans*-HOOO are not present in Earth's atmosphere contradicting previous claims.

5.1 Dissociation Energies

A series of calculations were carried out to predict the stability of the HOONO and HOOO conformers relative to dissociation. The relative importance of high-level correlation contributions, extrapolation to the infinite basis set limit and corrections for other factors such as the zero-point energy is greater when calculating the small dissociation energies of weakly bound species. The theoretical dissociation energies for *trans,perp* and *cis,cis-*

HOONO (15.9 and 19.2 kcal mol^{-1}, respectively, for HOONO $\rightarrow$ OH + NO_2) confirmed the experimental determinations, and provided additional predictions (23.4 and 26.7 kcal mol^{-1}, respectively, for HOONO $\rightarrow$ OH + NO_2). The dissociation energy predicted here is consistent with an early experimental value in that the calculated value (2.5 kcal mol^{-1}) is below the experimentally determined upper bound (5.3 kcal mol^{-1}), but the assumption that difference between the experimental upper bound and the true dissociation energy is small is not supported by this work. The theoretical prediction that the *trans*-HOOO radical is significantly less stable than previously inferred from experiment is consistent with a recently published kinetics study which found that *trans*-HOOO is stable relative to dissociation by 3.0 kcal mol^{-1}.

5.2 Spectroscopic Features and Constants

Through the calculation of anharmonic force fields using high-level quantum-chemical methods, the prediction of vibrational transition energies for the *trans,perp* and *cis,cis* conformers of HOONO, *cis,cis*-DOONO and the *trans* conformer of HOOO and DOOO was possible. The predictions for HOONO and DOONO were used to aid the assignment of experimental spectra and demonstrated the accuracy of these methods. For multi-quantum vibrational transitions observed in the gas-phase, the differences between predicted and experimental values were less than 25 cm^{-1} for both conformers of HOONO and the *cis,cis* conformer of DOONO. Some of the fundamental transitions observed in a solid matrix appear to be perturbed by the surroundings,

but in most cases the agreement was better than 20 cm^{-1}. The *cis,perp* conformer of HOONO forms a shelf in the torsional potential of *cis,cis*-HOONO. This deviation from harmonic behavior presents a slight challenge to the VPT2 description of the potential surface. The very low frequency torsion in the HOOO molecule presents a greater challenge. Some of the initial work to address this through examination of the torsional potential is presented here (see chapter 4 and section 5.3 below) and work is ongoing.[146]

5.3 HOOO Potential Curves and Structures

An examination of the minimum energy path to dissociation for *trans*-HOOO suggested that a barrier to dissociation may be the cause of the difference between the experimental upper bound to the dissociation energy and the predicted true bond energy. However, at higher levels of theory this barrier may become insignificant. The recently published kinetics study suggests that there is no barrier to the formation of HOOO from OH and O_2. The lack of a barrier does not rule out the possibility of an impulsive dissociation in which the excess energy is channeled into rotational excitation of one fragment rather than the other or relative kinetic energy. Preferential rotational excitation was observed in the HF dimer[144] in the absence of a barrier to dissociation.[145] As a result of impulsive dissociation, some portion of the excess energy following dissociation of HOOO due to vibrational excitation would not be accounted for if only the rotational excitation of the OH fragment is monitored.

A torsional potential for HOOO has been constructed with care as it is

important to treat the nondynamic correlation, or multi-reference character, to obtain a qualitatively correct *cis*-*trans* energy difference. The torsional barrier is low, approximately 200 to 250 cm^{-1}relative to the *trans* minimum. Preliminary, results suggest that calculation of the torsional levels from a potential curve such as this may begin to resolve the discrepancies between experimentally observed and theoretically predicted vibrational transition energies for *trans*-HOOO. The torsional frequencies assigned to the *cis* conformer are more difficult to align with the theoretical description.[146]

5.4 Relevance to Atmospheric Chemistry

The prediction that the binding energy of OH and O_2 is approximately half that assumed elsewhere, has a large impact on the probability that significant quantities of HOOO will form in Earth's atmosphere — with a binding energy of approximately 3 kcal mol^{-1}, very little HOOO will form.[97] Formation of the more stable HOONO isomers will likely occur in the atmosphere, but the significance of these species lies in the likelihood for dissociation and reformation of the OH and NO_2 radicals. The formation of HOONO is in competition with the formation of nitric acid, which is a sink for these radical species. Recent studies support the formation of nitric acid from HOO and NO with HOONO serving as an intermediate.[16] Accurate theoretical predictions of the HOO + NO $\rightarrow$ HOONO energy may become useful as there has not yet been an accurate experimental determination.

5.5 Proposed Experiments

Continued investigation of HOONO as an intermediate in the formation of nitric acid from HOO and NO will likely have greater significance in atmospheric chemistry as the prediction of reactive radical concentrations is a continuing goal. However, to this researcher, the reason for the difference in the observed upper bound to the dissociation energy of *trans*-HOOO and the predicted bond energy is a more interesting puzzle. If the disagreement is due to a barrier to dissociation, a possibility that disputed by the researches conducting the recent kinetics experiments, the rate of dissociation would be effected. A determination of the kinetic energy of the OH and O_2 fragments following dissociation of *trans*-HOOO through vibrational excitation would provide a refinement of the upper bound to the dissociation energy. However, without an examination of the populated rotational levels of the O_2 fragment as well, a portion of the excess energy could remain unaccounted for following vibrational excitation and dissociation.

The electron photodetachment of the HOOO anion could provide some insight into this puzzling system.[148] The vibronic structure of the photoelectron spectrum would give another view of the HOOO vibrations and possibly the dissociation energy. Calculations are underway to predict the ionization energy of the HOOO anion and determine the Frank-Condon factors for simulation of the photoelectron spectrum.

5.6 Proposed Theoretical Studies

The description of the vibrational spectrum of HOOO is a challenging problem as the system defies the harmonic approximation and the complex electronic structure requires high-level quantum chemical methods and a fairly large basis set for a proper description of the potential energy surface. The fitting of an analytic curve along the torsional potential for the determination of the torsional levels is a first step to calculating the fundamental frequencies of HOOO, but the reason for the disagreement between theory and experiment for three of the in-plane modes (the HOO and OOO bending modes and the central OO stretching mode) remains unknown. A three-dimensional potential surface along the coordinates in question may allow for the determination of these fundamental frequencies. However, the HOO bending mode does appear to be strongly coupled to the OH stretching mode and the HOOO torsional mode and all three modes in question appear to be coupled to the OO stretching mode so a six-dimensional surface may be required.

Though the HOONO system is largely well-behaved compared to the HOOO system, some additional work could refine the results presented here. A calculation of the full four-electron correlation contribution at the CCSDTQ level could be significant to the prediction of the dissociation energy of HOONO to HO_2 and NO. The estimated four-electron contribution was relatively large and as there is no experimental determination of the dissociation energy of HOONO to HO_2 + NO (other than the estimation from heats of formation), a precise theoretical determination could prove useful.

Appendices

Appendix A

HNO_3 Equilibrium Structures

This appendix is a collection of equilibrium structures for the HNO_3 system determined for the calculations presented in chapters 2 and 3.

A.1 CCSD(T)/cc-pVQZ

The thermochemical calculations presented in chapter 2 consist of many calculations of the energy at various levels of theory to determine various contributions to the total dissociation energy. Each calculation was carried out the same molecular geometry, with the expection of the zero-point energy contribution. The molecular parameters of each molecule were optimized at the CCSD(T)/cc-pVQZ level of theory. For each of the close-shell species an RHF reference wavefunction was used and for the open-shell species a UHF reference wavefunction was used. The molecular geometries of *cis,cis* and *trans,perp*-HOONO, as well as the dissociation fragments, are in table A.1. The CCSD(T)/cc-pVQZ equilibrium structure of the HOONO conformers were also used in the determination of vibrationally-corrected rotational constants of chapter 3.

A.2 CCSD(T)/ANO1

Prior to the calculation of the anharmonic force fields for the determination of the vibrational frequencies presented in chapter 3, the molecular parameters of the two HOONO conformers, *trans,perp* and *cis,cis* were optimized at the CCSD(T)/ANO1 level of theory. These equilibrium structures are presented in table A.2. As the HOONO molecule is a closed-shell species, an RHF reference wavefunction was employed. Core electrons were excluded from the correlation treatment in these CCSD(T)/ANO1 calculations.

Table A.1: Equilibrium structual parameters for *trans,perp* and *cis,cis*-HOONO, as well as the dissociation fragments, calculated at the CCSD(T)/cc-pVQZ level of theory.

molecular parameter	*tp*[a]	*cc*[a]	$OH + NO_2$[a]	$HO_2 + NO$[a]
terminal NO distance	1.458	1.374	1.193	1.148
central ON distance	1.423	1.426	1.193	
ONO angle	105.8	113.2	134.3	
OO distance	1.164	1.186		1.328
OON angle	108.9	114.5		
ONOO dihedral	176.9	0		
OH distance	0.963	0.979	0.968	0.969
OOH angle	101.2	100.4		104.3
HOOO dihedral	98.2	0		

[a]Distances in Ångströms and angles in degrees. Root mean square deviation of the molecular energy gradient less than 10^{-5} Hartree $Bohr^{-1}$.

Table A.2: Equilibrium structual parameters for *trans,perp* and *cis,cis*-HOONO calculated at the CCSD(T)/ANO1 (fc) level of theory.

molecular parameter	*tp*[a]	*cc*[a]
terminal NO distance	1.467	1.381
central ON distance	1.433	1.436
ONO angle	105.6	113.1
OO distance	1.170	1.193
OON angle	108.6	114.4
ONOO dihedral	176.8	0
OH distance	0.967	0.983
OOH angle	100.9	100.0
HOOO dihedral	98.3	0

[a]Distances in Ångströms and angles in degrees. Root mean square deviation of the molecular energy gradient less than 10^{-10} Hartree $Bohr^{-1}$.

Appendix B

Almlöf/Taylor vs. Dunning Basis Sets

The harmonic frequencies calculated with a series of ANO and Dunning basis are included below to demonstrate the relative convergence. Fundamental frequencies are included as well and compared to experimental values.

Table B.1: Harmonic frequencies of the propargyl radical calculated with the ANO basis sets at the CCSD(T) level (fc) of theory.

mode	ANO0[a]	ANO1[a]	ANO2[a]
ω_1	3460	3460	3455
ω_2	3171	3165	3164
ω_3	1969	1983	1983
ω_4	1463	1465	1467
ω_5	1050	1058	1060
ω_6	638	667	668
ω_7	447	477	482
ω_8	367	389	389
ω_9	3280	3266	3267
ω_{10}	1031	1034	1034
ω_{11}	594	616	618
ω_{12}	314	330	331
δ^b_{max}	36	6	
δ^c_{std}	15	2	

[a]In units of cm^{-1}. [b]Maximum absolute error relative to ANO2 values. [c]Standard deviation of error relative ANO2 values.

Table B.2: Harmonic frequencies of the propargyl radical calculated with the Dunning basis sets at the CCSD(T) level (fc) of theory.

mode	cc-pVDZ[a]	cc-pVTZ[a]	cc-pVQZ[a]
ω_1	3448	3457	3452
ω_2	3164	3162	3164
ω_3	1969	1979	1983
ω_4	1457	1471	1468
ω_5	1056	1056	1060
ω_6	620	661	668
ω_7	423	448	472
ω_8	348	376	385
ω_9	3274	3263	3266
ω_{10}	1026	1034	1035
ω_{11}	571	593	613
ω_{12}	312	325	330
δ^b_{max}	69	44	
δ^c_{std}	23	12	

[a]In units of cm^{-1}. [b]Maximum absolute error relative to cc-pVQZ values. [c]Standard deviation of error relative cc-pVQZ values.

Table B.3: Harmonic frequencies of nitric acid calculated with the ANO basis sets at the CCSD(T) level (fc) of theory.

mode	ANO0[a]	ANO1[a]	ANO2[a]
ω_1	3748	3750	3746
ω_2	1768	1770	1763
ω_3	1347	1355	1358
ω_4	1324	1337	1338
ω_5	882	914	919
ω_6	637	664	669
ω_7	576	589	592
ω_8	769	778	781
ω_9	467	485	490
δ^b_{max}	37	6	
δ^c_{std}	14	4	

[a]In units of cm^{-1}. [b]Maximum absolute error relative to ANO2 values. [c]Standard deviation of error relative ANO2 values.

Table B.4: Harmonic frequencies of nitric acid calculated with the Dunning basis sets at the CCSD(T) level (fc) of theory.

mode	cc-pVDZ[a]	cc-pVTZ[a]	cc-pVQZ[a]
ω_1	3741	3753	3752
ω_2	1795	1772	1769
ω_3	1366	1358	1362
ω_4	1345	1338	1342
ω_5	901	914	920
ω_6	651	664	669
ω_7	580	588	593
ω_8	765	780	784
ω_9	477	486	491
δ^b_{max}	26	6	
δ^c_{std}	15	3	

[a]In units of cm^{-1}. [b]Maximum absolute error relative to cc-pVQZ values. [c]Standard deviation of error relative cc-pVQZ values.

Table B.5: Fundamental frequencies of the propargyl radical calculated with the ANO basis sets at the CCSD(T) level (fc) of theory compared to experimental values.

mode	ANO0[a]	ANO1[a]	ANO2[a,b]	exp[a,c]
ν_1	3321	3323	3318	3322
ν_2	3040	3037	3036	3028
ν_3	1906	1923	1923	1935
ν_4	1438	1444	1445	1440
ν_5	1043	1055	1056	1061
ν_6	665	689	690	687
ν_7	447	481	487	490
ν_8	380	398	398	396
ν_9	3126	3116	3117	3124
ν_{10}	1014	1018	1019	1017
ν_{11}	585	612	614	620
ν_{12}	321	338	339	352
δ^d_{max}	43	14	13	
δ^e_{std}	17	7	7	

[a]In units of cm^{-1}. [b]VPT2 corrections calculated with the ANO1 basis. [c]Ref. 115. [d]Maximum absolute error relative to Ref. 115 values. [e]Standard deviation of error relative to Ref. 115 values.

Table B.6: Fundamental frequencies of the propargyl radical calculated with the Dunning basis sets at the CCSD(T) level (fc) of theory compared to experimental values.

mode	cc-pVDZ[a]	cc-pVTZ[a]	cc-pVQZ[a,b]	exp[a,c]
ν_1	3306	3319	3314	3322
ν_2	3030	3035	3037	3028
ν_3	1905	1918	1921	1935
ν_4	1429	1447	1444	1440
ν_5	1047	1051	1055	1061
ν_6	654	690	697	687
ν_7	417	518	541	490
ν_8	373	441	451	396
ν_9	3117	3113	3116	3124
ν_{10}	1008	1020	1020	1017
ν_{11}	554	629	648	620
ν_{12}	314	342	347	352
δ^d_{max}	73	45	55	
δ^e_{std}	23	18	23	

[a]In units of cm^{-1}. [b]VPT2 corrections calculated with the cc-pVTZ basis. [c]Ref. 115. [d]Maximum absolute error relative to Ref. 115 values. [e]Standard deviation of error relative to Ref. 115 values.

Table B.7: Fundamental frequencies of nitric acid calculated with the ANO basis sets at the CCSD(T) level (fc) of theory compared to experimental values.

mode	ANO0[a]	ANO1[a]	ANO2[a,b]	exp[a,c]
ν_1	3557	3561	3556	3551
ν_2	1721	1725	1719	1710
ν_3	1319	1327	1330	1326
ν_4	1292	1310	1311	1303
ν_5	858	886	892	879
ν_6	617	647	651	647
ν_7	563	577	581	580
ν_8	752	763	767	763
ν_9	434	454	459	458
δ^d_{max}	30	16	12	
δ^e_{std}	14	7	4	

[a]In units of cm^{-1}. [b]VPT2 corrections calculated with the ANO1 basis. [c]Ref. 120. [d]Maximum absolute error relative to Ref. 120 values. [e]Standard deviation of error relative to Ref. 120 values.

Table B.8: Fundamental frequencies of nitric acid calculated with the Dunning basis sets at the CCSD(T) level (fc) of theory compared to experimental values.

mode	cc-pVDZ[a]	cc-pVTZ[a]	cc-pVQZ[a,b]	exp[a,c]
ν_1	3550	3567	3566	3551
ν_2	1746	1728	1724	1710
ν_3	1332	1331	1335	1326
ν_4	1318	1313	1317	1303
ν_5	873	888	894	879
ν_6	631	647	653	647
ν_7	568	577	582	580
ν_8	750	765	770	763
ν_9	446	456	461	458
δ^d_{max}	37	18	15	
δ^e_{std}	17	8	5	

[a]In units of cm^{-1}. [b]VPT2 corrections calculated with the cc-pVTZ basis. [c]Ref. 120. [d]Maximum absolute error relative to Ref. 120 values. [e]Standard deviation of error relative to Ref. 120 values.

Bibliography

1. Finlayson-Pitts, B. J.; Pitts, J. N. *Chemistry of the Upper and Lower Atmosphere*; Academic Press: New York, **2000**.

2. Wayne, R. P. *Chemistry of Atmospheres*; Clarendon Press: Oxford, **1991**.

3. Robertshaw, J. S.; Smith, I. W. M. *Journal of Physical Chemistry* **1982**, *86*, 785–790.

4. Golden, D. M.; Smith, G. P. *Journal of Physical Chemistry A* **2000**, *104*, 3991–3997.

5. Donahue, N. M.; Mohrschladt, R.; Dransfield, T. J.; Anderson, J. G.; Dubey, M. K. *Journal of Physical Chemistry A* **2000**, *105*, 1515–1520.

6. Hippler, H.; Nasterlack, S.; Striebel, F. *Physical Chemistry Chemical Physics* **2002**, *4*, 2959–2964.

7. Nizkorodov, S. A.; Wennberg, P. O. *Journal of Physical Chemistry A* **2002**, *106*, 855–859.

8. Pollack, I. B.; Konen, I. M.; Li, E. X. J.; Lester, M. I. *Journal of Chemical Physics* **2003**, *119*, 9981–9984.

9. Matthews, J.; Sinha, A.; Francisco, J. S. *Journal of Chemical Physics* **2004**, *120*, 10543–10553.

10. Golden, D. M.; Barker, J. R.; Lohr, L. L. *Journal of Physical Chemistry A* **2003**, *107*, 11057–11071.

11. Zhang, J.; Donahue, N. M. *Journal of Physical Chemistry A* **2006**, *110*, 6898–6911.

12. D'Ottone, L.; Bauer, D.; Campuzano-Jost, P.; Fardy, M.; Hynes, A. J. *Faraday Discussions* **2005**, *130*, 111–123.

13. Srinivasan, N. K.; Su, M.-C.; Sutherland, J. W.; Michael, J. V.; Ruscic, B. *Journal of Physical Chemistry A* **2006**, *110*, 6602–6607.

14. Hippler, H.; Krasteva, N.; Nasterlack, S.; Striebel, F. *Journal of Physical Chemistry A* **2006**, *110*, 6781–6788.

15. Butkovskaya, N. I.; Kukui, A.; Pouvesle, N.; Le Bras, G. *Journal of Physical Chemistry A* **2005**, *109*, 6509–6520.

16. Butkovskaya, N.; Rayez, M.-T.; Rayez, J.-C.; Kukui, A.; Le Bras, G. *Journal of Physical Chemistry A* **2009**, *113*, 11327–11342.

17. Butkovskaya, N.; Kukui, A.; Le Bras, G. *Journal of Physical Chemistry A* **2007**, *111*, 9047–9053.

18. Cariolle, D.; Evans, M. J.; Chipperfield, M. P.; Butkovskaya, N.; Kukui, A.; Le Bras, G. *Atmospheric Chemistry and Physics* **2008**, *8*, 4061–4068.

19. McGrath, M. P.; Francl, M. M.; Rowland, F. S.; Hehre, W. J. *Journal of Physical Chemistry* **1988**, *92*, 5352–5357.

20. Zhang, X.; Nimlos, M. R.; Ellison, G. B.; Varner, M. E.; Stanton, J. F. *Journal of Chemical Physics* **2006**, *124*, 084305.

21. Chen, M. M. L.; Wetmore, R. W.; Schaefer III, H. F. *Journal of Chemical Physics* **1981**, *74*, 2938–2944.

22. Dupuis, M.; Fitzgerald, G.; Hammond, B.; Lester, W. A.; Schaefer III, H. F. *Journal of Chemical Physics* **1986**, *84*, 2691–2697.

23. Dodd, J. A.; Lipson, S. J.; Lowell, J. R.; Armstrong, P. S.; Blumberg, W. A. M.; Nadile, R. M.; Adlergolden, S. M.; Marinelli, W. J.; Holtzclaw, K. W.; Green, B. D. *Journal of Geophysical Research - Atmospheres* **1994**, *99*, 3559–3585.

24. Varandas, A.; Yu, H. *Molecular Physics* **1997**, *91*, 301–318.

25. Dodd, J. A.; Lockwood, R. B.; Hwang, E. S.; Miller, S. M.; Lipson, S. J. *Journal of Physical Chemistry A* **1999**, *103*, 7834–7842.

26. Fabian, W. M. F.; Kalcher, J.; Janoschek, R. *Theoretical Chemistry Accounts* **2005**, *114*, 182–188.

27. Sridharan, U. C.; Klein, F. S.; Kaufman, F. *Journal of Chemical Physics* **1985**, *82*, 592–593.

28. Setokuchi, O.; Sato, M.; Matuzawa, S. *Journal of Physical Chemistry A* **2000**, *104*, 3204–3210.

29. Silveira, D. M.; Caridade, P. J. S. B.; Varandas, A. J. C. *Journal of Physical Chemistry A* **2004**, *108*, 8721–8730.

30. McCabe, D. C.; Smith, I. W. M.; Rajakumar, B.; Ravishankara, A. R. *Chemical Physics Letters* **2006**, *421*, 111–117.

31. Vincent, M. A.; Hillier, I. H.; Burton, N. A. *Chemical Physics Letters* **1995**, *233*, 111–114.

32. Vincent, M.; Burton, N.; Hillier, I. *Molecular Physics* **1996**, *87*, 945–959.

33. Jungkamp, T.; Seinfeld, J. *Chemical Physics Letters* **1996**, *257*, 15–22.

34. Blint, R. J.; Newton, M. D. *Journal of Chemical Physics* **1973**, *59*, 6220–6228.

35. Mathisen, K. B.; Gropen, O.; Skancke, P. N.; Wahlgren, U. *Acta Chemica Scandinavica A* **1983**, *37*, 817–822.

36. Mathisen, K. B.; Siegbahn, P. E. M. *Chemical Physics* **1984**, *90*, 225–230.

37. Speranza, M. *Inorganic Chemistry* **1996**, *35*, 6140–6151.

38. Cacace, F.; Speranza, M. *Science* **1994**, *265*, 208–209.

39. Cacace, F.; de Petris, C.; Pepi, F.; Troiani, A. *Science* **1999**, *285*, 81–82.

40. Suma, K.; Sumiyoshi, Y.; Endo, Y. *Science* **2005**, *308*, 1885–1886.

41. Murray, C.; Derro, E. L.; Sechler, T. D.; Lester, M. I. *Journal of Physical Chemistry A* **2007**, *111*, 4727–4730.

42. Derro, E. L.; Sechler, T. D.; Murray, C.; Lester, M. I. *Journal of Physical Chemistry A* **2008**, *112*, 9269–9276.

43. Mansergas, A.; Anglada, J. M.; Olivella, S.; Ruiz-Lopez, M. F.; Martins-Costa, M. *Physical Chemistry Chemical Physics* **2007**, *9*, 5865–5873.

44. Braams, B. J.; Yu, H.-G. *Physical Chemistry Chemical Physics* **2008**, *10*, 3150–3155.

45. Denis, P. A.; Ornellas, F. R. *Journal of Physical Chemistry A* **2009**, *113*, 499–506.

46. Murray, C.; Derro, E. L.; Sechler, T. D.; Lester, M. I. *Accounts of Chemical Research* **2009**, *42*, 419–427.

47. Wennberg, P. O. *Nature* **2006**, *442*, 145–146.

48. Canty, T.; Pickett, H. M.; Salawitch, R. J.; Jucks, K. W.; Traub, W. A.; Waters, J. W. *Geophysical Research Letters* **2006**, *33*, 1–5.

49. Fehsenfeld, F.; Moseman, M.; Ferguson, E. *Journal of Chemical Physics* **1971**, *55*, 2115–2120.

50. Cheng, B. M.; Lee, J. W.; Lee, Y. P. *Journal of Physical Chemistry* **1991**, *95*, 2814–2817.

51. Troe, J. *International Journal of Chemical Kinetics* **2001**, *33*, 878–889.

52. Vaida, V.; Headrick, J. E. *Journal of Physical Chemistry A* **2000**, *104*, 5401–5412.

53. Ruscic, B.; Pinzon, R. E.; Morton, M. L.; von Laszevski, G.; Bittner, S. J.; Nijsure, S. G.; Amin, K. A.; Minkoff, M.; Wagner, A. F. *Journal of Physical Chemistry A* **2004**, *108*, 9979.

54. Ruscic, B.; Pinzon, R. E.; Morton, M. L.; Srinivasan, N. K.; Su, M.-C.; Sutherland, J. W.; Michael, J. V. *Journal of Physical Chemistry A* **2006**, *110*, 6592–6601.

55. Ruscic, B.; Feller, D.; Dixon, D. A.; Peterson, K. A.; Harding, L. B.; Asher, R. L.; Wagner, A. F. *Journal of Physical Chemistry A* **2000**, *105*, 1–4.

56. Flowers, B. A.; Szalay, P. G.; Stanton, J. F.; Kallay, M.; Gauss, J.; Csaszar, A. G. *Journal of Physical Chemistry A* **2004**, *108*, 3195–3199.

57. Tasi, G.; Izsak, R.; Matisz, G.; Csaszar, A. G.; Kallay, M.; Ruscic, B.; Stanton, J. F. *Chemical Physics Physical Chemistry* **2006**, *7*, 1664–1667.

58. Raghavachari, K.; Curtiss, L. A. In *Quantum-Mechanical Prediction of Thermochemical Data*, Cioslowski, J., Ed.; Kluwer: Netherlands, **2001**.

59. Petersson, G. A. In *Quantum-Mechanical Prediction of Thermochemical Data*, Cioslowski, J., Ed.; Kluwer: Netherlands, **2001**.

60. Martin, J. M. L.; Parthiban, S. In *Quantum-Mechanical Prediction of Thermochemical Data*, Cioslowski, J., Ed.; Kluwer: Netherlands, **2001**.

61. Schuurman, M. S.; Muir, S. R.; Allen, W. D.; Schaefer III, H. F. *Journal of Chemical Physics* **2004**, *120*, 11586–11599.

62. Karton, A.; Rabinovich, E.; Martin, J. M. L.; Ruscic, B. *Journal of Chemical Physics* **2006**, *125*, 144108.

63. Feller, D.; Peterson, K. A.; Dixon, D. A. *Journal of Chemical Physics* **2008**, *129*, 204105.

64. Tajti, A.; Szalay, P. G.; Császár, A. G.; Kállay, M.; Gauss, J.; Valeev, E. F.; Flowers, B. A.; Vázquez, J.; Stanton, J. F. *Journal of Chemical Physics* **2004**, *121*, 11599–11613.

65. Čížek, J. *The Journal of Chemical Physics* **1966**, *45*, 4256–4266.

66. Bartlett, R. J.; Stanton, J. F. In *Reviews of Computational Chemisty*, Lipkowitz, K. B. and Boyd, D. B., Eds.; VCH: New York, **1994**.

67. Crawford, T. D.; Schaefer III, H. F. In *Reviews of Computational Chemisty*, Lipkowitz, K. B. and Boyd, D. B., Eds.; VCH: New York, **1999**.

68. Gauss, J.; Tajti, A.; Kallay, M.; Stanton, J. F.; Szalay, P. G. *Journal of Chemical Physics* **2006**, *125*, 144111.

69. Helgaker, T.; Klopper, W.; Halkier, A.; Bak, K. L.; Jørgensen, P.; Olsen, J. In *Quantum-Mechanical Prediction of Thermochemical Data*, Cioslowski, J., Ed.; Kluwer: Netherlands, **2001**.

70. Purvis, G. D.; Bartlett, R. J. *Journal of Chemical Physics* **1982**, *76*, 1910.

71. Raghavachari, K.; Trucks, G. W.; Pople, J. A.; Head-Gordon, M. *Chemical Physics Letters* **1989**, *157*, 479 – 483.

72. Karton, A.; Rabinovich, E.; Martin, J. M. L.; Ruscic, B. *Journal of Chemical Physics* **2006**, *125*, 1144108.

73. Harding, M. E.; Vazquez, J.; Ruscic, B.; Wilson, A. K.; Gauss, J.; Stanton, J. F. *Journal of Chemical Physics* **2008**, *128*, 114111.

74. Almlöf, J.; Taylor, P. R. *Journal of Chemical Physics* **1987**, *86*, 4070–4077.

75. Cramer, C. J. *Essentials of Computational Chemistry*; Wiley: Chichester, **2004**.

76. Löwdin, P.-O. *Physical Review* **1955**, *97*, 1509–1520.

77. Vazquez, J.; Stanton, J. F. *Molecular Physics* **2006**, *104*, 377–388.

78. Dunning, Jr., T. H. *Journal of Chemical Physics* **1989**, *90*, 1007–1023.

79. Wilson, A. K.; van Mourik, T.; Dunning, Jr., T. H. *Journal of Molecular Structure* **1996**, *388*, 339–349.

80. Feller, D. *Journal of Chemical Physics* **1992**, *96*, 6104–6114.

81. Helgaker, T.; Klopper, W.; Koch, H.; Noga, J. *Journal of Chemical Physics* **1997**, *106*, 9639–9646.

82. Kendall, R. A.; Dunning, Jr., T. H.; Harrison, R. J. *Journal of Chemical Physics* **1992**, *96*, 6796–6806.

83. Pyykko, P. *Chemical Physics* **1988**, *88*, 563–594.

84. Boese, A. D.; Oren, M.; Atasoylu, O.; Martin, J. M. L.; Kallay, M.; Gauss, J. *Journal of Chemical Physics* **2004**, *120*, 4129–4141.

85. Valeev, E. F.; Sherrill, C. D. *Journal of Chemical Physics* **2003**, *118*, 3921–3927.

86. Noga, J.; Bartlett, R. J. *Journal of Chemical Physics* **1987**, *86*, 7041–7050.

87. Scuseria, G. E.; Schaefer III, H. F. *Chemical Physics Letters* **1988**, *152*, 382–386.

88. Watts, J. D.; Bartlett, R. J. *Journal of Chemical Physics* **1990**, *93*, 6104–6105.

89. Bomble, Y. J.; Stanton, J. F.; Kállay, M.; Gauss, J. *Journal of Chemical Physics* **2005**, *123*, 054101.

90. Kállay, M.; Gauss, J. *Journal of Chemical Physics* **2005**, *123*, 214105.

91. Tilson, J.; Ermler, W.; Pitzer, R. *Computer Physics Communications* **2000**, *128*, 128–138.

92. Szalay, P. G.; Vazquez, J.; Simmons, C.; Stanton, J. F. *The Journal of Chemical Physics* **2004**, *121*, 7624–7631.

93. Kraka, E.; Konkoli, Z.; Cremer, D.; Fowler, J.; Schaefer, H. *Journal of the American Chemical Society* **1996**, *118*, 10595–10608.

94. Varner, M. E.; Harding, M. E.; Gauss, J.; Stanton, J. F. *Chemical Physics* **2008**, *346*, 53–55.

95. CFOUR, Coupled Cluster techniques for Computational Chemistry, a quantum-chemical program package by J. F. Stanton, J. Gauss, M. E. Harding, P. G. Szalay with contributions from A. A. Auer, R. J. Bartlett, U. Benedikt, C. Berger, D. E. Bernholdt, Y. J. Bomble, O. Christiansen, M. Heckert, O. Heun, C. Huber, D. Jonsson, J. Jusélius, K. Klein, W. J. Lauderdale, D. A. Matthews, T. Metzroth, D. P. O'Neill, D. R. Price, E. Prochnow, K. Ruud, F. Schiffmann, S. Stopkowicz, and the integral packages: MOLECULE (J. Almlöf and P. R. Taylor); PROPS (P. R. Taylor); ABACUS (T. Helgaker, H. J. Aa. Jensen, P. Jørgensen, and J. Olsen) and ECP routines by A. V. Mitin and C. van Wüllen. For the current version, see: www.cfour.de.

96. MRCC, a string-based quantum chemical program suite written by M. Kállay. See also: Kállay; M. Surján, P. R. *J. Chem. Phys.* **2001**, *115* 2945-2954. As well as: www.mrcc.hu.

97. Le Picard, S. D.; Tizniti, M.; Canosa, A.; Sims, I. R.; Smith, I. W. M. *Science* **2010**, *328*, 1258–1262.

98. Konen, I. M.; Pollack, I. B.; Li, E. X. J.; Lester, M. I.; Varner, M. E.; Stanton, J. F. *Journal of Chemical Physics* **2005**, *122*, 094320.

99. Feierabend, K. J.; Havey, D. K.; Varner, M. E.; Stanton, J. F.; Vaida, V. *Journal of Chemical Physics* **2006**, *124*, 124323.

100. Zhang, X.; Nimlos, M. R.; Ellison, G. B.; Varner, M. E.; Stanton, J. F. *Journal of Chemical Physics* **2007**, *126*, 174308.

101. Atkinson, R.; Baulch, D.; Cox, R.; Hampson, R.; Kerr, J.; Rossi, M.; Troe, J. *Journal of Physical and Chemical Reference Data* **1997**, *26*, 521–1011.

102. Wagman, D. D.; Evans, W. H.; Parker, V. B.; Schumm, R. H.; Halow, I.; Bailey, S. M.; Churney, K. L.; Nuttall, R. L. *Journal of Physical and Chemical Reference Data* **1982**, *11*, 1–&.

103. Kerr, J. A. In *CRC Handbook of Chemistry and Physics*, 75th ed., Lide, D. R., Ed.; CRC: Florida, **1994**.

104. McGrath, M. P.; Rowland, F. S. *Journal of Chemical Physics* **2005**, *122*, 134312.

105. Yu, H.; Varandas, A. *Chemical Physics Letters* **2001**, *334*, 173–178.

106. Denis, P.; Kieninger, M.; Ventura, O.; Cachau, R.; Diercksen, G. *Chemical Physics Letters* **2002**, *365*, 440–449.

107. Derro, E. L.; Murray, C.; Sechler, T. D.; Lester, M. I. *Journal of Physical Chemistry A* **2007**, *111*, 11592–11601.

108. Derro, E. L.; Sechler, T. D.; Murray, C.; Lester, M. I. *Journal of Chemical Physics* **2008**, *128*, 244313.

109. Karton, A.; Parthiban, S.; Martin, J. M. L. *Journal of Physical Chemistry A* **2009**, *113*, 4802–4816.

110. Campuzano-Jost, P.; Croce, A. E.; Hippler, H.; Siefke, M.; Troe, J. *Journal of Chemical Physics* **1995**, *102*, 5317–5326.

111. Mills, I. M. In *Molecular Spectroscopy: Modern Research*, Rao, K. N. and Matthews, C. W., Eds.; Academic Press: New York, **1972**.

112. Matthews, J.; Sinha, A. *Journal of Chemical Physics* **2005**, *122*, 104313.

113. Burkholder, J. B.; Hammer, P. D.; Howard, C. J. *Journal of Physical Chemistry* **1987**, *91*, 2136–2144.

114. Nelander, B.; Engdahl, A.; Svensson, T. *Chemical Physics Letters* **2000**, *332*, 403–408.

115. Jochnowitz, E. B.; Zhang, X.; Nimlos, M. R.; Varner, M. E.; Stanton, J. F.; Ellison, G. B. *Journal of Physical Chemistry A* **2005**, *109*, 3812–3821.

116. Fry, J. L.; Nizkorodov, S. A.; Okumura, M.; Roehl, C. M.; Francisco, J. S.; Wennberg, P. O. *Journal of Chemical Physics* **2004**, *121*, 1432–1448.

117. Fry, J. L.; Drouin, B. J.; Miller, C. E. *Journal of Chemical Physics* **2006**, *124*, 084304.

118. Califano, S. *Vibrational States*; Wiley: London, **1976**.

119. Feierabend, K. J.; Havey, D. K.; Vaida, V. *Spectrochimica Acta A* **2004**, *60*, 2775–2781.

120. Perrin, A. *Spectrochimica Acta A* **1998**, *54*, 375–393.

121. Pauling, L. C.; Wilson, E. B. *Introduction to Quantum Mechanics*; McGraw-Hill: New York, **1935**.

122. Meal, J. H.; Polo, S. R. *Journal of Chemical Physics* **1956**, *24*, 1119–1125.

123. Stanton, J. F.; Lopreore, C. L.; Gauss, J. *Journal of Chemical Physics* **1998**, *108*, 7190–7196.

124. Konen, I. M.; Li, E. X. J.; Stephenson, T. A.; Lester, M. I. *Journal of Chemical Physics* **2005**, *123*, 204318.

125. Lo, W.-J.; Lee, Y. P. *Journal of Chemical Physics* **1994**, *101*, 5494–5499.

126. Bean, B. D.; Mollner, A. K.; Nizkorodov, S. A.; Nair, G.; Okumura, M.; Sander, S. P.; Peterson, K. A.; Francisco, J. S. *Journal of Physical Chemistry A* **2003**, *107*, 6974–6985.

127. McCoy, A. B.; Fry, J. L.; Francisco, J. S.; Mollner, A. K.; Okumura, M. *Journal of Chemical Physics* **2005**, *122*, 104311.

128. McCoy, A. B.; Sprague, M. K.; Okumura, M. *Journal of Physical Chemistry A* **2009**, *114*, 1324–1333.

129. Maciel, G. S.; Bitencourt, A. C. P.; Ragni, M.; Aquilanti, V. *Journal of Physical Chemistry A* **2007**, *111*, 12604–12610.

130. Zhang, X. *private communication.*

131. Yu, H.; Muckerman, J. *Journal of Molecular Spectroscopy* **2002**, *214*, 11–20.

132. Dutta, A.; Sherrill, C. D. *Journal of Chemical Physics* **2003**, *118*, 1610–1619.

133. Bomble, Y. J.; Saeh, J. C.; Stanton, J. F.; Szalay, P. G.; Kállay, M.; Gauss, J. *Journal of Chemical Physics* **2005**, *122*, 154107.

134. Allen, W. D.; Bodi, A.; Szalay, V.; Csaszar, A. G. *Journal of Chemical Physics* **2006**, *124*, 224310.

135. Manohar, P. U.; Stanton, J. F.; Krylov, A. I. *Journal of Chemical Physics* **2009**, *131*, 114112.

136. Saeh, J. C.; Stanton, J. F. *Journal of Chemical Physics* **1999**, *111*, 8275–8285.

137. Stanton, J. F.; Gauss, J. *Theoretica Chimica Acta* **1996**, *93*, 303–313.

138. Stanton, J. F.; Gauss, J. *Theoretica Chimica Acta* **1997**, *95*, 97–98.

139. Stanton, J. F.; Gauss, J. *Journal of Chemical Physics* **1994**, *101*, 8938–8944.

140. Kallay, M.; Gauss, J. *Journal of Chemical Physics* **2004**, *121*, 9257–9269.

141. Woon, D. E.; Dunning, Jr., T. H. *Journal of Chemical Physics* **1994**, *100*, 2975–2988.

142. Varner, M. E.; Harding, M. E.; Vázquez, J.; Gauss, J.; Stanton, J. F. *Journal of Physical Chemistry A* **2009**.

143. Mordaunt, D. H.; Osborn, D. L.; Neumark, D. M. *Journal of Chemical Physics* **1998**, *108*, 2448–2457.

144. Bohac, E. J.; Marshall, M. D.; Miller, R. E. *Journal of Chemical Physics* **1992**, *96*, 6681–6695.

145. Quack, M.; Suhm, M. A. *Journal of Chemical Physics* **1991**, *95*, 28–59.

146. Beames, J. M.; Murray, C.; Varner, M. E.; Stanton, J. F. and Lester, M. I. *in progress.*

147. Demaison, J.; Császár, A. G.; Dehayem-Kamadjeu, A. *Journal of Physical Chemistry A* **2006**, *110*, 13609–13617.

148. Lester, M. I.; Stanton, J. F. and Lineberger, W. C. *private communication.*

Vita

Mychel E. Varner grew up in Independence, Missouri; spent four years in Kirksville, Missouri; a summer in Minneapolis, Minnesota; and seven years in Austin, Texas.

Permanent address: mychelv@gmail.com

This dissertation was typeset with LaTeX[†] by the author.

[†]LaTeX is a document preparation system developed by Leslie Lamport as a special version of Donald Knuth's TeX Program.